Paul Christian, BSc

Polymorphism of the Drug Carbamazepine in Proximity to Solid Surfaces

MASTER THESIS

For obtaining the academic degree
Diplom-Ingenieur

Master's Program of
Technical Physics

GRAZ UNIVERSITY OF TECHNOLOGY

Supervisor:

Ao.Univ.-Prof. Dipl.-Ing. Dr.techn. Roland Resel
Institute of Solid State Physics
Graz University of Technology

Graz, December 2014

EIDESSTATTLICHE ERKLÄRUNG

AFFIDAVIT

Ich erkläre an Eides statt, dass ich die vorliegende Arbeit selbstständig verfasst, andere als die angegebenen Quellen/Hilfsmittel nicht benutzt, und die den benutzten Quellen wörtlich und inhaltlich entnommenen Stellen als solche kenntlich gemacht habe. Das in TUGRAZonline hochgeladene Textdokument ist mit der vorliegenden Masterarbeit/Diplomarbeit/Dissertation identisch.

I declare that I have authored this thesis independently, that I have not used other than the declared sources/resources, and that I have explicitly indicated all material which has been quoted either literally or by content from the sources used. The text document uploaded to TUGRAZonline is identical to the present master's thesis/diploma thesis/doctoral dissertation.

_____   _____
Datum / Date   Unterschrift / Signature

Acknowledgment

First and foremost I want to thank my supervisors:

Roland Resel, who always supports his students in the best possible way. I am deeply grateful for giving me the rare chance to participate in a synchrotron experiment which was a memorable experience.

Oliver Werzer, who's passion for his work is infectious and who provided me with the freedom to explore and experiment apart from pre-defined paths. His encouraging attitude and scientific guidance made this thesis a pleasant and most valuable experience.

I am most grateful to Christian Röthel who spent not only the beamtime in Berlin with me and who was responsible for all the synchrotron data conversion but whom I also consider as one of my closest friends.

I was pleased to meet Ingo Salzmann of the Humboldt University of Berlin who kindly invited us to join his beamtime at the BESSY II synchrotron facility. It was a pleasure to share an office with Stefan Pachmajer, Andrew Jones, Magdalena Truger and Benedikt Schrode in the *k-Raum*. Our fruitful discussions, the willingness to help each other and the cheerful atmosphere made our office a unique place to work at.

A special "thank you" is dedicated to my fellow students and friends Gernot Kraberger, Georg Urstöger and Manuel Zingl. Without you, these years would not have been so educational and so much fun.

Last but not least, I want to express my deepest gratitude to my family for being always morally supportive and for encouraging me on my path.

Abstract

Defined morphologies and crystallographic structures of active pharmaceutical ingredients (APIs) are highly desired for drug administration as these properties are directly linked to their bioavailability due to changes in their dissolution properties. Within this work, the molecular arrangement of a model substance, the anticonvulsant drug carbamazepine, is investigated at solid surfaces. For thin film preparation, various techniques including spin coating, drop casting and dip coating as well as physical vapor deposition by thermal evaporation were employed. By using specular X-ray diffraction and grazing incidence X-ray diffraction (GIXD), polymorphic forms and their orientation with respect to the substrate surface are elucidated. Optical microscopy and atomic force microscopy (AFM) are used complementarily for morphology characterization. While a preferred orientation is present for most of the films, the quality of alignment is poor and a large mosaic spread is displayed. The quality of alignment can be drastically improved by the inclusion of iminostilbene. Iminostilbene is a precursor in carbamazepine synthesis that does not contain the carboxamide end group. This molecule forms homogeneous films with a dendritic morphology and a preferred 010 texture is present independent of the preparation technique. On the intermixing of carbamazepine with iminostilbene in solution no co-crystal forms on deposition, but as iminostilbene crystallizes prior to carbamazepine, it acts as a crystallization template for the latter. The findings of this work show various methods to induce defined order and polymorph selection which are expected to have a direct impact on the dissolution properties within transdermal patches or particle coatings typically used in pharmaceutical drug formulation.

Kurzfassung

Arzneistoffe mit definierter Morphologie und kristallographischen Struktur sind von besonderer Relevanz für die medizinische Verabreichung, da diese Eigenschaften das Lösungsverhalten verändern und sich damit direkt auf die Bioverfügbarkeit im Körper auswirken. In dieser Arbeit wird die strukturelle Anordnung einer Modellsubstanz, die des Antiepileptikums Carbamazepin, an Oberflächen untersucht. Zur Präparation dünner Filme wurden Lösungsmittel basierende Techniken wie Rotationsbeschichtung, Auftropfen, Tauchbeschichtung sowie auch thermisches Bedampfen verwendet. Mittels spekularer Röntgendiffraktometrie und Röntgendiffraktometrie mit streifendem Einfall wurden die verschiedenen polymorphen Formen charakterisiert und die jeweilige Orientierung in Bezug auf die Substratoberfläche untersucht. Die Oberflächenbeschaffenheit selbst wurde mittels optischer Mikroskopie und Rasterkraftmikroskopie näher analysiert. Obwohl die meisten Filme eine gewisse Vorzugsorientierung der Kristalle zeigen, ist die Qualität der Ausrichtung gering und eine weite Verteilung der Mosaizität wird beobachtet. Eine deutliche Verbesserung kann durch die Beigabe von Iminostilbene erreicht werden. Iminostilbene ist ein Ausgangsstoff in der Synthese von Carbamazepin, welches auf Grund der fehlenden Carbonsäureamide-Gruppe homogene Filme mit dendritischen Strukturen in einer 010 Vorzugsorientierung, unabhängig von der Präparationsmethode, bildet. Beim Mischen von Carbamazepin mit Iminostilbene in Lösung kommt es nicht zur Bildung von Co-Kristallen, jedoch wirkt das schneller kristallisierende Iminostilbene als eine Art Template für die nachfolgende Kristallisation von Carbamazepin. Die Ergebnisse dieser Arbeit zeigen verschiedenste Methoden um gerichtetes Wachstum sowie bestimmte polymorphe Phasen zu induzieren, von welchen ein direkter Einfluss auf das Löslichkeitsverhalt in transdermalen Pflastern oder in Partikelbeschichtung, wie sie in der Pharmazie üblich sind, erwartet wird.

Contents

Contents

1. Introduction

Poorly soluble drug compounds for oral delivery are becoming an increasing problem in pharmaceutical application over the recent years [1]. It is estimated that nowadays 40 – 70 % out of all the new chemical entities that enter drug development exhibit an insufficient aqueous solubility [2].

There are several ways to increase the solubility such as particle size reduction, use of surfactants or the formation of co-crystals [3–5]. While an amorphous form most often exhibits favorable dissolution properties, it is usually also the least stable one, thus being avoided in practical application [6]. Among the most important factors which influence the solubility in solid state pharmaceutical formulations are the crystallographic structure and the morphology of the compound [7]. In this context polymorph screening and control have become crucial parts within drug development. Crystallization in different polymorphic phases alters various critical properties such as bioavailability, solubility, dissolution rate as well as the chemical and physical stability [8]. While conventional polymorph control is established through methods such as recrystallization via seeding, more recent approaches include techniques such as solvent control or template-induced crystallization processes [8, 9].

Within the field of organic electronics polymorphism in the form of thin film phases is often observed [10, 11]. The formation of such phases can be the result of solvent exposure [12] or likewise the presence of substrates during the crystallization process [13]. Typical techniques employed for thin film preparation include drop casting, spin coating as well as vacuum deposition. Such techniques are not common in the pharmaceutical sciences and thus exhibit new possibilities to find and/or stabilize so-far unknown polymorphic phases.

1. Introduction

Within this master thesis the presence of surfaces during the crystallization process of an active pharmaceutical ingredient (API) is evaluated as a possible way to achieve polymorph control. Thin films of a drug compound are prepared on defined surfaces to gain a more detailed understanding on the API - surface interactions. This is of relevance in practical application where drug administration routes such as the buccal ones from patches can profit [14]. Preparation of thin films of APIs has previously been demonstrated to enhance the dissolution properties and morphology control (shape, size) can be accomplished directly via the process parameters [15]. Using thin film preparation techniques well-established within the organic electronics research community, this allows for scalability but also minimizes the imminent danger of an unintended phase transition, as usually only a single process step is required. A phase transition may result in strongly altered properties and thus deviating therapeutic action.

In pharmaceutical sciences, characterization is mostly performed by techniques such as X-ray powder diffraction, infrared or Raman spectroscopy. By the preparation of thin films on solid surfaces, different techniques such as atomic force microscopy, specular X-ray diffraction and most notably grazing incidence diffraction can additionally be employed. These are established techniques for thin film characterization and allow a detailed insight into the crystallographic properties and the relative alignment between substrate and deposited film.

Part I.

Fundamentals and experimental section

2. Fundamentals

Within this chapter a short introduction to the fundamental principles of crystal growth is given. The intention is to familiarize the reader with the basic concepts and to point out the parameters important in crystallization experiments. A short section on polymorphism completes this chapter to provide a basic knowledge of this phenomena and its importance in pharmaceutical application.

2.1. Nucleation and crystal growth

Among the different drug administration routes the oral route is still by far the most common one, usually formulated in tablets or other solid forms (e.g. capsules) [16]. Metastable crystalline or amorphous forms always bear the risk of sudden transformation upon handling or storage. Consequently, they are usually not desired for practical application, thus stable crystalline forms are mostly applied [17]. A detailed understanding of the mechanisms behind crystal growth is therefore necessary. While this section mostly deals with crystallization from solution, the presented theories can likewise be applied to crystallization from the melt.

In the following, two different approaches to describe cluster formation during crystal nucleation in solutions are introduced: classical nucleation theory (CNT) and *non-classical* approaches such as the two-step mechanism. In Figure 2.1 these processes are schematically depicted. In conventional theory the formation of clusters within the supersaturated solution is assumed, which already exhibit the structure of possible polymorphs of the solute. The cluster formation is the consequence of order and density fluctuations concomitant with supersaturation. On the contrary,

order and density fluctuations are assumed to be disconnected from each other in the two-step mechanism. Here the separation of a dense, disordered liquid phase precedes crystalline order so that initial clusters are liquid-like and structural order emerges over time [18].
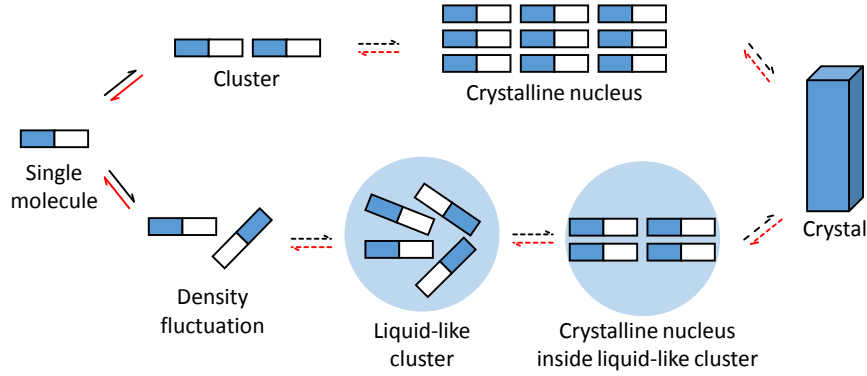
Figure 2.1.: Cluster formation during nucleation as described by the conventional and the two-step theory. Figure based on [18].

2.1.1. Classical nucleation theory

The classical nucleation theory (CNT) [19] is well established in describing the processes associated with crystal growth due to supersaturation (from solution/melt). It is a model of a first order phase transition which can be used to describe homogeneous as well as heterogeneous nucleation processes. Supersaturation is commonly expressed as the ratio of the actual concentration of the solute C before any crystallization event and the solubility C_s (i.e. concentration at equilibrium):

$$\beta = \frac{C}{C_s}. \tag{2.1}$$

As the chemical potential in supersaturation is different to that in saturation, a driving force

$$\Delta\mu = k_\mathrm{B} T \ln(\beta), \tag{2.2}$$

is experienced by a single molecule. In this equation k_B denotes the Boltzmann constant and T the absolute temperature [20]. When a cluster of size n is formed,

this leads to a gain of $-n\Delta\mu$ in bulk free energy. However, this process competes with the increase in total interface energy

$$E = A\gamma, \tag{2.3}$$

where γ represents the surface energy of the nucleus-solution interface and A the surface area [18]. Describing the competing processes in terms of the Gibbs free energy (also called *enthalpy*) yields

$$\Delta G = -n\mu + E = -nk_{\mathrm{B}}T\ln(\beta) + A\gamma. \tag{2.4}$$

For a cubic nucleus of length a which consists out of n blocks of volume v (i.e. molecular volume of the crystalline form), the surface area A can be expressed by

$$V = nv = a^3 \rightarrow A = a^2 = (nv)^{2/3}. \tag{2.5}$$

To account for other shapes and keep a more general expression, a shape factor s is introduced so that the surface area is now connected to the molecular volume by $A = s(nv)^{2/3}$. The free enthalpy from Equation 2.4 is then expressed in terms of the building block number n:

$$\Delta G = \underbrace{-nk_{\mathrm{B}}T\ln(\beta)}_{\substack{Volume \\ term}} + \underbrace{s(nv)^{2/3}\gamma}_{\substack{Surface \\ term}}. \tag{2.6}$$

This equation describes the competing processes of bulk free energy (volume term) and interface energy (surface term). As long as the surface term is dominant, the enthalpy change for a growing nucleus (that is increasing n) will be positive, meaning that the formed cluster is disfavored. In Figure 2.2 this is demonstrated for a spherical nucleus (shape factor $s = (36\pi)^{1/3}$) with radius r. At small cluster sizes the surface term dominates and the change in enthalpy is positive, meaning that the formed cluster is unfavorable and dissolves spontaneously. However, above a critical radius r^* the enthalpy change becomes negative, thus further growth proceeds spontaneously. This means that ΔG reaches a maximum at r^*, above which the nucleus is stable, i.e. there is an energy barrier G^* above which growth of the nucleus is favored.
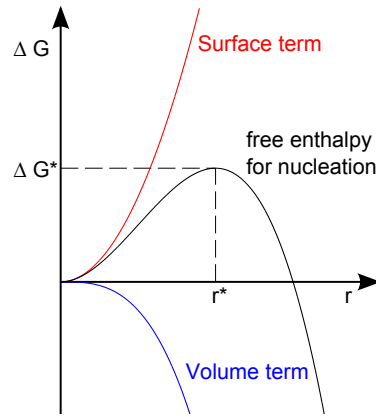
Figure 2.2.: Total free energy of the nucleation process as a function of the nucleus radius r. The position of the critical radius r^* and the corresponding free enthalpy G^* is indicated.

Anyway, this energy barrier can be derived in a more general form from the equation 2.6 by calculating the maximum in ΔG. This yields a critical nucleus size

$$\Delta n^* = \frac{8}{27} v^2 \left(\frac{s\gamma}{k_B T \ln(\beta)} \right)^3 \tag{2.7}$$

with a corresponding energy barrier of

$$\Delta G^* = \frac{4}{27} \frac{v^2 s^3 \gamma^3}{(k_B T \ln(\beta))^2}. \tag{2.8}$$

This also allows the determination of the steady-state crystal nucleation rate which generally can be expressed by

$$J = K_0 \exp\left(\frac{-\Delta G^*}{k_B T} \right) \tag{2.9}$$

with the kinetic coefficient K_0 [Nucleation sites $\cdot s^{-1}$] (as opposed to the exponential factor containing the structure of the nucleus) [20]. While the actual nucleation rate is the consequence of a consecutive series of attachments and separations resulting in differently sized clusters (compare with Szilard-Farkas model [21]), usually a stationary state with a constant cluster concentration is assumed. The kinetic coef-

ficient can then be expressed by

$$K_0 = z f^* C_0, \tag{2.10}$$

where z denotes the Zeldovich factor, f^* the frequency of building unit attachment and C_0 the concentration of nucleation sites [18]. The Zeldovich factor characterizes the flatness of the free enthalpy around the critical size where size variations are mainly random and can also lead to dissolution of a cluster. Consequently, this factor also limits the nucleation rate [22]. For the steady-state nucleation case this factor is

$$Z = \frac{3\ln^2(\beta)}{4v\sqrt{\pi}} \left(\frac{k_B T}{s\gamma} \right)^{3/2} = \frac{\ln(\beta)\sqrt{k_B T}}{\sqrt{12\pi\Delta G^*}}, \tag{2.11}$$

which is supersaturation-dependent [18]. The frequency f^* can be described by a diffusion process D from/to the surface area A^* of the nucleus in contact with the solution:

$$f^* = \lambda A^* D \frac{X_1}{d}. \tag{2.12}$$

The concentration of available building units in the solution is denoted with X_1 and d can be assumed by the diameter of these units. The sticking coefficient λ describes molecules which do not get transferred to the adsorbed state despite being in proximity to the nucleus. The diffusion term D can be modeled by an energy barrier $D = D_0 \exp(-E/RT)$ which is associated with conformational changes and/or partial loss of the solvent shell upon incorporation into the nucleus [18]. The energy term E refers to a mole of the substance, thus the gas constant R is used instead of the Boltzman constant k_B.

So far only homogeneous nucleation (HEN) had been considered, an ideal case most likely observed from pure solutions well above the supersaturation mark. However, in real experiments mostly heterogeneous nucleation (HON) is observed as interfaces with solid surfaces (e.g. vessel, stirrer) as well as contamination with other solids (e.g. dust) lower the the surface energy γ and provide additional nucleation sites [20]. The decrease in surface energy is depicted in Figure 2.3 where depending on the contact angle (the angle between the solid/liquid contact interface) the interface to the surrounding fluid is reduced. This is taken into account by using an effective surface energy $\gamma_{HON} = \psi\gamma$. The activity factor ψ ranges from 0 to 1

and will thus decrease the energy barrier G^* in Equation 2.8. The same applies to the concentration of nucleation sites C_0 in Equation 2.10 which likewise has to be changed from the molecular density ($C_0 = v^{-1}$) to the effective concentration taking the heterogeneous nucleation sites into account ($C_0 = C_a$) [18].

Figure 2.3.: Decreasing contact angle (from left to right) for three droplets on a solid surface.

2.1.2. Two-step mechanism

Classical nucleation theory has a major shortcoming: While most parameters used in this model can be determined precisely, there are usually several orders of magnitude between the experimental nucleation rate and the one predicted from CNT [23]. To overcome this issue and to account for experimental observations made for protein crystallization in solution, two-step models were developed more recently [24].

As already depicted in Figure 2.1, a two-step process describes the formation of metastable, disordered dense liquid clusters in solution as a precursor to crystalline order rather than the formation of nuclei already exhibiting the final crystalline structure. This is inferred from the observation made by dynamic light scattering (DLS) in protein systems such as lysozyme and lumazine synthase. In these systems cluster formation is present immediately after preparation but exhibiting relatively steady radii. From this it is concluded that these clusters are of dense liquid. Their lifetime is significant longer (15 ms for lysozyme and ~ 10 s for lumazine synthase) than that of single proteins in Brownian motion ($\sim 10 \times 10^{-5}$ s for proteins) [24]. Sufficiently strong short-range forces (e.g. van der Waals, hydrophobic) are assumed to play a key role in the formation of those dense areas [25]. While their formation is fast, subsequent crystallization inside them is rate determining [24].

While initially developed for protein crystallization, subsequently this mechanism was successfully matched to observed crystallization mechanisms of various other systems including small molecules [25] and polymers [26].

2.1.3. Crystal growth from the nucleus

The formation of a nucleus is only the initial step in the growth of a macroscopic crystal. Subsequently, these nuclei start to grow in size by further molecular attachment to the surface. In Figure 2.4 a schematic representation of a crystal surface with potential growth sites is given. One can identify different faces on such a structure: Flat regions called terraces, steps where a consequent layer begins and kinks, vacant positions in a step. A solute molecule adsorbing to the surface is most likely to attach to a kink as these sites involve the formation of at least one strong bond in excess of the other faces. This makes kinks fast growing faces while likewise flat faces are the slowest one. In the final habit (shape) of the crystal the slow growing faces will therefore become the largest while fast growing ones become small [27].
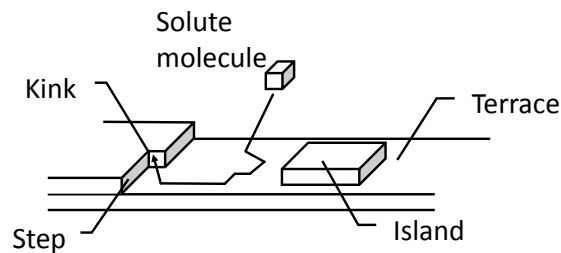
Figure 2.4.: Potential growth sites on an arbitrary crystal surface: Flat, stepped and kinked faces. Figure based on [28].

Further, dislocations and impurities play an important role in crystal growth. For a screw dislocation steps are always present, thus solute molecules can attach more easily. This leads to a much more regular growth. Impurities on the other hand, can have a great effect on the crystal growth rates. While from a thermodynamical point of view the growth rates should increase (as the impurity adsorption decreases the edge free energy), usually the kinetic factor is much more affected. The blocking of several kinks by impurities can already decrease the growth rate by several orders of magnitude [20].

To describe the growth kinetics theoretically, many assumptions about the pathways of mass transfer have to be made. However, even with very basic assumptions one

can obtain useful results. The following derivation is based on De Yoreo *et al.* [28]. For this only the steps are considered as sites of crystal growth and concentration and activity are assumed equal. The step speed v then corresponds to the step advancement rate R_s times the depth of a kink b. As the step advancement rate is simply the difference of molecules attaching/detaching, this can be expressed as

$$\frac{v}{b} = R_s = R_a - R_b, \tag{2.13}$$

with R_a and R_b denoting the attachment and detachment rate, respectively. The attachment rate is simply the flux of molecules F to the step times the area of a step site $c \cdot h$ multiplied by the probability of attachment P_a. The step height is here denoted by h and the distance between molecules along the step by c. Likewise, detachment can be expressed by a probability P_d and an attempt frequency f. However, as different sites exhibit different detachment rates, one has to sum over all sites independently. With these terms Equation 2.13 becomes

$$\begin{aligned} \frac{v}{b} &= R_a - R_b \\ &= chFP_a - f \sum_i n_i P_{d,i}. \end{aligned} \tag{2.14}$$

The flux is proportional to the solution concentration C times a factor B and the detachment probability can be expressed by an energy barrier $\exp(-E_i/k_B T)$:

$$\frac{v}{b} = chBC - f \sum_i n_i \exp(-E_i/k_B T). \tag{2.15}$$

The concentration-independent factor B accounts for the geometry, the temperature and mass terms describing the dynamics of the solute in proximity to the surface. This equation for the step speed can easily be evaluated for equilibrium where f becomes zero and the concentration corresponds to the equilibrium reactant concentration C_e. From this, one can express the step speed as

$$\begin{aligned} v &= cbhB(C - C_e) \\ &= \Omega\beta(C - C_e), \end{aligned} \tag{2.16}$$

with Ω the molecular volume and β the kinetic coefficient. This equation demon-

strates that the step speed scales with absolute supersaturation rather than actual supersaturation, meaning that under same conditions a crystal with higher solubility exhibits faster growth.

2.2. Polymorphism

Polymorphism is becoming increasingly important in pharmaceutical application, both as a deliberately induced state for enhanced properties in the one API but also as a random occurrence to be avoided at all cost in another. Polymorphism describes the ability of a certain compound to exist in more than one distinct crystalline structure while the stoichiometry stays the same. If this is the result of a conformer of the same molecule, this is termed *conformational polymorphism*. The change in molecular arrangement alters many properties such as solubility, dissolution rates and stability [8]. These changes can be favorable in terms of an increased bioavailability but can also drastically decrease the efficiency of a certain compound. Polymorphism is a common phenomena in drug molecules which is emphasized by what is labeled *McCrone's rule*: He stated in 1965 that

> "every compound has different polymorphic forms, and that, in general,
> the number of forms known for a given compound is proportional to the
> time and money spent in research on that compound." [29]

For example Stahly reports on the basis of 245 polymorph screens that more than 90 % exist in multiple crystalline/non-crystalline forms (e.g. hydrates, solvates, allotropes) while 50 % exhibit polymorphism [30].

However, not every change in crystal structure is the result of the formation of a "real" polymorph. If the crystal structure is altered by the incorporation of solvent molecules, this is termed *pseudo-polymorphism*. Noteworthy examples are hydrates, formed by the incorporation of water molecules into the crystal structure. Though sometimes desired in pharmaceutical application, hydrate formation will mostly result in decreased bioavailability and dissolution rates are often negatively influenced by this transition [31, 32]. The formulation of an API in hydrate/solvate form should

therefore be carefully considered. In the case of non-volatile molecules which get systematically incorporated into the structure, this is called a co-crystal [16].

2.2.1. Polymorph formation and Ostwald's rule of stages

Despite the practical importance in many fields (e.g. pharmaceutical application, dye industry) and being vastly researched in academia, polymorphism is still not fully understood. The root of polymorph formation is most likely found in pre-nucleation aggregates (preparation from solutions or melts), which already mimic all the possible polymorphic configurations [33]. Whether these *embryos* are in an ordered state (according to CNT) or in a disordered form (two-step nucleation) is still up to debate. It is, however, known that the formation of polymorphic phases is influenced by a variety of processing parameters such as solvent effects (e.g. polar/unpolar), temperature, degree of supersaturation, surface interactions and additives [8].

In the context of polymorph formation also Ostwald's rule of stages [34] should be mentioned. Ostwald studied highly supersaturated solutions and resulting precipitates which led him to his statement that the fastest solidifying form is usually also the least thermodynamically stable one. Though not a law but only a possible tendency in nature, it is often followed [35, 36].

2.2.2. Polymorph control

As already mentioned in the previous section, there are multiple parameters influencing polymorph formation. According to Ostwald's rule of stages also the timescales of the employed techniques have a major influence. This leads to a quite large parameter space in which polymorphism can be studied/possibly be observed. In Figure 2.5 a variety of different experiments are schematically depicted with their corresponding time scale. These are techniques commonly employed in the control/screening of polymorphs [8]. Since solution-based techniques are mostly used

within this work, solvent-mediate effects will be briefly considered in the following.
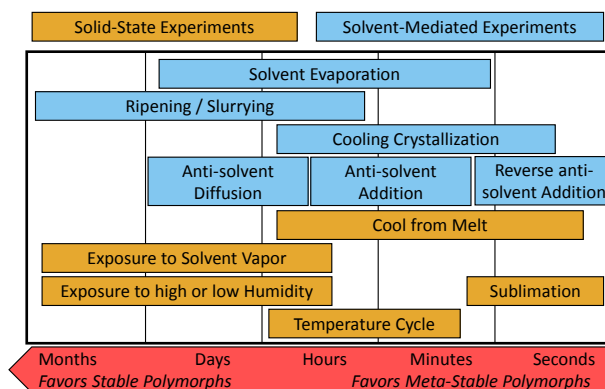
Figure 2.5.: Crystallization techniques for polymorph control. Utilizing different timescales will favor the formation of stable or metastable forms, respectively. Figure based on [8].

As discussed previously, a general assumption in crystal growth is the presence of clusters during the nucleation process which contain all the possible polymorphic arrangements. In this state other molecules (e.g. solvents) can be regarded as additives, which may interfere with the nucleation or crystal growth rates, thus promoting a certain phase over the others [8]. Solvents are basically additives which are present in vast amounts around the solute. Depending on the solvent-solute interactions, different associates are formed which transfer their structural information to the final crystal form [18]. This is schematically depicted in Figure 2.6. Herein not only hydrogen bonding but also electrostatic and van der Waals interactions play an important role [37].
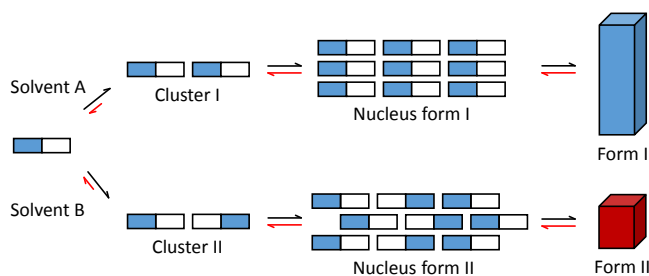
Figure 2.6.: Polymorph selction promoted by solvent selection. Figure based on [18].

3. Experimental

Within this chapter the materials used in this work, their properties and the methods employed for sample preparation are presented. A brief introduction to the experimental techniques and the actual measurement setup is given as well.

3.1. Materials

This section introduces carbamazepine and iminostilbene, the two molecules investigated within this study. While similar in molecular structure, only the former is used in pharmaceutical application.

3.1.1. Carbamazepine

Carbamazepine (CBZ) is an active pharmaceutical ingredient (API) with the systematic name 5H-Dibenz[b,f]azepine-5-carboxamide. The structural formula is depicted in Figure 3.1. In pharmaceutical application the anticonvulsant drug is used to treat serious medical conditions such as epilepsy and trigeminal neuralgia. Carbamazepine is included in the WHO Model List of Essential Medicines, a table containing APIs which are thought to be crucial for human health care needs [38].

Despite its importance in human medicine, carbamazepine is rated only a class II API by the Biopharmaceutics Classification System (BCS), meaning that aqueous solubility is low while permeability is still high [39]. The low water solubility ($205\,\mu g\,mL^{-1}$ reported by Tsinman *et al.* [40]) combined with the many different
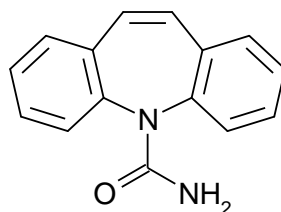
**Figure 3.1.:** Structural formula of carbamazepine ($C_{15}H_{12}N_2O$).

polymorphic phases reported in literature, make the drug an ideal model compound for this study.

To date five anhydrous polymorphs of carbamazepine are known in literature [41] together with various pseudopolymorphs such as hydrates and solvates as well as co-crystals [42]. The unit cells of the anhydrous polymorphs are depicted in Figure 3.2 while the corresponding lattice constants are given in Table 3.1. For carbamazepine dihydrate a *P*-monoclinic and an orthorhombic form are reported [43]. Their unit cells are depicted in Figure 3.3 and their lattice constants are given in Table 3.2. These and all the other images in this work depicting molecular packings were rendered by using the "Visual molecular dynamics" (VMD) software [44].

Table 3.1.: Unit cell parameters of five anhydrous phases of carbamazepine. Lattice constants a, b and c are given in Å and the angles α, β, γ between the sites in degree. The CSD field refers to the Cambridge Structural Database reference code.

	Form I	Form II	Form III	Form IV	Form V
a	5.1705(6)	35.454(3)	7.5500(16)	26.609(4)	9.1245(5)
b	20.574(2)	35.454(3)	11.186(3)	6.9269(10)	10.4518(5)
c	22.245(2)	5.253(1)	13.954(3)	13.957(2)	24.8224(11)
α	84.124(4)	90	90	90	90
β	88.008(4)	90	92.938(8)	109.702(2)	90
γ	85.187(4)	120	90	90	90
CSD	CBMZPN11	CBMZPN03	CBMZPN14	CBMZPN12	CBMZPN16
lattice	triclinic	trigonal	*P*-monoclinic	*C*-monoclinic	orthorhombic
Source	[45]	[46]	[47]	[48]	[41]

All polymorphs except for form V exhibit the formation of dimer structures which act as the main packing motif. The carboxamide moieties of two adjacent molecules

Triclinic Form I
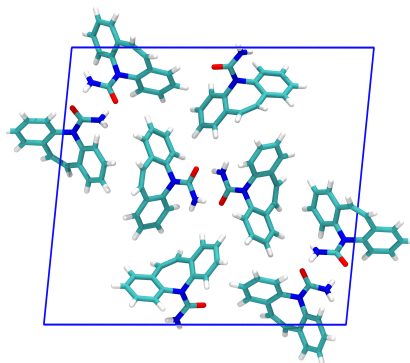
Trigonal Form II
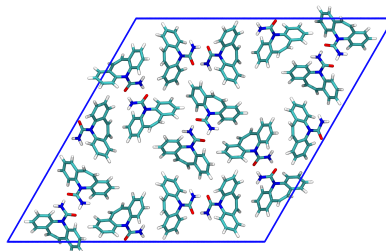
P-monoclinic Form III
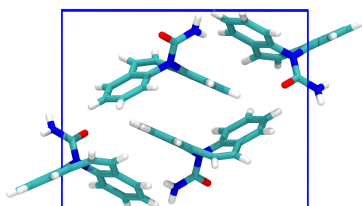
C-monoclinic Form IV
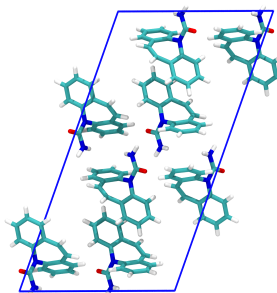
Orthorhombic Form V
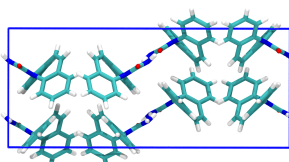
Figure 3.2.: Unit cells of the five anhydrous polymorphic phases of carbamazepine as known in literature, shown along arbitrary directions.

form these dimers through hydrogen-bonding which then (for a given crystal structure) arrange accordingly [49]. A different situation is observed in the orthorhombic form V where catermeric hydrogen bonds are formed. This means that instead of two hydrogen bonds between two adjacent carboxamide groups, one of these bonds is formed with another molecule, thus a chain of interconnected molecules emerges [41].

Another interesting observation can be made in the trigonal polymorph (Form II). This crystal tructure has a comparable lower density caused by cavities expanding throughout the crystal. There is also evidence that in these channels solvent incorporation is possible without even changing the polymorphic phase [50].

The carbamazepine powder used in this work was purchased from Alfa Aesar. A purity of 98 % is specified by the manufacturer together with a melting point in the range of 189 – 192 °C. The powder itself was continuously stored in a fridge at temperatures slightly above zero.
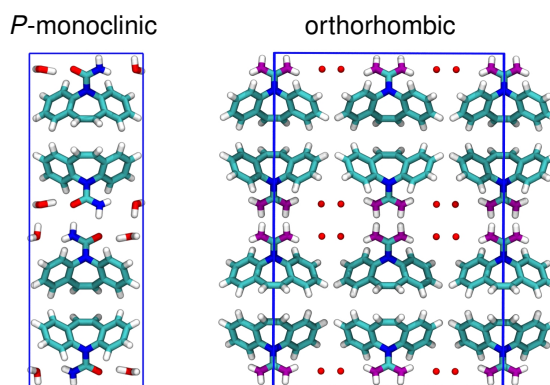

Figure 3.3.: Unit cells of the *P*-monoclinic and orthorhombic carbamazepine dihydrate. For the latter the carboxamide moiety is disordered, thus both possible arrangements of this group are indicated for each molecule in purple.

Table 3.2.: Unit cell parameters of two hydrous phases of carbamazepine. Lattice constants a, b and c are given in Å and the angles α, β, γ between the sites in degree. The CSD field refers to the Cambridge Structural Database reference code.

	P-monoclinic	orthorhombic
a	10.066(2)	19.779(2)
b	28.719(5)	4.9369(4)
c	4.831(1)	28.714(3)
α	90	90
β	103.45(1)	90
γ	90	90
CSD	FEFNOT02	FEFNOT05
Source	[51]	[43]

3.1.2. Iminostilbene

Iminostilbene is a precursor in carbamazepine synthesis and exhibits a similar structure to the latter except for the missing carboxamide group [52]. The structural name is 5H-Dibenz[b,f]azepine and the structural formula is depicted in Figure 3.4.
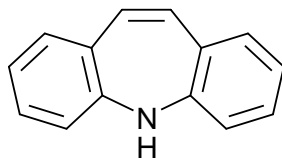
Figure 3.4.: Structural formula of iminostilbene ($C_{14}H_{11}N$).

Although iminostilbene has no direct application in pharmaceutical application, the similarity in structure to carbamazepine makes it an interesting compound for this study. While the carboxamide group plays an important part in the molecular packing of carbamazepine due to strong hydrogen bonding, this group is absent for iminostilbene. Indeed, for iminostilbene only one crystal structure is known as reported by Reboul *et al.* [53]. The molecule packs in an orthorhombic unit cell (depicted in Figure 3.5) with the lattice parameters being $a = 8.226(3)\,\text{Å}^{-1}$, $b = 20.413(6)\,\text{Å}^{-1}$, $c = 6.035(2)\,\text{Å}^{-1}$, $\alpha = \beta = \gamma = 90°$.

The iminostilbene powder was purchased from Sigma Aldrich in 97 % purity and is used without further treatment. The powder is of yellow color and a melting point in the range of 196–199 °C is specified by the manufacturer.
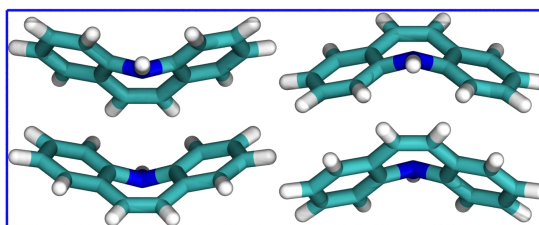

Figure 3.5.: Unit cell of the orthorhombic iminostilbene.

3.2. Sample preparation

In this section the techniques employed for thin film preparation on defined surfaces are explained. Also the substrate cleaning procedure is briefly described as it is of high relevance.

3.2.1. Substrates and cleaning procedure

While different substrates were evaluated within this work, most thin film preparation was done either on microscopy slides or on silicon wafers with defined grown thermal oxide layers. To distinguish them from each other, the former is referred to as "glass" and the latter as "silicon oxide" or "SiO_x" from here on.

The glass substrates were manually cut to quadratic shape (2.5 cm x 2.5 cm) from microscopy slides made out of soda-lime glass (company Roth) or crown glass (company Menzel). Prior to the film preparation, these substrates were cleaned for fifteen minutes by sonication while inserted into acetone. Subsequently, they were washed with 2-propanol and dried using pressurized air.

Pre-cut silicon wafers (2 cm x 2 cm) with 150 nm thermal oxide were used equally with uncut wafers. The former were cleaned by plasma etching for 40 s at maximum plasma power with the commercial equipment "Femto" from Diener electronics. This procedure does not only remove any organic residuals but also activates the surface by increasing the number of OH moieties, thus increasing the hydrophilicity. Manually cut wafers were washed in acetone prior to etching in concentrated NaOH for 15 min. Afterwards they are also cleaned with 2-propanol and dried using pressurized air. These surfaces have a similar hydrophilicity compared to the plasma etched ones.

3.2.2. Dip coating, drop casting, and spin coating

The methods employed in this work are well established within the research community and within our group. As such only a short reminder for each technique is given. For more detailed description see for instance [54] or any textbook.

Dip coating is a method to produce thin films with directed growth. The substrate is inserted into a solution containing the compound to be deposited. After complete insertion, the sample is then withdrawn at a certain speed. The wetting layer on the substrate at the gas/liquid interface will consequently evaporate. By this the dissolved material is deposited on the surface with, in an ideal case, a preferred orientation present along the withdrawal direction. Depending on solvent evaporation rate and withdrawal speed, different coating thicknesses can be reached [55]. The dip coater used is a product of SDI Company Ltd. and is located on a benchtop isolator under a covering hood. This is done to minimize vibrations and to limit solvent evaporation from the dip coating recipient.

Drop casting is a simple technique to deposit material from solution onto a given surface. A solution is dropped onto a substrate so that ideally full surface coverage can be reached. Subsequently, the solvent evaporates and the dissolved material precipitates. The speed of this process is greatly influenced by the used concentration and the evaporation rate of the solvent. In this work drop casting was done with the constant amount of 100 μL solution per sample to ensure comparability of

the individual batches. Additionally, the samples were covered with the lid of a petri dish to promote controlled solvent evaporation. Otherwise the volatile environment of the fume hood has a considerable influence.

Spin coating is a technique which allows the formation of thin, uniform films on a substrate surface. The sample is fastened on a rotatable chuck and solution is added to the surface. Subsequently, the sample is accelerated to a certain rotation speed. While spinning the rotational forces and solvent evaporation will remove excess solution/solvent so that an homogeneous residual layer is formed [56]. The results presented in this work were achieved with a SSC-200 spin coater from Schaefer. Spin coating was performed with 200 μL solution and a rotational speed of 17 rps for one minute was applied. Other speeds and duration times were also evaluated but are omitted from this work for clarity.

3.2.3. Thermal evaporation

Thermal evaporation was performed under high vacuum (below 10^{-4} mbar) in an evaporation chamber, schematically depicted in Figure 3.6. The recipient is made out of glass and operating conditions can be reached within thirty minutes. Such a setup may be also practicable for pharmaceutical application, for which processing time is of great importance. The used compound is put in a Knudsen cell, a crucible made out of quartz glass with a small orifice. The cell is resistively heated via a tungsten wire. With this setup deposition rates below $0.5\,\text{Å}\,\text{s}^{-1}$ can be reached. The deposition process itself is started/terminated via a manually operated shutter after the desired evaporation rate is established.

In situ monitoring of the deposition rate is performed via a quartz crystal microbalance (QCM) which is water cooled for increased precision and stability. The quartz crystal is oscillating at its resonance frequency which is disturbed by a change in its mass (i.e. deposition or removal of material from its surface). This frequency shift correlates with the mass change as described by the Sauerbrey equation [57] in 3.1. This equation can be rewritten by using $\Delta m = \rho A h$ so that the frequency shift is directly proportional to the deposited film thickness. For the 6 MHz QCM used in
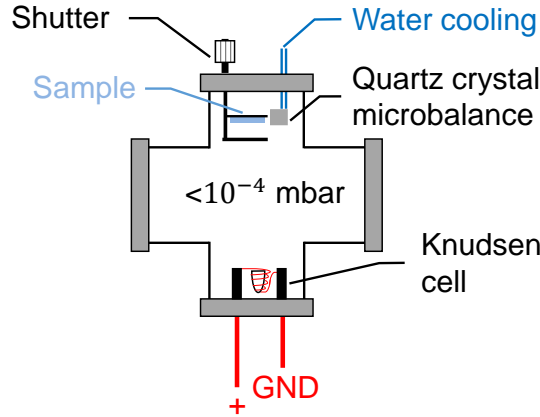
**Figure 3.6.:** Schematic diagram of the thermal evaporator.

this work and an assumed density of $1.2\,\text{g/cm}^3$ for carbamazepine a change of $1\,\text{Hz}$ corresponds to a thickness of $1\,\text{Å}$. The density of carbamazepine is assumed from its crystalline forms and will not only vary for the different polymorphic phases but also when not in the crystalline form at all. Anyway, the obtained values correspond well to X-ray reflectivity results which is one of the most accurate techniques for layer thickness determination.

$$\Delta f = -\frac{2\Delta m f_0^2}{A\sqrt{\rho_q \mu_q}} \qquad \rightarrow \qquad \Delta h = -\frac{\sqrt{\rho_q \mu_q}}{2f_0^2}\frac{\Delta f}{\rho} \tag{3.1}$$

Where:

Δf : is the frequency shift (Hz)

Δm : is the change in mass (g)

f_0 : is the resonant frequency (Hz)

A : is the active area (cm^2)

ρ_q : is the density of quartz ($\rho_q = 2.643\,\text{g/cm}^3$)

μ_q : is the shear modulus (AT-cut crystal $\mu_q = 2.947 \times 10^{11}\,\text{g}\cdot\text{cm}^{-1}\cdot\text{s}^{-2}$)

Δh : is the film thickness in (cm)

ρ : is the density of the deposited material (g/cm^2)

3.3. Characterization techniques

In this section the main techniques used in sample characterization are introduced and a brief explanation of the working principle is given.

3.3.1. Optical and atomic force microscopy

Optical microscopy was performed either on an Axiovert 40 CFL microscope or an Olympus BX51 microscope. Images were usually taken in a crossed polarizers setup. In this configuration the sample is illuminated with polarized light and a second polarizer is used as an analyzer in the optical path after the specimen. Their respective position is chosen in such way that all intensity is canceled out for the absence of any birefringent material (i.e. crystals) on the specimen. If a birefringent material is brought into the optical path, the incident polarized light will be split again into two perpendicular wave components. As long as the optical axis of the material does not coincide with the analyzer, this will result in an observable image.

Atomic force microscopy (AFM) was performed with a Nanosurf easyScan 2 Flex-AFM mounted on a Zeiss Observer Z1 microscope. Atomic force microscopy is a powerful, nondestructive technique used to map the surface morphology. A sharp tip (only a few atoms in size) mounted on a cantilever is piezoelectrically driven across the sample in proximity to the surface where intermolecular forces such as van der Waals or capillary forces interact with the tip. While there are different operation modes, only the tapping mode is relevant for this work. In this particular mode the cantilever is deliberately oscillated close to its resonant frequency. As the tip approaches the surface, the intermolecular forces will change both amplitude and phase of this vibration which can be used for feedback control. To hold the amplitude constant the tip is lowered or heighten so that it follows the morphology of the surface. The feedback signal (height signal) can therefore be used to measure the topography of the sample [58]. The cantilever used in this work is the Tap190-Al from BudgetSensors.

3.3.2. Specular X-ray diffraction

Specular X-ray diffraction is a powerful method usually used to characterize randomly oriented crystallites (often referred to as a three dimensional powder). In such a setup the crystallites are illuminated by a monochromatic X-ray source of wavelength λ under specular condition, meaning that incident $\vec{k}_i$ and scattered $\vec{k}_s$ wave vectors are coplanar and make likewise the same angle to the surface normal (depicted in Figure 3.7). Their respective length is $\frac{2\pi}{\lambda}$.
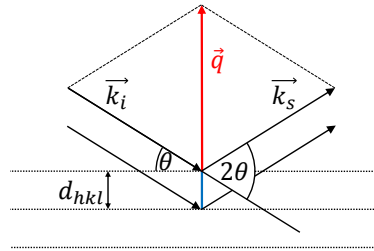

Figure 3.7.: Schematic representation of specular X-ray diffraction.

The scattering vector $\vec{q} = \vec{k}_s - \vec{k}_i$ is then normal to the surface. The path difference $\delta = d_{hkl} \sin \theta$ resulting from scattering with different net planes of the crystal (net plane distance d_{hkl}) yields only constructive interference for $2\delta = n\lambda$. This gives the so-called Bragg equation:

$$n\lambda = 2d \sin(\theta) \tag{3.2}$$

A specular scan probes therefore the net plane distance d as a function of the angle θ. As the scattering vector $\vec{q}$ is orthogonal to the surface, only net planes oriented parallel to the surface will be detected. In the case of a three dimensional powder, the crystallites are randomly oriented and likewise are the net planes. This will lead to a powder spectrum where all sufficiently strong net planes (having a high electron density) should be observable. As this measurement is dependent on the λ used in experiment, it is more convenient to plot the measured intensities over the scattering vector $|\vec{q}| = \frac{2\pi}{d}$. The brief introduction given here is based on [59], where a more detailed discussion of this technique can be found.

Specular X-ray diffraction experiments were mostly carried out on a PANalytical

Empyrean diffractometer with a PIXcel³ᴰ detector. For this a setup a 20 mm mask, a 7.5 mm anti-scatter slit and a $1/8°$ divergence slit were used. The detector was set to the 1D scanning line mode with a counting time of 29 seconds per data point.

3.3.3. Grazing incidence diffraction

Grazing incidence diffraction (GIXD) is a surface sensitive method to determine the in-plane structure of thin films. The incident wave vector hits the surface close to the critical angle of the substrate so that total reflection occurs. This leads to the formation of an evanescent wave which exhibits a penetration depth of below 10 nm. Also due to refraction effects, an intensity enhancement up to a factor of four can be observed, thus allowing for the detection of even smallest quantities. For a more detailed description see the thesis of Moser [60] or Werzer [61] or textbooks like "High Resolution Scattering" [62].
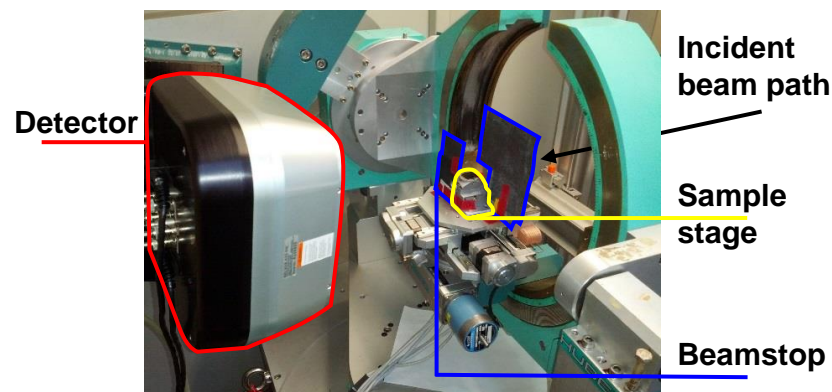
Figure 3.8.: Experimental setup of the KMC-2 beamline at the synchrotron facility BESSY II in Berlin.

Grazing incidence diffraction was performed at the KMC-2 beamline at the synchrotron facility BESSY II in Berlin. In Figure 3.8 the experimental setup is shown. The sample is mounted on 6-axis HUBER goniometer and a beamstop is fasten to the stage in such a way that it blocks any non-diffracted primary beam, thus minimizing the background signal. The diffracted intensity is recorded by the Bruker Vantec 2000, a 2-dimensional cross-wire detector with an active area of 14 cm x 14 cm [63].

The wavelength of the X-ray beam was chosen to $1\,\text{Å}$ in agreement with the beamline scientist's information for optimal experimental conditions. The incident angle was always chosen close to the critical angle of the substrate (for silicon the critical angle at this wavelength is $0.144°$) in order to achieve the best surface diffraction signal.

GIXD was measured to determine the in-plane structure of the prepared films. The angular measurements are recalculated to reciprocal vectors using the Python script package *xrayutilities* by Kriegner *et al.* [64]. The result is a distribution of the measured intensities in dependence of the in-plane ($q_p = \sqrt{q_x^2 + q_y^2}$) and out-of-plane component (q_z) of the momentum transfer $\vec{q}$. This is best represented by the so-called "reciprocal space map" (RSM), a two dimensional pseudo-color plot. The obtained RSMs show an aberration for higher values of the scattering vector q, especially along the in-plane axis q_p. The tools provided within the *xrayutilities* expect a flat detector while it is in fact a curved one. However, this error becomes only significant above a value of $q = 2\,\text{Å}^{-1}$ whereas the important information is usually contained in a much lower region for the samples investigated. The aberration is illustrated in Figure 3.9 on a corundum powder. At higher q values a misfit in shape and position between the literature Deybe-Scherrer rings and the experimental data is observed.
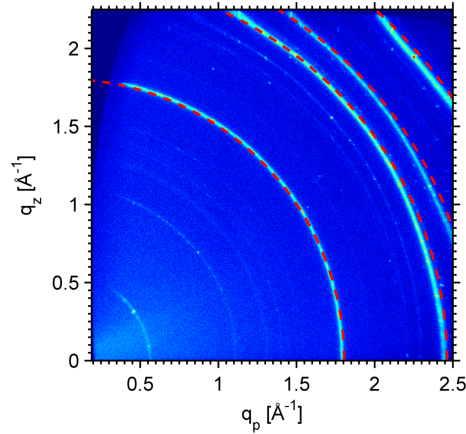

Figure 3.9.: Reciprocal space map illustrating the aberration for higher q values. Expected Deybe-Scherrer rings of corundum powder are indicated by the red dashed lines.

3.3.4. Pole figure measurements

In specular scans net planes parallel to the substrate surface are probed as a function of the interplanar distance d. On the contrary, pole figure measurements monitor a specific d-spacing as a function of the Euler angles ϕ and Ψ which describe the tilting of the respective net planes in respect to the surface normal. The angle ϕ describes the rotation within the surface while Ψ describes the inclination to the surface normal [59].

The pole figures depicted in this work were recorded on a Philips X'Pert diffractometer with an ATC 3 texture cradle. The obtained data is depicted in stereographic projection and analyzed by using the software *STEREOPOLE* [65].

Part II.

Results and Discussion

4. Carbamazepine

Within this chapter the crystallization behavior of the substance carbamazepine is studied as a function of the used solvent, preparation technique and substrate selection. These factors are expected to influence not only the resulting morphologies but also act selectively on certain polymorphic phases, thus promoting the formation of particular crystal structures. Controlling these parameters is of particular interest to the pharmaceutical sciences as it influences properties such as bioavailability and stability.

4.1. Characterization of the carbamazepine powder

The as delivered carbamazepine powder is investigated by X-ray powder diffraction to characterize the polymorphic phase of the original material and to check for any contamination. Also the solubility of carbamazepine in tetrahydrofuran and ethanol is determined.

4.1.1. X-ray powder diffraction pattern

The as-purchased carbamazepine powder is analyzed by X-ray powder diffraction on a Siemens 500D diffractometer. The pattern in Figure 4.1 shows various peaks in the range of $q = 0.3$ - $2.5\,\text{Å}^{-1}$. This is typical for a powder where all sufficiently strong Bragg reflections can be observed. A comparison of this spectrum with the structures known in literature identifies the main component as the *P*-monoclinic carbamazepine polymorph ($a = 7.55\,\text{Å}$, $b = 11.186\,\text{Å}$, $c = 13.954\,\text{Å}$, $\alpha = \gamma = 90°$,

$\beta = 92.938°$) as reported by Eccles *et al.* [47]. This polymorph is the commercial form i.e. it is typically used in a pharmaceutical relevant application [66]. Not all the observed peaks can be attributed to this phase, however, most prominently the one located at $q = 0.63\,\mathring{A}^{-1}$. This peak can solely be explained by an hydrous carbamazepine form. Either this peak corresponds to the 100 Bragg reflection of the *P*-monoclinic dihydrate ($a = 10.066\,\mathring{A}$, $b = 28.719\,\mathring{A}$, $c = 4.831\,\mathring{A}$, $\alpha = \gamma = 90°$, $\beta = 103.45°$) reported by Harris *et al.* [51] or by the 200 Bragg reflection of the orthorhombic dihydrate ($a = 19.779\,\mathring{A}$, $b = 4.9369\,\mathring{A}$, $c = 28.714\,\mathring{A}$, $\alpha = \beta = \gamma = 90°$) as reported by Kogan *et al.* [43]. Carbamazepine in hydrous form is usually an unwanted contamination as its dissolution properties and its bioavailability is unfavorable compared to the anhydrous form [67]. The presence of more than one distinct polymorphic phase in the original powder is not considered a limitation to this work, as all the used thin film preparation techniques result in recrystallization of the original material.
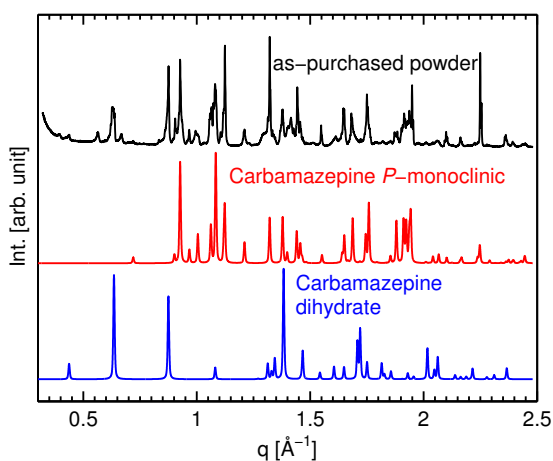

Figure 4.1.: Experimental X-ray powder diffraction patterns of the as-purchased carbamazepine powder and two reference phases from literature.

4.1.2. Solubility of carbamazepine in tetrahydrofuran and ethanol

The saturation concentration of carbamazepine both in tetrahydrofuran and in ethanol was determined. Solvent is dropwise added to a given amount of carbamazepine under ambient conditions, until complete dissolution is reached. The mole fraction solubility is then calculated by Equation 4.1:

$$x = \frac{\frac{m_1}{M_1}}{\frac{m_1}{M_1} + \frac{m_2}{M_2}} \tag{4.1}$$

Where:

m_x : is the mass of component x

M_x : is the molar mass of component x

In Table 4.1 the experimental data and the calculated mole fraction solubility is given as well as carbamazepine solubility data previously reported by Liu *et al.* [68]. The molar masses of carbamazepine, tetrahydrofuran and ethanol are $236.27\,\mathrm{g\,mol^{-1}}$, $72.11\,\mathrm{g\,mol^{-1}}$ and $46.07\,\mathrm{g\,mol^{-1}}$, respectively. The solubility found for tetrahydrofuran ($x = 157.1 \times 10^{-4}$) is slightly above the literature value with a deviation of $3\,\%$. The ethanol solubility ($x = 45.3 \times 10^{-4}$) is of same magnitude as the one reported in literature but differs by approximately $15\,\%$. As the solubility is also a function of temperature and no exact control of the ambient environment is established, this is most likely due to a lower experimental temperature. Another source of error is the way complete dissolution was determined. Solvent was added until no undissolved particles remained observable by the unaided eye.

Knowing the solubility is of especial importance when performing crystallization experiments from solution, as both solubility and solvent evaporation rate have a tremendous impact on the crystallization behavior. These factors determine the effective time until crystallization due to supersaturation emerges, hence the speed of crystallization can be influenced by the choice of solvent.

Table 4.1.: Mole fraction solubility of carbamazepine in tetrahydrofuran and ethanol.

m_{carba}/mg....Mass of carbamazepine
$m_{solvent}$/mg...Mass of solvent
$10^4 x$ ....Mole fraction solubility reported in this work
$10^4 x_{Liu}$ ....Mole fraction solubility at 22.5 °C as reported by Liu *et al.* [68]

	m_{carba}/mg	$m_{solvent}$/mg	$10^4 x$	$10^4 x_{Liu}$
Tetrahydrofuran	100.04	1913.14	157.1	152.6
Ethanol	100.46	4298.56	45.3	53.9

4.2. Drop casting

In this section morphologies and crystallographic properties of carbamazepine drop casted onto different surfaces (e.g. SiO_x, mica, gold) are reported. The influence of solvent selection (e.g. tetrahydrofuran, ethanol) and solute concentration on the crystallization behavior is elucidated.

4.2.1. Carbamazepine-tetrahydrofuran solution on glass surfaces

A solution series of 5.0, 1.2, 0.62 and 0.14 wt% carbamazepine dissolved in tetrahydrofuran is drop casted on conventional glass substrates. Different morphologies are obtained as a function of solute concentration. Optical polarization microscopy images of the predominant structures are depicted in Figure 4.2 together with atomic force microscopy images. The highest concentration yields large needles randomly dispersed over the substrate surface (Figure 4.2a). As this concentration is close to the maximum solubility (i.e. close to supersaturation) and as the needles are located on top of each other, it can be concluded that the crystallization process takes place in solution rather than on the substrate surface. The needles depicted in the AFM image of Figure 4.2b exhibit thicknesses in the range of 200 to 1500 nm. In general, the structures obtained from this concentration are too large to be characterized by atomic force microscopy, thus these needles are just an example. With a decrease in

carbamazepine concentration also the amount of needles decreases and spherulitic structures growing on the substrate surface emerge (Figure 4.2c). When observed under an optical microscope with crossed polarizers, spherulites are often recognizable by a dark area in the shape of a cross emerging from the center of the crystallite structure. This is called "Maltese Cross" for the similarity in shape. These dark areas are the result of crystallites oriented within the spherulite in such a way, that they do not alter the polarization of the incident light. Therefore the transmitted light is then blocked by the analyzer. As within a spherulite arrays of microcrystals are radially aligned in 360° around the nuclei, this will always lead to four perpendicular directions coinciding with the polarizers [69]. In the atomic force image in Figure 4.2d radial growth from a nuclei towards the boundary is observed where it intersects with a neighboring spherulite.

Decreasing the carbamazepine concentration further leads to initially isolated crystallization dispersed on an otherwise amorphous layer (Figure 4.2e). Upon storage this layer will fully crystallize leading to a relatively homogeneous surface when compared to the other structures (root mean squared surface roughness below 90 nm determined from the AFM scan in Figure 4.2f). At the lowest concentration dewetting of the amorphous layer is observed which leads to crystallization in individual droplets (Figure 4.2g). The corresponding AFM image in Figure 4.2h shows a rupture which allows a thickness determination of the amorphous film to $\sim 540\,\text{nm}$.

Specular X-ray diffraction with the Philips X'Pert diffractometer yields an observable diffraction pattern only for samples prepared from 5.0 and 1.2 wt% carbamazepine as depicted in Figure 4.3. The observed Bragg reflections are compared to the structures known in literature. By this the trigonal polymorph of carbamazepine ($a = b = 35.454\,\text{Å}$, $c = 5.253\,\text{Å}$, $\alpha = \beta = 90°$, $\gamma = 120°$) is identified as reported by Lowes *et al.* [46]. As Bragg reflections from different sets of net planes are observed, it can be concluded that the carbamazepine crystals are randomly oriented in respect to the substrate surface. This is consistent with the conclusions drawn from optical microscopy and also grazing incidence diffraction confirms the powder-like orientation of the crystallites (Appendix A.1). The sample prepared from 1.2 wt% shows additional reflections which are related to the presence of another polymorphic phase, namely the triclinic one ($a = 5.1705\,\text{Å}$, $b = 20.574\,\text{Å}$, $c = 22.245\,\text{Å}$,

4. Carbamazepine

$\alpha = 84.124°$, $\beta = 88.008°$, $\gamma = 85.187°$) as reported by Grzesiak *et al.* [45]. Optical microscopy (Figure 4.2c) revealed the presence of two distinct morphologies for this concentration, needles and spherulites. As the former is also observed at higher concentrations while the latter not, this is an indication that these spherulites might be in fact the triclinic carbamazepine polymorph.
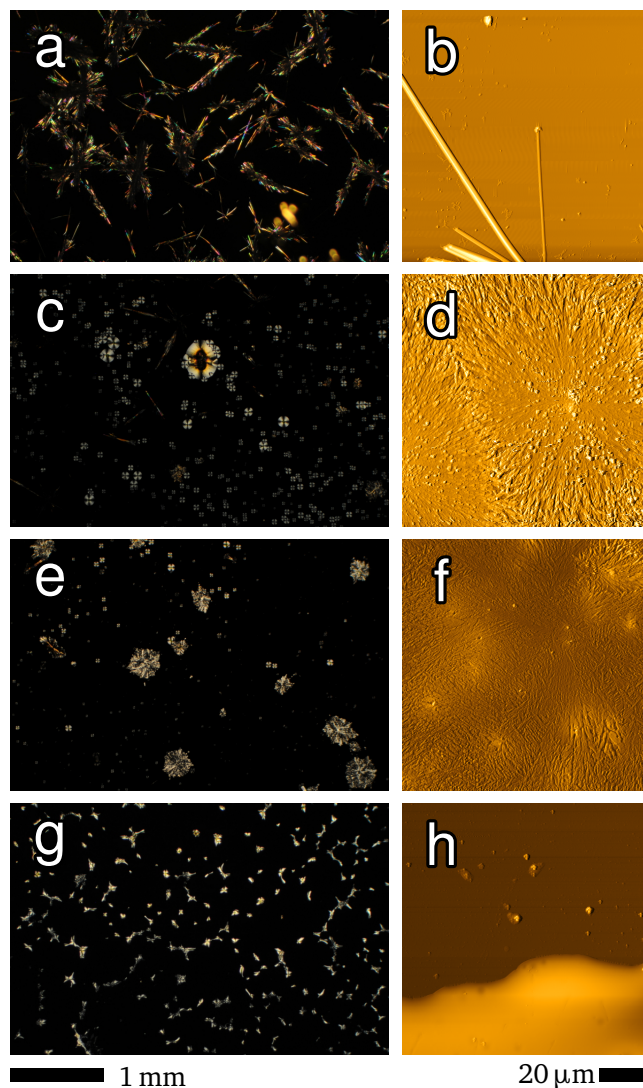

Figure 4.2.: Optical (left) and atomic force (right) microscopy images of carbamazepine drop casted from 5.0 wt% (a,b), 1.2 wt% (c,d), 0.62 wt% (e,f) and 0.14 wt% (g,h) THF solutions on glass substrates.
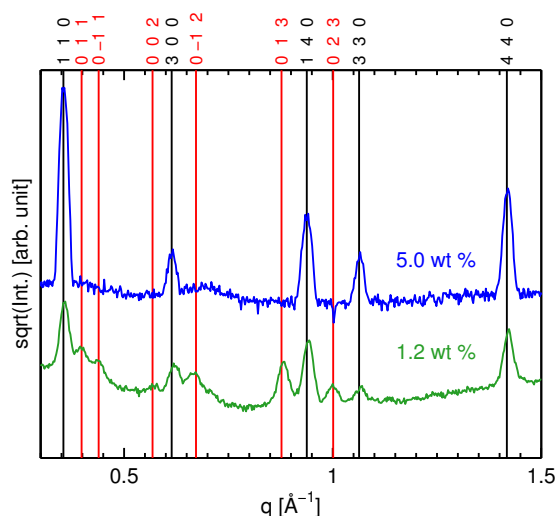
Figure 4.3.: Specular X-ray diffraction pattern of 5.0 wt% and 1.2 wt% carbamazepine solution drop casted on glass surfaces. Vertical lines indicate the Bragg peak positions of the trigonal (black) and the triclinic (red) carbamazepine polymorph.

4.2.2. Carbamazepine-tetrahydrofuran solution on SiO_x surfaces

Another series of carbamazepine films was prepared on NaOH etched silicon oxide surfaces by drop casting from 4.5, 2.3, 1.1, 0.57, 0.28 and 0.14 wt% tetrahydrofuran solution, respectively. Optical microscopy images under crossed polarizers are depicted in Figure 4.4. The observed morphologies are similar in shape to those demonstrated in Section 4.2.1 on glass surfaces. For a high carbamazepine concentration randomly dispersed needles are observed which diminish as the concentration decreases. Instead, spherulitic structures emerge which cover the surface homogeneously (Figure 4.4d,e). At a concentration of 0.14 wt% small needles crystallize independently from each other, dispersed all over the surface area (Figure 4.4f). Also a larger structure with a radial symmetry is observed, which is a growing spherulite.

While optical microscopy does not hint any significant difference to the films prepared on glass surfaces, specular X-ray diffraction draws a different conclusion. The
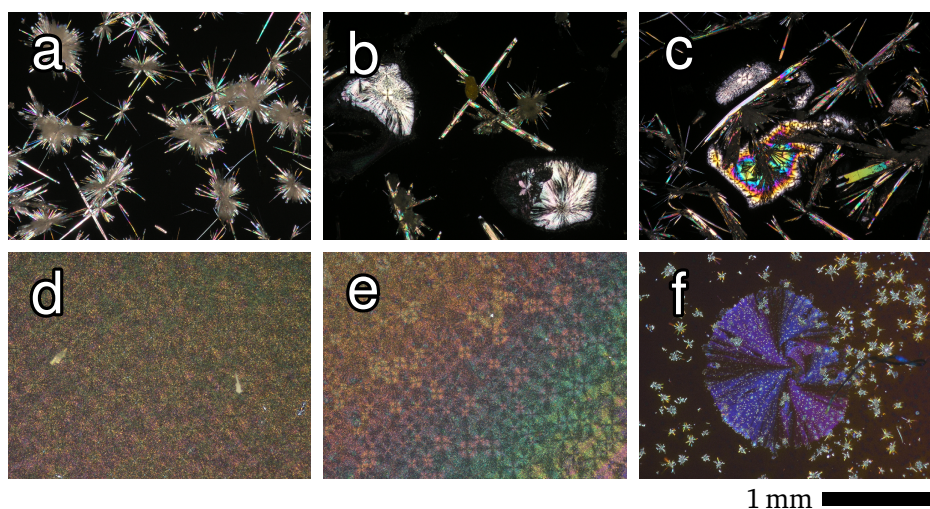
Figure 4.4.: Morphological changes of carbamazepine drop casted from 4.5 wt% (a), 2.3 wt% (b), 1.1 wt% (c), 0.57 wt% (d), 0.28 wt% (e) and 0.14 wt% (f) THF solutions on silicon oxide substrates. (a) needles; (b,c) needles and spherulites; (d-f) spherulites.

diffraction patterns of samples as-prepared are depicted in Figure 4.5a. Preparation from 4.5 to 1.1 wt% solution yields a high intensity reflection at $q = 0.354 \text{Å}^{-1}$, characteristic for the trigonal polymorph. This is expected as the morphology depicted in Figure 4.4a-c consists mainly of thin needles, another indicator for this very polymorph. While the experimental peak positions are well matched by the literature structure for the highest concentration, they do not fit particularly well for the lower ones. Also new Bragg reflections emerge as the concentration decreases, located next to the ones attributed to the trigonal polymorph but at lower q values. A shift to lower q values corresponds to an increase in the interplanar distances, thus increasing the overall volume. These peaks come in pairs located at $q = 0.878$ and 0.913Å^{-1} as well as at $q = 1.33$ and 1.37Å^{-1}. While some of these peaks can be explained by other structures known in literature, the one located at $q = 0.91 \text{Å}^{-1}$ can not.

A diffraction pattern recorded four months later (Figure 4.5b) shows that from these pairs of unexplained peaks, only the ones respectively located at the lower q value have remained, while their intensity increased. By indexation with the known literature structures the orthorhombic carbamazepine dihydrate is identified. The un-

explained peaks in the diffraction pattern of the as-prepared samples are in fact trigonal crystallites undergoing a phase transition to the hydrous phase by the incorporation of water molecules, thus increasing their volume. This in return causes the shift of certain Bragg reflections to lower q values. The trigonal form of carbamazepine is known for its relatively large voids, forming channels throughout the crystal along its c axis [46]. Cabeza *et al.* were able to show that within these voids solvent incorporation can take place [50].

From these results it is also assumed that the NaOH treatment of the silicon oxide substrate is the reason for the the enhanced hydrate formation as previous results on glass did not show such behavior (Section 4.2.1). The etching process makes the surface more hydrophilic which promotes water condensation at the surface in return.
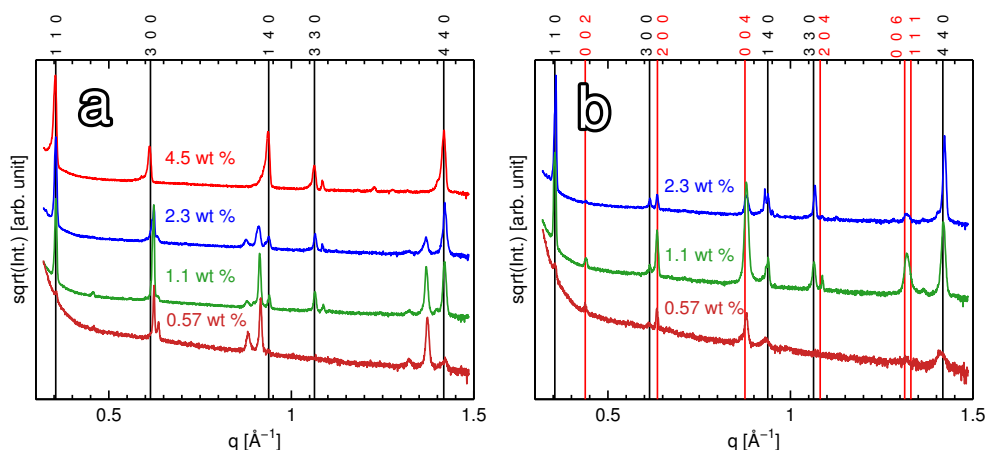

Figure 4.5.: Specular X-ray diffraction pattern for a fraction series of carbamazepine/THF as-prepared (a) and after four months (b). Vertical lines indicate Bragg reflections of the trigonal carbamazepine polymorph (black) and the orthorhombic dihydrate (red).

4.2.3. Carbamazepine-ethanol solution on glass

A solution series of 2.3, 1.2, 0.58, 0.29 and 0.15 wt% carbamazepine dissolved in ethanol is drop casted on glass substrates. Again the obtained morphologies are

characterized by optical microscopy under crossed polarizers (see Figure 4.6). Large needles are observed independent of the carbamazepine concentration which is different to the behavior previously displayed by the tetrahydrofuran solutions. Although needles are present within all the films, different types can be distinguished by their size and shape. The highest concentration yields straight, thin needles (Figure 4.6a) similar to those obtained from 5 wt% tetrahydrofuran. Both consist of the trigonal polymorph as shown later on by X-ray diffraction. With a decrease in concentration the needles start to bend and form larger networks which resemble a feather for its branched structure (Figure 4.6b-e). In between shorter, bulky needles (or rods) are located, corresponding to the very bright areas observed in the optical microscopy image (this is most prominently depicted in Figure 4.6c). At the lowest concentration also small droplets, dispersed on the substrate surface, can be observed which indicates dewetting (Figure 4.6e). Nevertheless, this film also exhibits the feather-like structures of bend needles as depicted in the center.
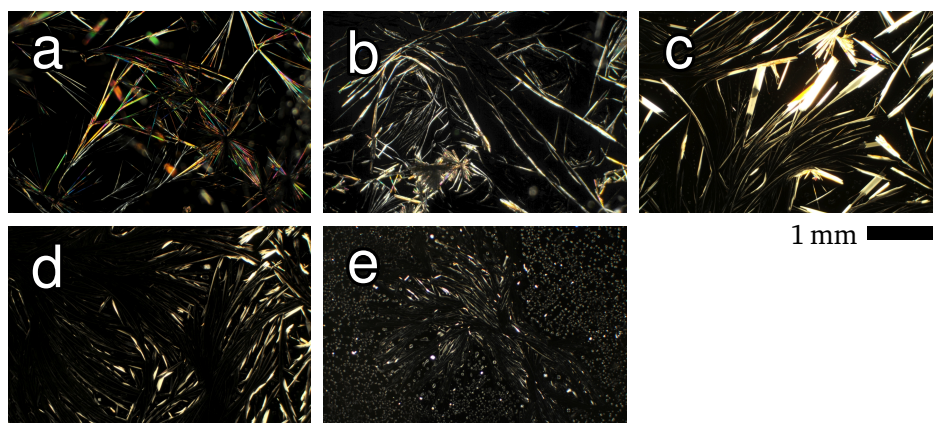

Figure 4.6.: Morphology changes of carbamazepine drop casted from 2.3 wt% (a), 1.2 wt% (b), 0.58 wt% (c), 0.29 wt% (d) and 0.15 wt% (e) ethanol solution onto glass substrates.

The samples were subsequently characterized by specular X-ray diffraction using a PANalytical Empyrean diffractometer with the obtained patterns depicted in Figure 4.7. For the sample prepared from 2.3 wt% solution the trigonal carbamazepine polymorph is identified through the presence of the strong reflection at $q = 0.35\,\text{Å}^{-1}$, corresponding to the (110) net plane. However, several peaks remain unexplained by this phase and also a mismatch between the literature and the measured posi-
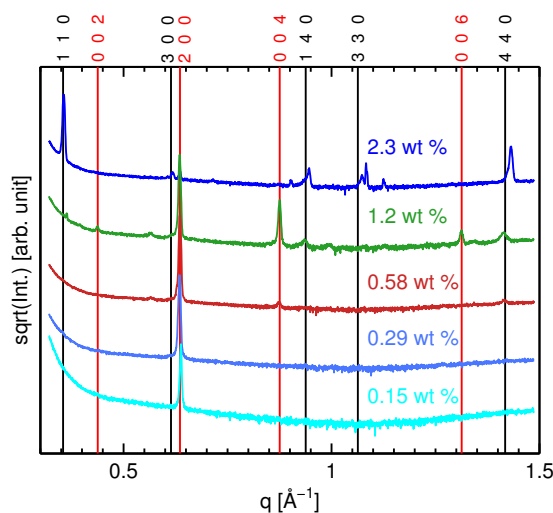
Figure 4.7.: Specular X-ray diffraction pattern for a carbamazepine/ethanol concentration series drop casted on glass. Selected Bragg reflections of the trigonal carbamazepine (black) and the orthorhombic carbamazepine dihydrate (red) are indicated by vertical lines.

tions of the Bragg reflections is observed. For lower concentrations the trigonal 110 peak decreases rapidly and vanishes completely for samples with a carbamazepine content equal or below 0.58 wt%. Instead, a reflection of high intensity emerges at $q = 0.64\text{\AA}^{-1}$. This peak represents an orthorhombic carbamazepine dihydrate ($a = 19.779\,\text{\AA}$, $b = 4.9369\,\text{\AA}$, $c = 28.714\,\text{\AA}$, $\alpha = \beta = \gamma = 90°$) for all these lower concentrations. The orthorhombic dihydrate reported by Kogan *et al.* is a less stable form of the carbamazepine hydrates, in which the carboxamide moiety is disordered [43]. As ethanol always contains water to some extent ($\sim 4\%$) under ambient conditions, the formation of a hydrate seems plausible. Still, not all the observed reflections can be explained by this pseudo-polymorph. Although low in intensity, small peaks are observed at $q = 0.57$, 0.94, 0.99, 1.31 and $1.41\,\text{\AA}^{-1}$, respectively. While only some of them can be explained by the trigonal polymorph, all of them can be matched by the triclinic one. The low peak intensities indicate that only a small amount of this polymorph is present. It is assumed that the hydrate form is partially transformed back to the anhydrous triclinic form which would also explain the low quantity of the latter. Indeed, it has been shown in literature that a transformation of the dihydrate under low humidity will result in the triclinic polymorph [70]. As the

specular X-ray diffraction pattern shows mostly one distinct peak for the dihydrate form, a preferred orientation in respect to the substrate surface is likely present.

These results also hint a possible explanation for the mismatch between the literature and the measured pattern of the sample prepared from 2.3 wt% solution. The unexplained peaks together with the shift in peak position might be a gradual transition to the hydrate form as observed previously for the THF samples on silicon oxide.
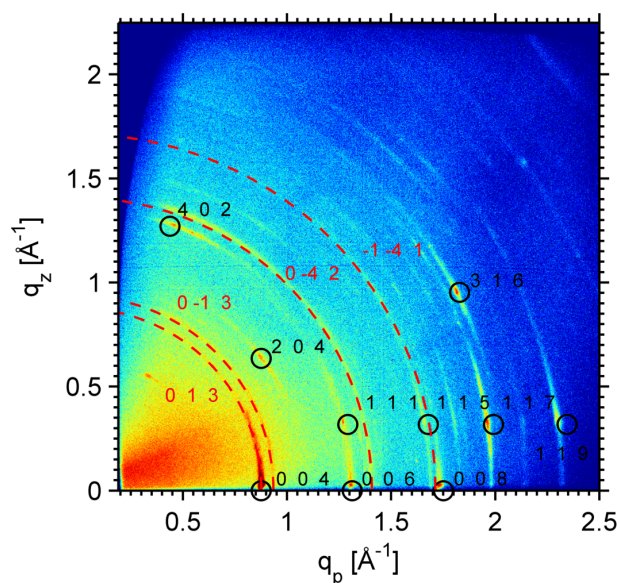

Figure 4.8.: Grazing incidence diffraction pattern of drop casted carbamazepine from 0.58 wt% ethanol solution. ○ Bragg reflection spots of the orthorhombic carbamazepine dihydrate in 100 texture. Dashed lines in red indicate Debye-Scherrer rings of the triclinic polymorph.

The sample prepared from 0.58 wt% ethanol solution is further investigated by grazing incidence diffraction with the reciprocal space map depicted in Figure 4.8. In this map spots of high intensity are observed together with intensity distributed along rings. The former pattern is matched by the orthorhombic carbamazepine dihydrate in a 100 texture. This means that the contact plane of the crystallites with the substrate surface is along the {100} planes. These spots are also smeared out to some degree indicating a not perfect alignment. They do, however, not explain the rings in the diffraction pattern. The constant intensity distributed along the so-

called Deybe-Scherrer rings indicates the absence of a preferred orientation. With the triclinic form already hinted by specular X-ray diffraction these rings are accordingly indexed. As the quantity of this polymorph is probably very low, only a few rings corresponding to reflections with a large structure factor are observed.

4.2.4. Carbamazepine drop casted from other solvents

Acetone, isopropyl alcohol, chloroform and dichloromethane were evaluated for carbamazepine recrystallisation. Morphologies obtained by drop casting carbamazepine from these solvents are depicted in Figure 4.9. Acetone and isopropyl alcohol both yield long, bulky needles with a lateral length of approximately one millimeter (Figure 4.9a,b), distinct in shape and size to the ones obtained previously from tetrahydrofuran (compare Figure 4.2). Samples prepared from chloroform and dichloromethane both display the formation of spherulitic structures. While the former exhibits


1 mm
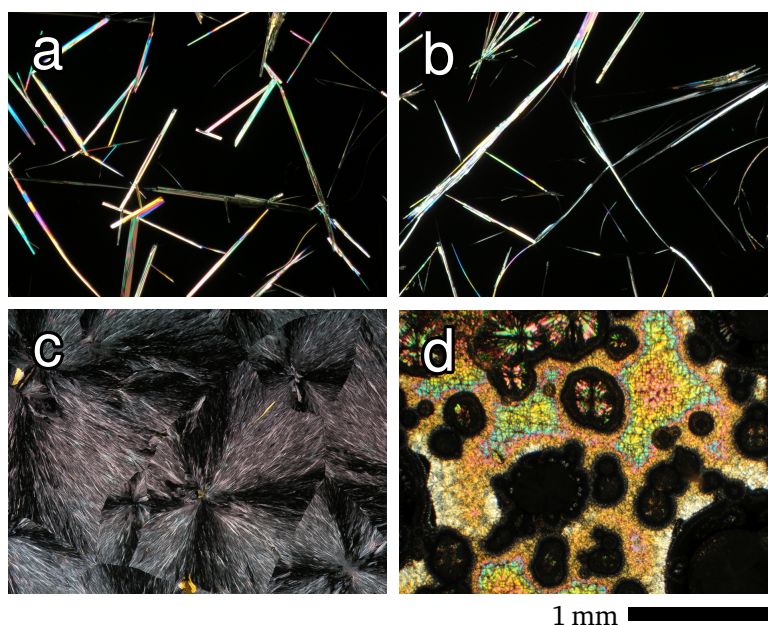
Figure 4.9.: Carbamazepine drop casted from different solvents: 0.67 wt% in acetone (a), 0.99 wt% in isopropyl alcohol (b), 1.2 wt% in chloroform (c) and 9.1 wt% in dichloromethane (d).

homogeneous spherulite sizes (Figure 4.9c), the latter shows a broader distribution (Figure 4.9d). In addition, a wetting structure is present for the dichloromethane sample indicating that a full film might form for a different preparation method.
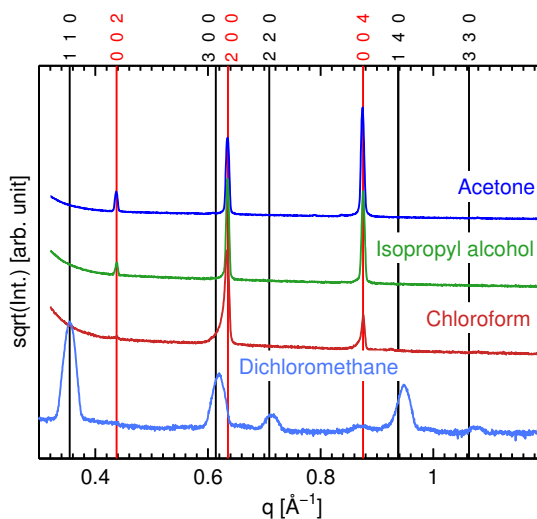

Figure 4.10.: Specular X-ray diffraction pattern of drop casted carbmazepine from different solvents: 0.67 wt% acetone, 0.99 wt% isopropyl alcohol, 1.2 wt% chloroform and 9.1 wt% dichloromethane. Vertical lines indicate the position of Bragg reflections of the trigonal (black) and the orthorhombic dihydrate (red) carbamazepine polymorph.

The specular X-ray diffraction pattern of the aforementioned samples is depicted in Figure 4.10. The broader shape of the reflections observed for dichloromethane is caused by the usage of the Philips X'Pert diffractometer instead of the PANalytical Empyrean. These measurements reveal an orthorhombic carbamazepine dihydrate ($a = 19.779\,\text{Å}$, $b = 4.9369\,\text{Å}$, $c = 28.714\,\text{Å}$, $\alpha = \beta = \gamma = 90°$) present for all the films except the one prepared from dichloromethane, which is in the trigonal form. While no final explanation can be given for the occurrence of the hydrate form, there are two possible explanations for this phenomena. First, the solvents themselves could be contaminated with water. As all the solvents are stored under ambient environment, this is not unlikely but does not explain why this behavior is only observable from particular solvents. Secondly, carbamazepine is presumably able to rapidly transit to the hydrate form simply by exposure to high humidity [6]. This is also the most likely explanation. Not only were the samples exhibiting the

dihydrate form prepared at a different date but also the used substrates were cleaned in NaOH which modifies the surface to become more hydrophilic. Interestingly, no co-crystallization with acetone is observed, even though this has been reported in literature [49].

4.2.5. Drop casting on kapton, mylar, gold and muscovite mica substrates

Carbamazepine crystallization was studied on different surfaces by specular X-ray diffraction. Film preparation on kapton and mylar surfaces was done by drop casting from tetrahydrofuran solution with 1 wt% carbamazepine content and on gold with 5 wt%. Similarly, 2.3 wt% ethanol solution was prepared on a gold surface. Specular X-ray diffraction of the samples results in multiple Bragg reflections in the range of $q = 0.3 - 1.5 \text{Å}^{-1}$, as depicted in Figure 4.11. They correspond to the Bragg reflections characteristic for the trigonal carbamazepine polymorph. The reflections originate from different crystallographic net planes, thus a powder-like distribution of the crystallites is present. Both kapton and mylar display an increase in background intensity distributed over a wide q range. This is the result of diffuse scattering with the amorphous substrates which is termed an "amorphous hump". The mylar substrate also exhibits Bragg reflections at $q = 0.90$, 0.92 and 1.09Å^{-1} which remain unexplained by the trigonal carbamazepine polymorph. Another unexplained, low intensity Bragg reflection right next to the carbamazepine 330 peak is observed at $q = 1.09 \text{Å}^{-1}$ for the gold substrates. These peaks can be matched to various polymorphic phases or might even be the result of a crystalline contamination within the substrates themselves. As these reflections are of low intensity and thus represent only a low quantity, they are not of further relevance.

While substrates such as gold, kapton and mylar do not alter the carbamazepine crystallization with the tested solutions, a different behavior is observed on mica. Mica is a sheet silicate mineral with a highly ordered surface structure which has been demonstrated, for instance, to induce fully defined epitaxial order within needle-shaped caffeine crystallites [71]. The mica surface was prepared by cleaving and carbamazepine is subsequently prepared on top by drop casting from 2.3 wt% ethanol
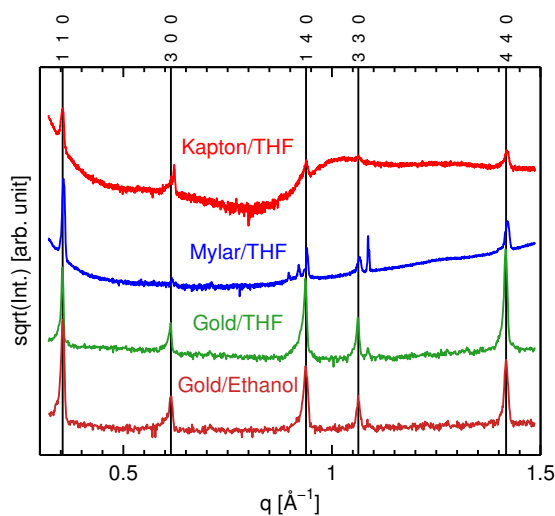
Figure 4.11.: Specular X-ray diffraction pattern for carbamazepine drop casted on different substrates: 1 wt% on kapton/mylar and 5 wt% on gold from THF; 2.3 wt% on gold from ethanol; Vertical lines indicate Bragg reflections of trigonal carbamazepine.

solution. In Figure 4.12 an atomic force microscopy image of the obtained structures together with the corresponding specular X-ray diffraction pattern is shown. Carbamazepine needles with a thickness of several 100 nm are growing on the surface, seemingly *climbing* a ledge of the mica substrate. If the needles would grow in solution instead and stick only afterwards to the surface, the needles would not be attached to the ledge itself as observed here. The specular X-ray diffraction pattern consists of a series of higher order reflections with high intensity. These Bragg reflections correspond to {001} net planes of mica. For the remaining reflections the indexation is not decisive as both the triclinic polymorph as well as the dihydrate form of carbamazepine match. Both forms are known for their needle morphology [43, 45] which makes them difficult to distinguish. In Figure 4.12b the triclinic polymorph is chosen over the hydrous form for the following reason: The hydrate is ultimately not able to explain a small though present peak at $q = 1.149 \, \text{Å}^{-1}$ as well as the smeared out left shoulder of the 008 mica Bragg reflection at $q = 2.515 \, \text{Å}^{-1}$. Still, this is not a final exclusion of the hydrous form but reasonable. In the Appendix A.2 therefore an alternative indexation with the hydrous form is given. However,

even without knowing the exact carbamazepine polymorph the presence of a partial fiber texture can be concluded from the Bragg reflection series at $q = 0.437$, 0.874, 1.31, 1.75 and $2.19\,\text{Å}^{-1}$. In case of the triclinic polymorph these reflections would correspond to $\{0\text{-}11\}$ net planes. This means that these planes form the contact layer as specular X-ray diffraction probes only net planes parallel to the substrate surface.

In conclusion, it seems that the influence of the substrate selection is negligible in the case of kapton, mylar and gold with the tested solvents. On the other hand, oriented growth of carbamazepine is very likely present on a mica surface as verified by specular X-ray diffraction.
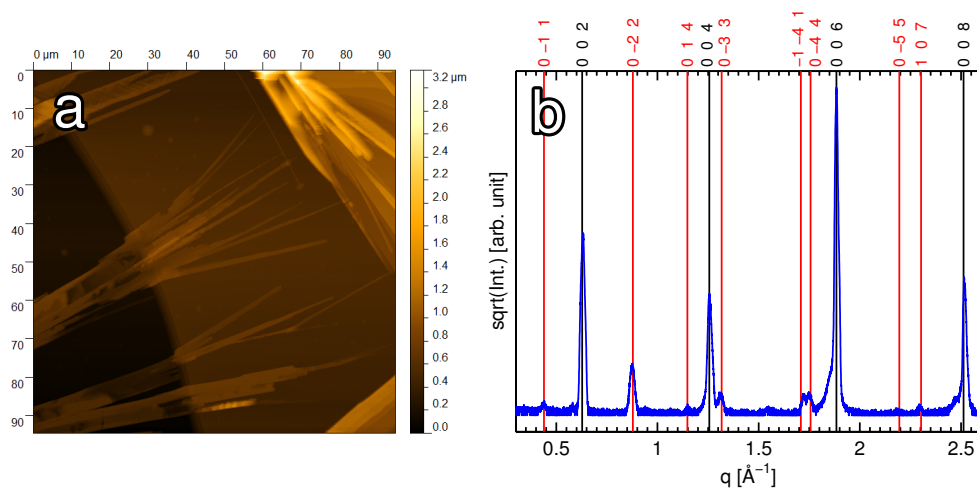

Figure 4.12.: (a) Atomic force height image of carbamazepine on a mica substrate drop casted from a 2.3 wt% ethanol solution. (b) Corresponding specular X-ray diffraction pattern with Bragg reflections of the triclinic carbamazepine (red) and the mica reference (black) indicated as vertical lines.

4.2.6. Thermally induced phase transition

Trigonal carbamazepine prepared by drop casting from 5.0 wt% THF solution is heated at a rate of 5 °C min^{-1} up to 180 °C. X-ray diffraction patterns are collected by the stationary PIXcel^{3D} detector. This setup monitors simultaneously the 140 and 330 Bragg reflection of the trigonal form. The peaks are nearly constant at temperatures up to about 140 °C. At 140 °C these reflections start to decrease in intensity while new peaks emerge at $q = 0.88, 0.94, 0.99$ and 1.04Å^{-1}, corresponding to 013, 031, 0-31 and 032 Bragg reflections of the triclinic phase, respectively. Upon a subsequent cool-down time this *new* phase remains stable. This is a known phase transition for the bulk material as reported by authors such as Grzesiak *et al.* [45]. As this transition is very similar in thin films, it is suggested that the substrate is of little influence on this thermal behavior.
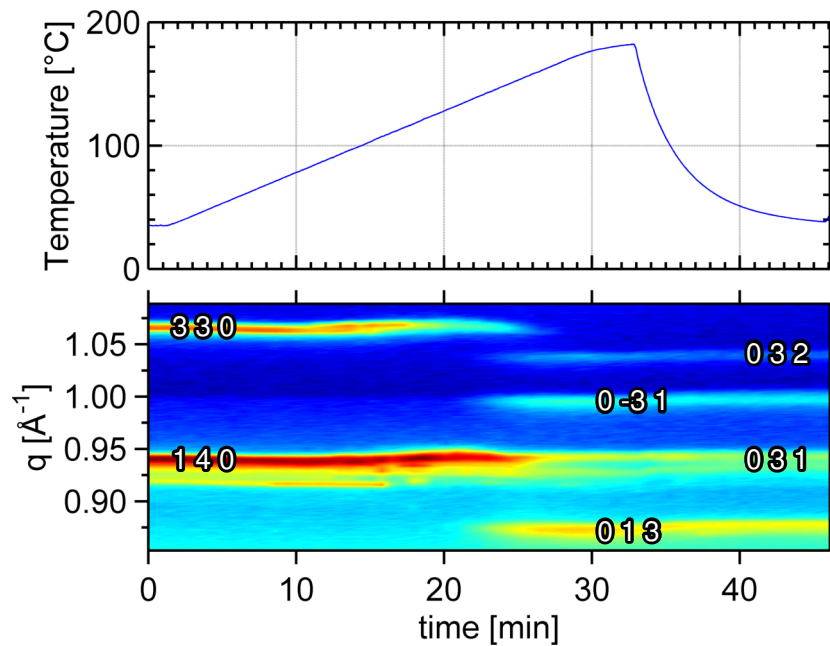

Figure 4.13.: Heating carbamazepine in the trigonal form while observing the 330 and 140 peaks with the stationary PIXcel^{3D} detector. At 145 °C a phase transition to the triclinic form is observed.

4.3. Dip coating

Dip coating was evaluated as a way to induce orientated crystal growth to thin films of carbamazepine which usually exhibits random orientation when prepared by drop casting. Carbamazepine was dip coated from 0.45 wt% tetrahydrofuran solution and from 0.50 wt% ethanol solution on plasma-etched SiO_x surfaces. The withdrawal speed was set to $3 \, \mu m \, s^{-1}$. Other speeds were tested but the best performance was achieved using this parameter set.

Optical microscopy images under crossed polarizers of the samples are depicted in Figure 4.14 together with atomic force microscopy images. Both solvents result in the formation of needles but while those grown from ethanol exhibit alignment along
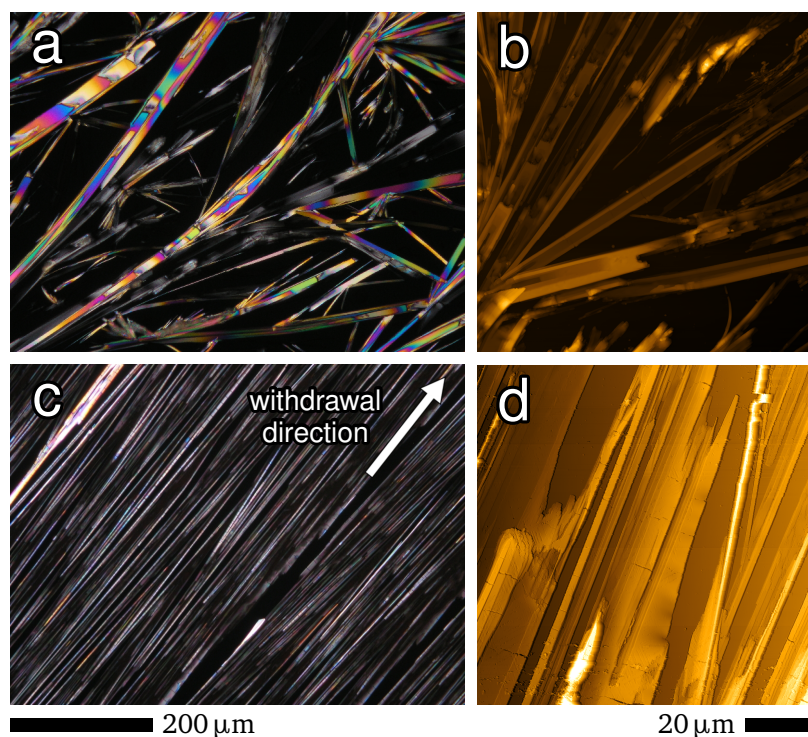

Figure 4.14.: Optical microscopy (left side) and atomic force microscopy (right side) images of dip coated carbamazepine at a withdrawal speed of $3 \, \mu m \, s^{-1}$ prepared form 0.45 wt% tetrahydrofuran solution (a,b) and from 0.50 wt% ethanol solution (c,d).

the withdrawal direction (Figure 4.14b), preparation from tetrahydrofuran does not (Figure 4.14a). The sample prepared from the latter shows large, bulky needles with smaller, thinner needles growing in between. These morphologies are reminiscent to the structures of the carbamazepine dihydrate and the trigonal form. As tetrahydrofuran is a fast evaporating solvent, the dip coating process is not governed by the withdrawal speed but the solvent evaporation rate. Therefore no preferred orientation is induced and the crystallites are growing randomly.

Interestingly, small cracks distributed periodically along the needles are observable for the sample prepared from ethanol. In the atomic force microscopy image (Figure 4.14d) these ruptures are clearly visible with an approximate periodicity of $11\,\mu$m. These cracks might be the result of how the needles are growing on the substrate surface at the liquid/vapor interface. Ethanol is also a volatile solvent so that immediate needle growth at the wetting layer is expected. As the sample is withdrawn further the needles growing along the contact angle in the interfacial region will start to attach to the substrate surface. As rigid bodies such as crystals can hardly bend, small cracks will therefore appear on the surface on account of stress release.

Specular X-ray diffraction (Figure 4.15) confirms the presence of both the orthorhombic hydrate as well as the trigonal carbamazepine polymorph in the sample dip coated from 0.45 wt% tetrahydrofuran solution. Both forms show Bragg reflections resulting from various, different net planes, hence no texture is present. The oriented growing needles prepared from 0.50 wt% ethanol are also identified as the dihydrate form. In the diffraction pattern this sample shows primarily the strong 200 Bragg reflection but also two higher order reflections of the 001 net planes are identified. This indicates that the needles are mainly oriented on the substrate surface along the 100 net plane but also that another orientation along the 001 plane exists, though of minor importance.
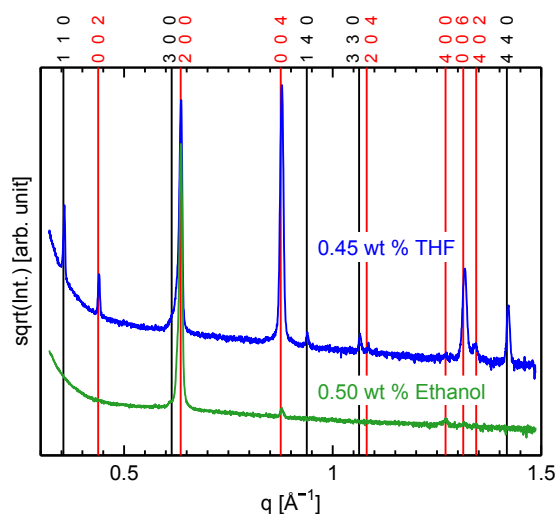
Figure 4.15.: Specular X-ray diffraction pattern of dip coated carbamazepine samples from tetrahydrofuran and from ethanol solution prepared at a withdrawal speed of $3\,\mu m\,s^{-1}$. The reflections are indexed with the trigonal carbamazepine polymorph (black) and the orthorhombic dihydrate (red).

4.4. Spin coating

Thin films of carbamazepine prepared by spin coating appear amorphous at first. Optical microscopy shows the presence of a layer but when observed under crossed polarizers, the film vanishes. This means that there is no birefringent material, e.g. a crystal, on the specimen. As spin coating enhances the solvent evaporation rate compared to drop casting, the given time for the single carbamazepine molecules to arrange properly in a specific crystal structure is most likely too short, thus leading to an amorphous film. Over the course of several days to weeks these films crystallize eventually. Morphologies typically obtained are depicted in Figure 4.16. For higher concentrations structures similar in shape and growth to spherulites are observed. With a decrease in carbamazepine content these structures get replaced by randomly oriented, small needles as depicted in Figure 4.16c. Both on silicon oxide and on glass surfaces a similar behavior is displayed but for the latter the decrease of larger structures as a function of concentration is happening slower (not shown).

silicon oxide   glass
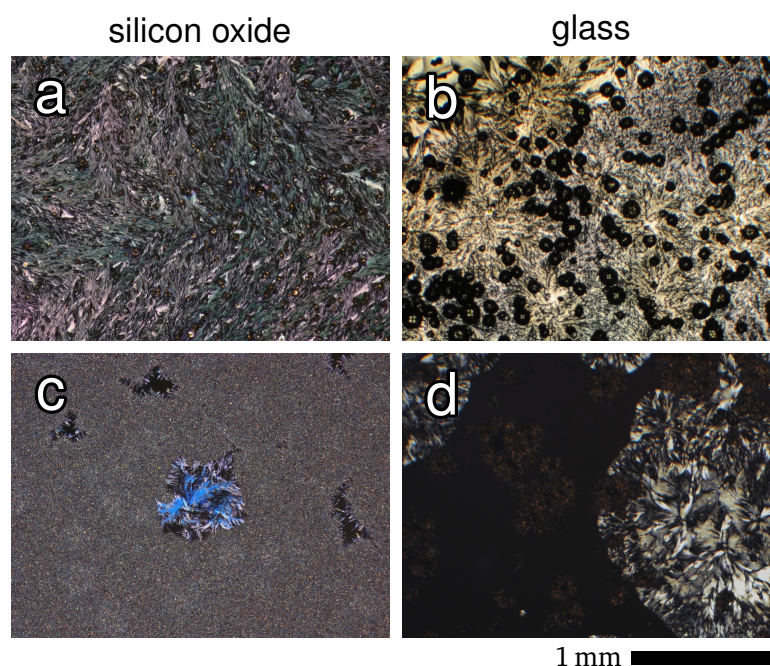
Figure 4.16.: Carbamazepine spin coated on silicon oxide (left column) and on glass (right column) from 4.5 wt% (a), 5.0 wt% (b), 1.1 wt% (c) and 1.2 wt% (d) tetrahydrofuran solution. Optical microscopy images are taken several weeks after film preparation.

Grazing incidence diffraction is used on the sample prepared from 4.5 wt% THF solution to identify the polymorphic phase as specular X-ray diffraction yields too little intensity, most likely due to the thickness of the layer being to thin. In Figure 4.17 the according reciprocal space map is shown where the diffracted intensity is located along rings. This is characteristic for a three dimensional powder where net planes have no distinct relation to the substrate surface. The scattering vector $\vec{q}$ can therefore interact with all the net planes independent of its own orientation (from being parallel $[\vec{q} = \vec{q}_p]$ up to being perpendicular $[\vec{q} = \vec{q}_z]$ to the substrate surface), hence the diffracted intensity is located on rings along a constant $|\vec{q}|$ value. However, along these rings also segments of higher intensities are found. This indicates that additionally some preferred orientation is present. Indexation with the phases known in literature allows the identification of the triclinic carbamazepine polymorph. The diffraction spots of higher intensity are matched to a partial 0-11 fiber texture, i.e. a larger part of the crystallites contacts the substrate surface along the 0-11 net plane.

In the reciprocal space map the positions of carbamazepine Bragg reflections in this particular alignment are marked by circles.
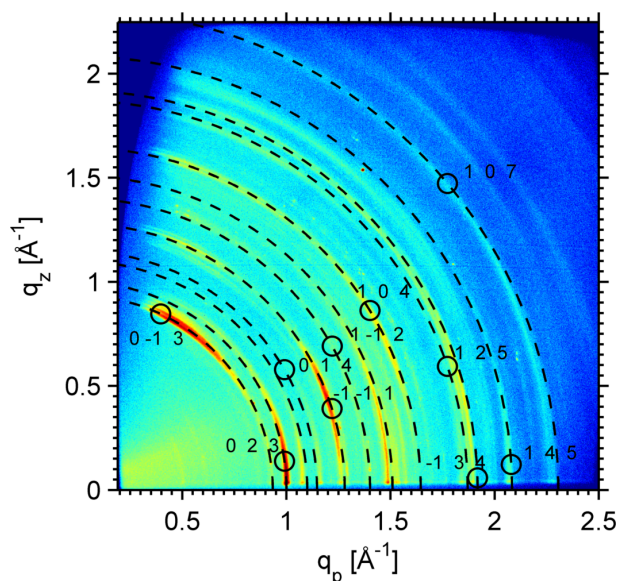

Figure 4.17.: Reciprocal space map of crystallized carbamazepine after spin coating from a 4.5 wt% THF solution onto a SiO$_x$ surface. The observed pattern is indexed by Deybe-Scherrer rings of the triclinic polymorph. ○ Position of the Bragg reflections for a 0-11 texture.

4.4.1. Solvent vapor and thermal annealing

Carbamazepine samples spin coated onto microscopy glass slides from 1 wt% THF solution were exposed to different solvent vapors as well as heat treated by storage at 40, 60 and 80 °C, respectively. The initially amorphous film crystallizes under these treatments resulting in different morphologies as depicted in Figure 4.18. Acetone, toluene and dichloromethane solvent vapor yields an homogeneous layer of what appears to be randomly oriented, thin needles (only acetone shown in Figure 4.18a). This layer is interrupted at random by some larger structures of different morphology. The formation of small, randomly oriented needles is also mostly observed for chloroform vapor (Figure 4.18b) and tetrahydrofuran (Figure 4.18c) annealing. Additionally, chloroform shows the formation of larger crystallites located in the middle of otherwise empty holes. Thermal annealing within a temperature range of 40 to

80 °C leads to the formation of larger needles which are again randomly distributed (Figure 4.18d). Specular X-ray diffraction does not result in any observable reflections. This is expected for randomly oriented crystallites of small size and quantity as the diffracted intensity is simply too low.


1 mm ▬
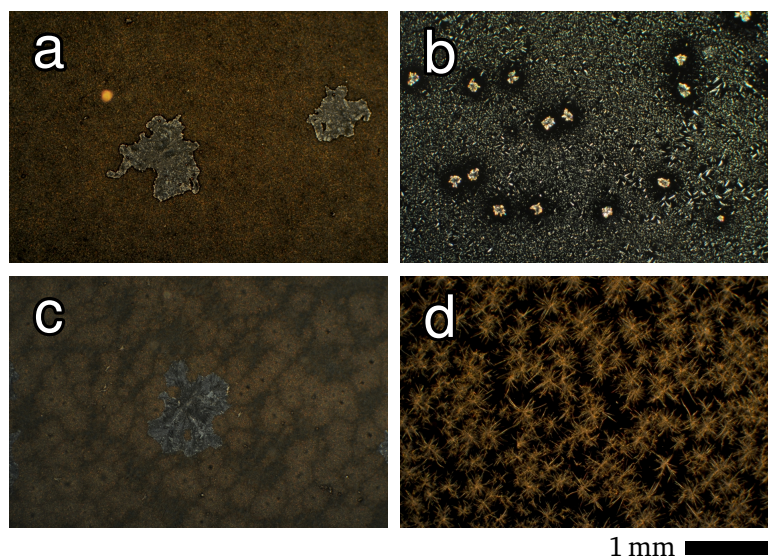
Figure 4.18.: Different morphologies achieved after 24 hours from solvent vapor annealing for acetone (a), chloroform (b), tetrahydrofuran (c) and by thermal annealing at 60 °C (d).

4.5. Physical vapor deposition

Carbamazepine recrystallization from solvent-based techniques faces various challenges. These processes yield a variety of different morphologies which exhibit often more than one polymorphic phase at a time, thus making characterization and practical application difficult or impossible. Moreover, hydrate formation is often observed which is undesired in application due to its poor solubility. To overcome these issues another preparation technique is applied. Within this chapter a solvent-free approach to carbamazepine recrystallization is presented by means of thermal evaporation under vacuum conditions.

4.5.1. Sample preparation

When carbamazepine is prepared by thermal evaporation onto solid surfaces with the experimental setup in use, not a crystalline but an amorphous layer is formed upon deposition. A similar behavior was previously observed from spin coating as reported in Section 4.4. The amorphous form is usually a favorable alternative to the crystalline state in terms of solubility and bioavailability [72]. However, as this is only a metastable state, these films usually lack long term stability and crystallization might occur on storage [6].

Anyway, as the initial films are amorphous they are typically homogeneous in thickness with a very low roughness, thus they can be characterized using X-ray reflectivity (XRR) measurement. By this method the film thickness as well as the interface roughness can be determined. To obtain these parameters the measured data is fitted with the commercial X'Pert Reflectivitiy software suite supplied with the PANalytical Empyrean equipment. This is also a reliable method to compare the actual film thickness to the one calculated by the Sauerbrey equation which was used for the determination of the mass load on deposition. In Figure 4.19 an exemplary XRR measurement is shown together with the fitted data for a sample prepared at a deposition rate of $3.5\,\text{Å}\,\text{s}^{-1}$. The pressure in the vacuum chamber was below 7×10^{-5} mbar during the preparation process. In the range of $q = 0.04 - 0.25\,\text{Å}^{-1}$ oscillations in intensity are observed, the so-called Kiessig fringes [73]. From the

periodicity of these fringes the film thickness can be determined while the slope represents the interface roughness and the damping of the amplitudes indicates the upper roughness at the sample/air interface. From the fit the thickness is determined to (54.0 ± 1.0) nm and an interface roughness of below 0.3 nm is obtained. From the Sauerbrey equation 3.1 a film thickness of approximately 52 nm was estimated which is in good agreement. The data presented shows that by thermal evaporation carbamazepine can be prepared with a controlled film thickness as well as a low roughness. Tests under different conditions yield films of similar quality meaning that this technique allows for adjusting the material quantity while conserving the film quality.
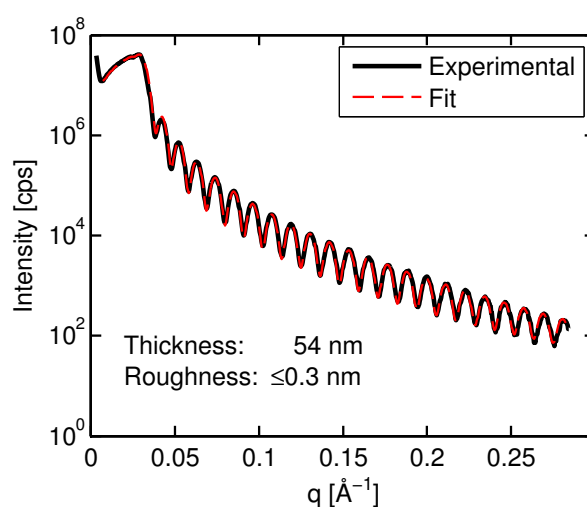
Figure 4.19.: X-ray reflectivity measurement of carbamazepine prepared by thermal evaporation on a silicon oxide surface.

4.5.2. Crystallization under ambient atmosphere

Though initially not of crystalline nature, the prepared amorphous carbamazepine films are not stable under ambient environment, thus subsequent crystallization is observed. This behavior is similar to the likewise amorphous films prepared by spin coating, reported in Section 4.4. In Figure 4.20 optical microscopy images taken two days after sample preparation are depicted, showing morphologies typically

obtained. The presented films had an initial thickness of approximately 200 nm and are prepared on silicon oxide (Figure 4.20a,c) and gold surfaces (Figure 4.20b).
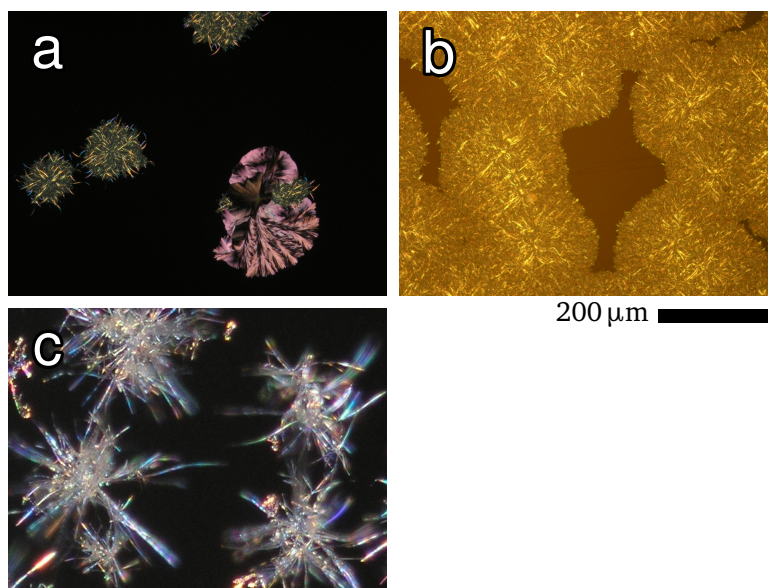
Figure 4.20.: Optical microscopy images of crystallizing carbamazepine taken two days after deposition: stored under ambient conditions (a,b) and at 60 °C (c). The samples are prepared on silicon oxide (a,c) and on gold (b).

Carbamazepine on silicon oxide stored under ambient conditions results mostly in aggregations of small, randomly oriented needles which resemble tumbleweed for their shape (Figure 4.20a). Occasionally, also radial grown structures with a more defined morphology are observed (e.g. in the right corner of the image). For the gold substrate a similar behavior is displayed (Figure 4.20b) with the main morphology consisting out of small, randomly oriented needles. However, the crystallization process seems to be enhanced compared to SiO_x as most of the film area is already covered with crystalline carbamazepine. Within this layer domains with a circular border are visible. While the circular shape indicates radial growth, this does not resemble spherulitic structures and needles grow in arbitrary directions. When the amorphous films are kept at elevated temperatures, the crystallization process gets further enhanced. In Figure 4.20c crystallized carbamazepine is shown after temperature treatment at 60 °C for 24 hours. Again randomly oriented needles are observed but larger in size than those obtained from storage at room temperature.

Further, the structures seem to have centers in common from which crystallization is initiated.

In conclusion, all the samples yield randomly oriented, small needles which are slowly forming under ambient environment. This can, however, be enhanced by storage at elevate temperature. The obtained morphology together with the previous results from spin coating indicates already that these needles are most likely the triclinic carbamazepine polymorph. Enhancements in the crystallization behavior may also be achieved by changes in the evaporation equipment via an introduction of a temperature controlled sample holder. Such a setup would allow higher temperatures to be applied during deposition which typically means enhanced molecular diffusion, thus fostering nucleation.
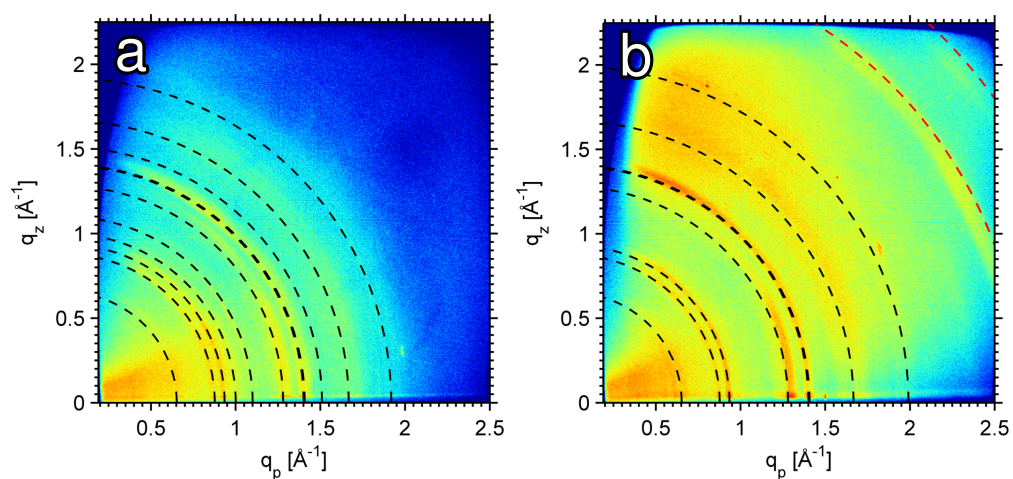
Figure 4.21.: Reciprocal space maps of carbamazepine prepared on silicon oxide (a) and gold (b) surface by thermal evaporation. Dashed lines indicate Deybe-Scherrer rings of triclinic carbamazepine (black) and gold (red).

The random orientation together with the low quantity of the crystallites, however, makes specular X-ray diffraction not feasible. Therefore grazing incidence diffraction is used to determine the polymorphic form. In Figure 4.21 reciprocal spaces maps of a sample prepared on silicon oxide (a) and of the aforementioned sample on gold (b) are depicted. The diffracted intensity is found located along rings which confirms the mainly random orientation of the crystallites (i.e. a three dimensional powder). As often observed some degree of texture is present. By indexation

with the structures known in literature the triclinic carbamazepine polymorph is confirmed for both samples with a very slight 0-11 texture.

4.5.3. Crystallization under argon inert atmosphere

Crystallization under ambient environment is never a controlled process as parameters such as temperature, humidity and atmospheric pressure are volatile. Even though the results previously obtained are consistent within their interpretation, the idea was to establish further control by storage under argon atmosphere.

A carbamazepine film of 100 nm thickness was deposited by thermal evaporation on a silicon oxide surface with a deposition rate of approximately $0.3\,\text{Å}\,\text{s}^{-1}$. The pressure in the vacuum chamber was 4×10^{-5} mbar. After the deposition, the sample was transferred to a storage kept under argon atmosphere. The transfer itself, though performed under ambient environment, is not expected to be of significant influence as the exposure time is short and carbamazepine crystallization in comparison slow. The sample was removed from the inert atmosphere after four days as most of the surface was covered with crystallized material by then.

An optical microscopy image of the sample is depicted in Figure 4.22a. The previously obtained "tumbleweed" structures are scarcely observed but instead radial grown structures cover the surface. From the detailed view shown in Figure 4.22b, a branched, dendritic structure is noted as the underlying growth pattern. While spherultic structures were previously observed for carbamazepine, this particular arrangement is new. In contrast to the previous results (mostly randomly distributed needles), this structure seems to grow more directed.

The specular X-ray diffraction pattern as depicted in 4.23 yields peaks at $q = 1.12$, 1.21, 1.44, 1.75 and $1.91\,\text{Å}^{-1}$. Though low in intensity and only slightly above the background signal, they can be matched by the structures known in literature. This reveals the *P*-monoclinic carbamazepine polymorph with the observed peaks corresponding to the (020), (021), (022), (031) and (032) net plane, respectively.

While more exhaustive research is still necessary, these first results indicate a possi-
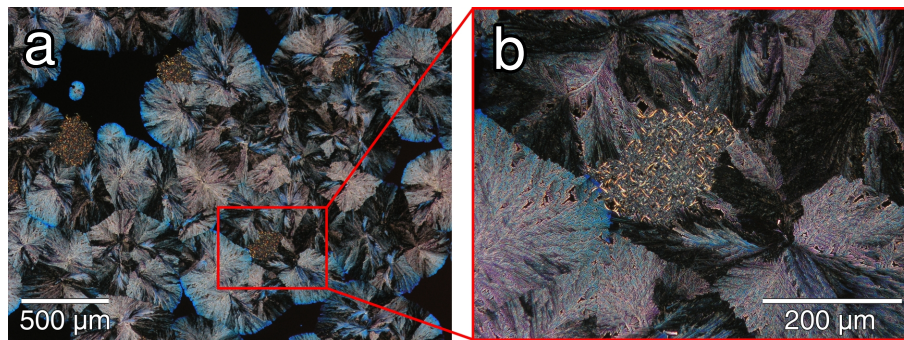
Figure 4.22.: Optical microscopy images under crossed polarizers (a) and detailed view (b) for carbamazepine crystallized under argon atmosphere.

ble way to recrystallize carbamazepine in the commercial form, i.e. the one used in medication. As this also avoids a problematic dihydrate formation and is independent of the polymorphic phases of the original material, this is of practical interest.
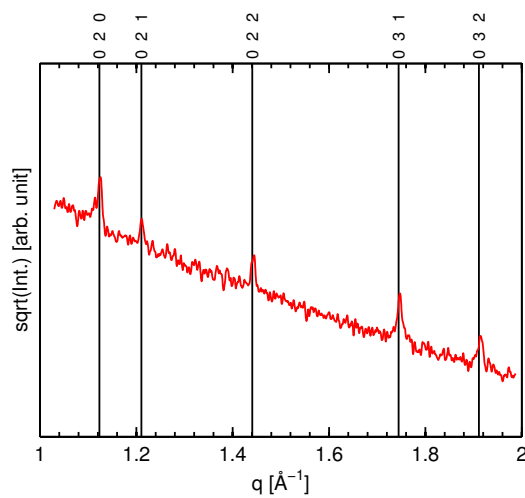
Figure 4.23.: Specular X-ray diffraction pattern for carbamazepine crystallized under argon atmosphere. The vertical lines in correspond to Bragg reflections of the *P*-monoclinic polymorph.

5. Iminostilbene

Within this chapter a characterization of the iminostilbene crystallization behavior in terms of crystal structure, orientation and achievable morphologies is provided for different solution-based preparation techniques. Given the similar molecular structure of carbamazepine and iminostilbene, the idea was to gain an understanding of how the carboxamide side chain influences the crystallization behavior. The experimental powder is pre-characterized by X-ray powder diffraction and the solubility in tetrahydrofuran and ethanol is evaluated. Iminostilbene from a THF solution series prepared by drop casting and spin coating is then investigated. With the crystallization behavior deduced from these experiments the focus is then laid on growing iminostilbene with a preferred in-plane orientation (texture), suitable as a template for carbamazepine crystallization.

5.1. Crystallization behavior in bulk and at solid surfaces

The as-purchased powder is investigated by X-ray powder diffraction to identify the crystalline phase and to check for a possible contamination. Solutions from 2-Propanol, tetrahydrofuran and xylenes were used in various concentrations for the formation of iminostilbene films, produced either by drop casting or spin coating. The resulting morphologies are compared by optical microscopy and specular X-ray diffraction.

5.1.1. X-ray analysis of iminostilbene powder

The X-ray powder diffraction pattern of the as-purchased iminostilbene powder was collected with a PANalytical Empyrean diffractometer using the 1d-mode of the detector with the obtained pattern depicted in Figure 5.1. The spectrum shows various peaks in the range $q = 0.4 - 2.8 \text{\AA}^{-1}$. A comparison of this pattern with a known phase presented in literature [53] reveals an excellent agreement of the peak positions. This shows that the as-purchased powder has an orthorhombic unit cell with $a = 8.226 \text{\AA}$, $b = 20.413 \text{\AA}$, $c = 6.035 \text{\AA}$, $\alpha = \beta = \gamma = 90°$.

While there is an excellent match of the peak positions, the peak intensity of the measured and the literature pattern varies significantly meaning that the measured powder sample is a result from a non-ideal powder. On the one hand, texture effects may be accounted for this as during preparation individual net planes are forced to a position parallel to the surface. On the other hand, preferred crystal growth along certain directions could have induced a preferred orientation to the original powder. Additionally, size and strain effects are able to alter the peak intensities.
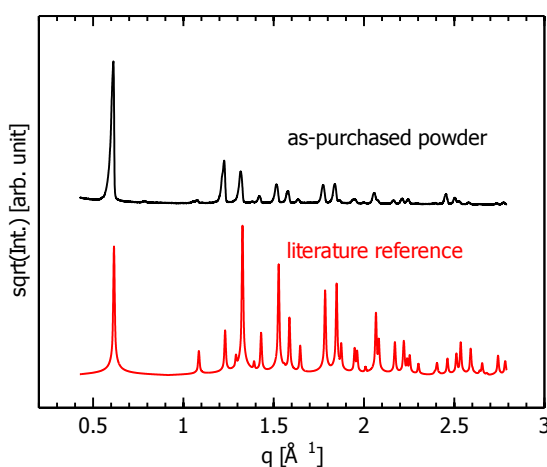

Figure 5.1.: Specular X-ray pattern of the experimental powder and the matching literature powder spectrum from [53].

Apart from a low-intensity Bragg reflection located at $q = 0.8 \text{\AA}^{-1}$, all the the other peaks are matched by the reference crystal structure. This means that the sample

consists almost exclusively of iminostilbene in a unique crystal structure. Furthermore, this indicates that impurities of crystalline nature or any other iminostilbene polymorphs are also below a few percent. Similarly, amorphous fractions of iminostilbene or impurities are, in the limit of the experiment, absent in the pattern.

5.1.2. Solubility of iminostilbene in tetrahydrofuran and ethanol

The saturation concentration of iminostilbene in tetrahydrofuran and ethanol solutions was determined in the same way as previously shown for carbamazepine (Section 4.1.2). The experiment was conducted again under ambient laboratory environment. In Table 5.1 the experimental data is given together with the mole fraction solubility calculated from Equation 4.1. The molar mass of iminostilbene is $193.24\,\mathrm{g\,mol^{-1}}$. While iminostilbene is highly soluble in tetrahydrofuran (mole fraction solubility is more than two times larger than that of carbamazepine), a significantly lower solubility is found in ethanol. It has to be noted that, in the limit of this experiment, the determined solubility should not be taken as an absolute value but rather as a tendency. A slightly different preparation temperature may already lead to deviating results.

Table 5.1.: Mole fraction solubility of iminostilbene in tetrahydrofuran and ethanol.

m_{carba}/mg....Mass of iminostilbene
$m_{solvent}$/mg...Mass of solvent
10^4x ....Mole fraction solubility reported in this work

	m_{carba}/mg	$m_{solvent}$/mg	10^4x
Tetrahydrofuran	49.97	406.21	439
Ethanol	50.41	7666.72	16

5.1.3. Drop casting and spin coating from tetrahydrofuran

The powder investigated in the previous section revealed a slight texture but with the material being in a unique polymorphic form. To see the effects of preparation

from solution onto a solid substrate, various films were prepared.
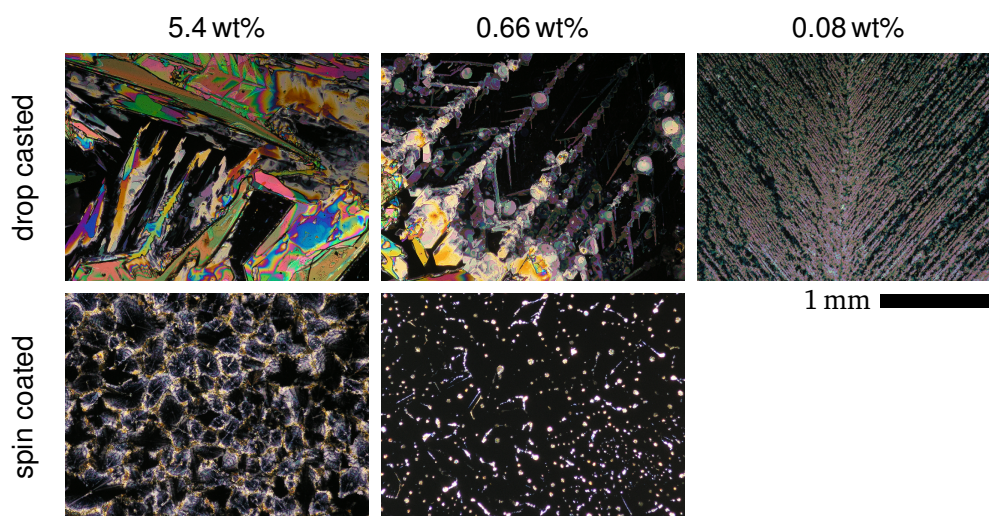
Figure 5.2.: Comparison of the different morphologies obtained by drop casting and by spin coating iminostilbene from THF solutions in different concentrations. Pictures are taken by an optical microscope under crossed polarizers.

In Figure 5.2 a concentration series from THF containing 5.4, 0.66 and 0.08 wt% iminostilbene prepared on SiO_2 surfaces by drop casting and spin coating is depicted by polarization microscopy. At high concentrations drop casting results in the formation of large crystals. With decreasing concentration dendritic structures start to occur around the larger structures. This results ultimately in the growth of defined dendrites, homogeneously covering the surface, for the lowest concentration. Different to the drop casted samples, spin coating results in a loosely attached network of ring-like structures for the highest concentration. For lower concentrations this structure breaks up and results in dispersed droplets. This is attributed to dewetting of the solution, forming smaller droplets which then crystallize independently. The ring-like assemblies are assumed to be caused by the coffee ring effect [74]. A flow towards the edges caused by a difference in evaporation rate transports the dissolved material to the border, leaving the inside of the droplet almost depleted. In these areas of low concentration dendritic growth is then observed, which is in agreement with the morphologies obtained from drop casting lower concentrations. For 0.08 wt% iminostilbene no crystalline material was observed as the amount is most likely too small to be detectable with the optical polarization microscope.
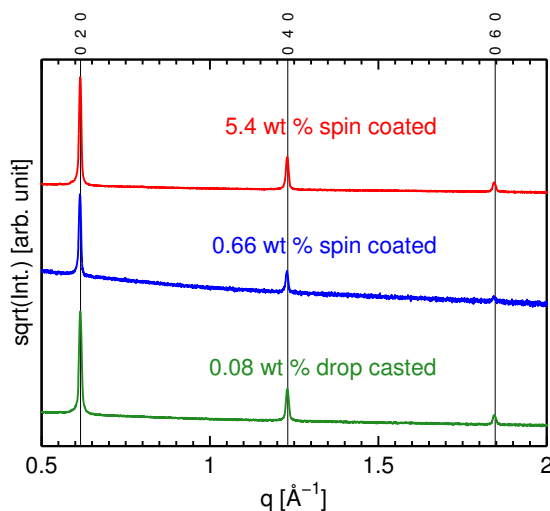
Figure 5.3.: Examples of specular X-ray diffraction patterns of iminostilbene prepared from three different THF solutions. The vertical black lines indicate the 010 peak series of the literature reference.

A qualitative characterization by specular X-ray diffraction was performed on all the samples. A representative selection is shown in Figure 5.3 as the scans yield similar patterns independently from preparation method and solution concentration used. A series of equidistant Bragg reflections corresponding to the {010} net planes of the literature reference is observed, showing that a preferred growth orientation with respect to the substrate surface exists. As specular X-ray diffraction probes just net planes which are parallel to the substrate surface, this means that most if not all crystallites have a 010 orientation with respect to the surface.

The samples were further investigated by grazing incidence diffraction to gain an understanding of the in-plane ordering of the crystallites. In Figure 5.4 reciprocal space maps of a drop casted and a spin coated sample are shown with high intensity spots indexed by the corresponding hkl values of the literature reference in a 010 orientation. While a good overall agreement is achieved for the drop casted sample, the spin coated sample exhibits a more smeared pattern indicating a deviation from a perfect preferred orientation, typically named mosaicity. Spin coating leads to rapid solvent evaporation thus fostering fast crystallization rates. This will ultimately result in non-conformal growth with respect to the surface to some extent. As grazing

incidence diffraction is very sensitive and no other orientations are observable under specular conditions, it can be concluded that the amount of non-oriented crystallites is absent or very low. As all high intensity peaks of the known structure are present, it can further be followed that the sample behaves like a 2-dimensional powder (or has a fiber texture), i.e. the individual crystallites are randomly rotated with respect to each other. A single crystal should only show one rod at a certain azimuth of the sample.
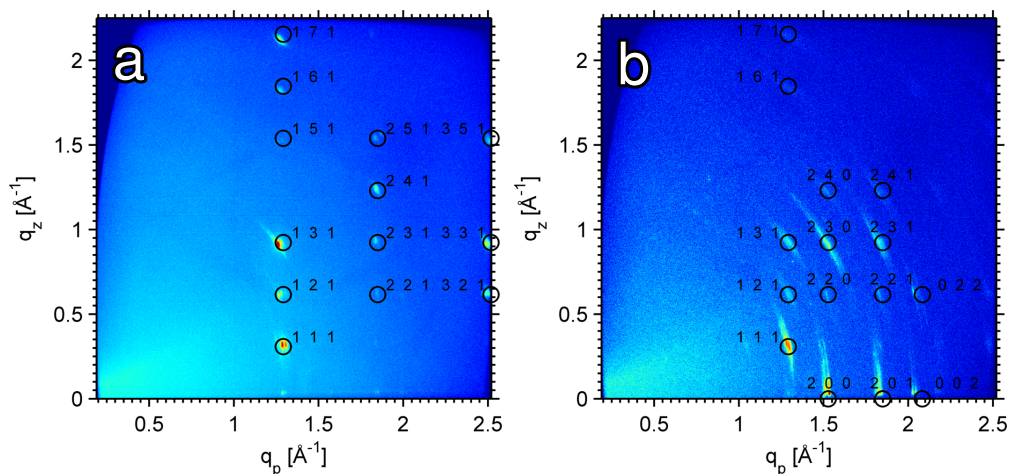
Figure 5.4.: Grazing incidence reciprocal space maps of iminostilbene drop casted from a 0.08 wt% THF solution (a) and spin coated from a 5.4 wt% THF solution (b).

5.1.4. Crystallization from other solvents

To determine a possible influence of the solvent polarity and the evaporation rate on the crystallization behavior, 2-propanol and xylenes solutions were prepared with 0.25 wt% and 0.23 wt% iminostilbene, respectively. The obtained morphologies from the drop casted solutions are depicted together with a sample from THF solution in Figure 5.5. Compared to THF the decrease in vapor pressure results in a more homogeneous morphology, leading to the growth of single crystalline rhombic plates from xylenes. The sample grown from 2-Propanol exhibits similar structures but stacked vertically on top of each other. As the vapor pressure of 2-Propanol and xylenes is of similar order, it can be assumed that the polarity of 2-Propanol is mainly

responsible for this effect [75]. Despite yielding different morphologies, specular X-ray diffraction shows no difference in crystal lattice or orientation for the different solvents used in preparation. This indicates that the facets along which the crystals grow are altered while the contact plane with the substrate is left unaffected. This means that by an exchange of the solvent a strong change in the morphology can be induced while the polymorph stays the same. This may have a great impact on dissolution properties.

1 mm
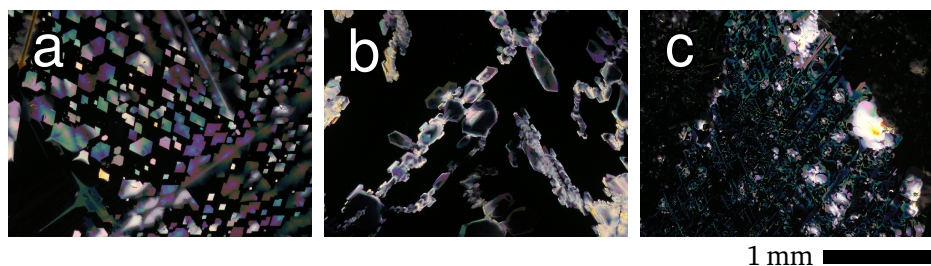
Figure 5.5.: Optical polarization microscopy of the different morphologies obtained by drop casting iminostilbene from 0.23 wt% xylenes (a), 0.25 wt% 2-Propanol (b) and from 0.16 wt% tetrahydrofuran (c) solution.

5.2. Preparing bi-axially aligned iminostilbene

Iminostilbene has been shown to exhibit a preferred 010 orientation to the substrate surface in the previous section and displays defined dendritic growth from lower concentrations. While a preferred orientation exists in the previous samples, in-plane order does not. By dip coating also in-plane ordering should be be achievable. Dip coating from different solvents is evaluated at first and factors leading to misorientation are discussed. To tackle these issues and to further enhance oriented growth, a polyimide alignment layer is finally evaluated as a suitable surface for the preparation of high quality films.

5.2.1. Dip coating from different solvents

Iminostilbene was dip coated from 0.45 wt% THF, 0.51 wt% ethanol, 0.25 wt% 2-Propanol and 0.23 wt% xylenes solutions at a withdrawal speed of $3\,\mu\mathrm{m\,s^{-1}}$ on a $\mathrm{SiO_x}$ substrate. Images by polarization microscopy were used to evaluate the obtained morphologies as depicted in Figure 5.6. Both THF and ethanol result in the formation of needles with the ones obtained from THF being more edgy and bulky when compared to those from ethanol. As THF is a solvent with a high vapor pressure, crystallization takes place much faster than in ethanol. In fact the high evaporation rate also puts the absolute withdrawal speed in perspective as the filling level in the recipient decreases significantly over the dip coating process while the concentration increases. Dip coating from 2-Propanol results in a segmented growth caused by a tearing of the wetting film which is attributed to the bad mixability between iminostilbene and 2-Propanol as well as to the hydrophilic solvent. Fractal growth is observed from xylene solution with perfectly perpendicularly growing structures. The constant color for the individual branches means that they have a unique height. This is confirmed by an AFM measurement (Figure 5.7c) which reveals a very homogeneous height ranging between 100 nm and 120 nm. Interest-

$200\,\mu\mathrm{m}$
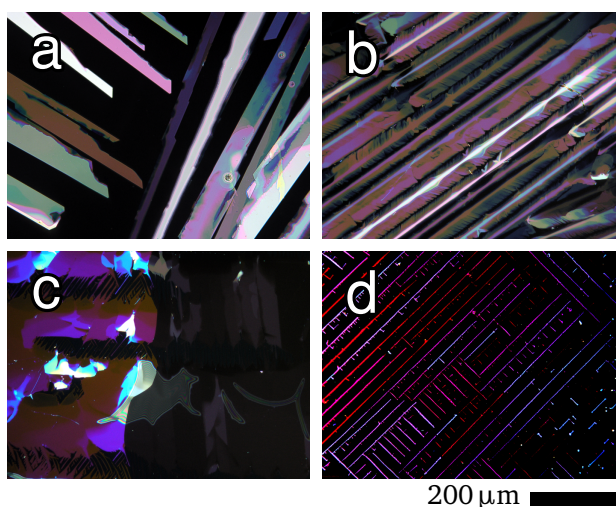
Figure 5.6.: Dip coating iminostilbene on a $\mathrm{SiO_2}$ surface at a withdrawal speed of $3\,\mu\mathrm{m\,s^{-1}}$ from different solutions: 0.45 wt% THF (a), 0.51 wt% ethanol (b), 0.25 wt% 2-propanol (c) and 0.23 wt% xylenes (d).

ingly, there is also strong indication that the side branches grow in the direction of the main orientation induced by dip coating (the long needles as observed in Figure 5.6d) and not from them. The side branches exhibit a larger *head* far from the main orientation which is also aligned in perpendicular orientation, being only connected to the main direction through a narrow structure if at all. Also needles grown from ethanol seem to exhibit such an underlying structure where the empty space is subsequently filled with further material, resulting in an observed main direction with feather-like branches to the side (see Figure 5.7a,b).
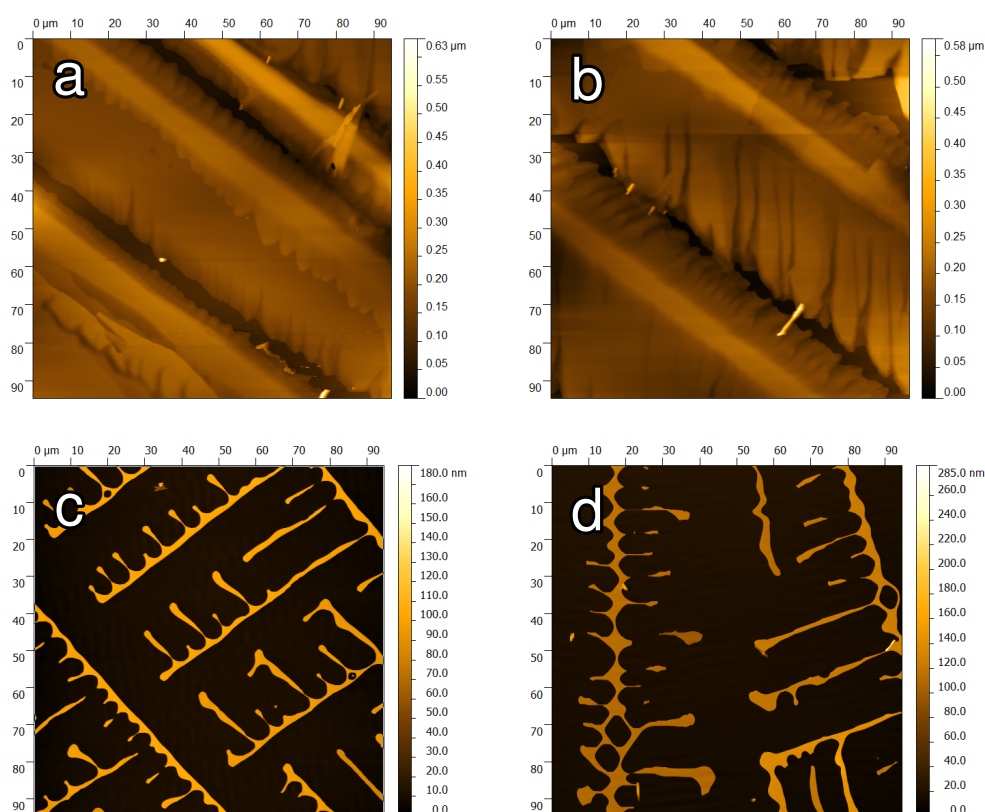
Figure 5.7.: Atomic force microscopy images of iminostilbene dip coated from 0.51 wt% ethanol (a,b) and from 0.23 wt% xylenes (c,d) at a withdrawal speed of $1\,\mu m\,s^{-1}$.

5.2.2. Effects causing misorientation

In order to minimize the formation of misorientations (which were present in the previous samples) to an acceptable degree (i.e. large, independent domains), the cause of these defects is investigated. In fact, main influence factors are the solution/substrate and solution/air interfaces, the solvent evaporation rate and the withdrawal speed. Decreasing the withdrawal speed too far leads to a tearing of the wetting layer at the substrate/air interface, leading to periodic segments which then crystallize independently. The limit in withdrawal speed is ultimately linked to the solvent choice as a fast evaporating solvent is more likely to cause film tearing. More importantly, the solution/air and solution/substrate interface have a huge impact on the obtained growing directions as depicted in Figure 5.8. Immediately after the substrate is inserted into the solution, a wetting layer will be formed on the substrate at the solution/air interface. This layer starts crystallizing early on, leading to larger crystallites without a orientation being induced by the dip coating process (see Figure 5.8a). These crystallites then act as seeds for further crystallization causing various orientations off the dip coating direction. Likewise, randomly oriented crystallites start to grow on the substrate/liquid border which then constantly act as new seeds for different growth orientations (see Figure 5.8b). Larger substrates can minimize this effect but are also limited to some extend as this will increase the necessary solution volume. Depending on the used recipient this can be a limiting factor in these experiments.
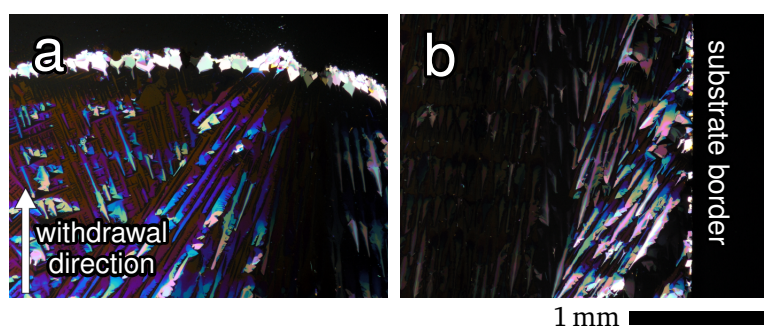

Figure 5.8.: The two main reasons for misoriented crystal growth during dip coating: formation of large, unoriented crystallites due to wetting at the top (a) and inhomogeneous growth from the solvent/substrate interface (b).

5.2.3. Enhanced orientation by using a polyimide alignment layer

To suppress the formation of crystal growth not parallel to the withdrawal direction, a rubbed polyimide alignment layer was tested. Such films were obtained by spin coating Liquicoat PI-Kit ZLI-2650 from Merck AG on silicon oxide substrates. To do so, 290 mg resin was dissolved in 10 mL solvent and subsequently kept in a sonicator to speed up dissolution. Before spin coating at 40 rps, the solution was filtered with the Phenex syringe filter RC 0.2 μm. The so produced samples were then kept at 100 °C, 200 °C and 300 °C for one hour, respectively, to induce the imidization process. Slow heating steps minimize cracks in the film and allow for a full chemical reaction. To induce a orientation to the polyimide surface, the samples are then manually rubbed on a velvet fabric along a ruler serving as a stabilizing edge. This results in grooves running along the rubbing direction which typically allows subsequent film alignment of deposited layers [76].
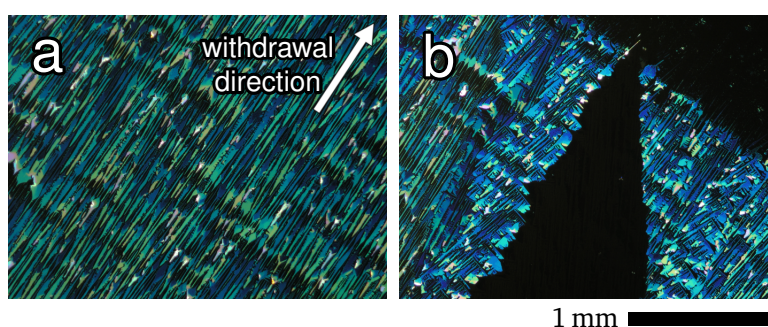
Figure 5.9.: Iminostilbene dip coated on a polyimide alignment substrate from a 0.51 wt% ethanol solution at a withdrawal speed of $3 \, \mu m \, s^{-1}$. Homogeneous growth inside large domains (a) and the presence of another growth direction at the top of the sample (b) is observed.

Deposition of 0.51 wt% iminostilbene from ethanol solution via dip coating onto the rubbed polyimide alignment layers decreases the amount of misorientations significantly, giving raise to larger domains which themselves are homogeneous. In Figure 5.9a a large domain of nearly perfectly grown crystallites is shown, revealing the impact of this technique on the growth direction. Similar to the previous samples misorientations are present at the very top of the sample and the sample border (example shown in Figure 5.9b). The overall reduction of misorientations and the

homogeneous growth inside the single domains, however, allows the specific selection of well-oriented domains by splitting the sample in such a way that other orientations are omitted.
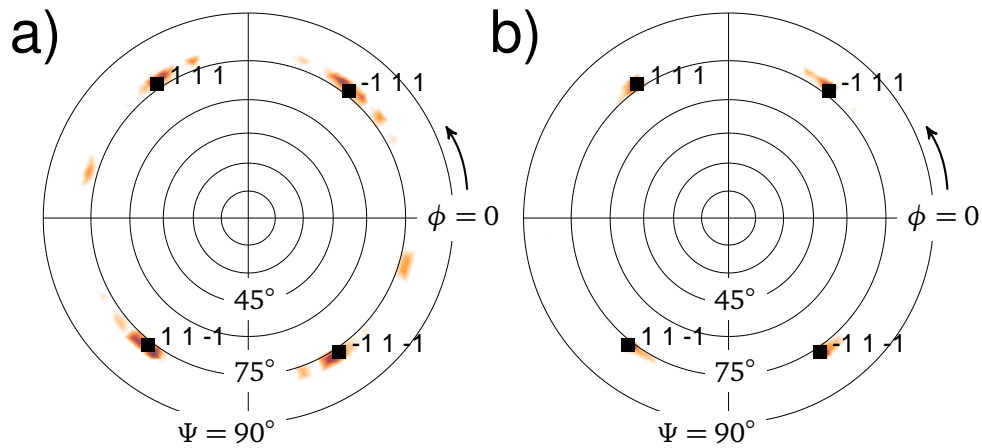
Figure 5.10.: Pole figures taken at $|q| = 1.33\,\text{Å}^{-1}$ for iminostilbene dip coated on a polyimide alignment layer from 0.51 wt% ethanol solution as-prepared (a) and after removing misorientations (b).

Pole figure measurements on the 111 peak ($|q| = 1.33\,\text{Å}^{-1}$) were performed for iminostilbene dip coated on the polyimide alignment layer as-prepared i.e. with some misorientations (Figure 5.10a) and after removing misorientations (Figure 5.10b). The observed reflections for the as-prepared film are found oriented on a ring at $\Psi = 47°$ in accordance with a 010 orientation. In azimuthal direction (i.e. along ϕ) a main orientation is present (indexed with the corresponding hkl values). Additional, small poles are also present. This indicates that there exists not only one preferred in-plane orientation but rather different domains with distinct growth directions, as already observed by optical microscopy (5.9a). After reduction to only one domain by sample splitting, the pole figure reveals a unique aligned iminostilbene layer with the observed intensities being perfectly matched by the indexation and the small poles being canceled out (compare Figures 5.10a and b). As the needle-like crystallites have an underlying dendritic structure with growth directions perpendicular to each other (as seen in Figure 5.7), this also indicates that all the molecules are aligned in the same direction on the substrate despite exhibiting perpendicular structures.

6. Carbamazepine and iminostilbene mixtures

Within this chapter the crystallization behavior of carbamazepine intermixed with iminostilbene is investigated. Even though the molecular structure of carbamazepine and iminostilbene is similar, their crystallization behavior is different as demonstrated in the previous chapters. Anyway, the fact that the former has already been shown to form cocrystals with a variety of different molecules [49, 77, 78], a cocrystallization upon intermixing was anticipated, by which the carbamazepine crystallization properties hopefully improve. Different mixing ratios are studied and a possible influence of the preparation temperature is assessed. Finally, amorphous carbamazepine is prepared by thermal evaporation on top of dip-coated iminostilbene to evaluate the latter as a possible template for defined crystallization.

6.1. Intermixing from solution

In the following section only results obtained from tetrahydrofuran solutions are shown, though comparable results have also been achieved with ethanol (see Appendix A.3). Different mixing ratios of carbamazepine and iminostilbene were prepared in 0.61 wt% and 4.9 wt% tetrahydrofuran solutions. Film preparation on silicon oxide surfaces was done by drop casting and spin coating under ambient conditions as well as by drop casting at 60 °C. Analysis of the obtained crystal structures is performed by specular X-ray diffraction as shown in Figure 6.1 for selected samples. Despite the differences in solvent concentration and preparation, the X-ray patterns show similar results for all the investigated samples. The spectrum reveals various

peaks over the entire pattern but unlike the powder-like samples, these peaks correspond either to the 110 or higher order reflections of carbamazepine or the 010 and higher order reflections of iminostilbene. This suggests that carbamazepine and iminostilbene crystallize independently. The absence of any unexplained peaks is a further indication that cocrystals did not form. This means that a phase separation took place and that each molecule crystallizes in its respective lattice. While a preferred 010 orientation of pure iminostilbene was observed previously, the same was absent for carbamazepine. The mono-axial alignment is in contrast to the otherwise powder-like crystallizing pure carbamazepine at solid surfaces. This suggests that iminostilbene induces/helps carbamazepine to align along certain directions during the preparation.
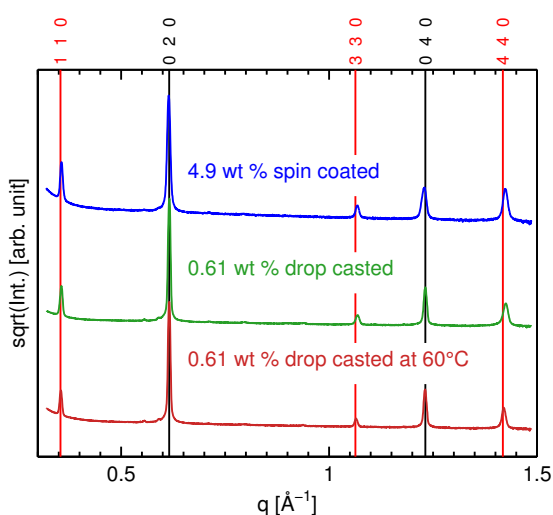

Figure 6.1.: Specular X-ray diffraction pattern of carbamazepine/iminostilbene mixtures (ratio $\sim 1 : 1.5$) prepared from THF solution by different preparation techniques. Vertical lines indicate certain Bragg reflections from iminostilbene (black) and trigonal carbamazepine (red).

6.1.1. Grazing incidence diffraction

Although specular X-ray diffraction yields similar results for the crystallographic properties independent of the preparation conditions, further investigation by grazing incidence X-ray diffraction reveals a more complex behavior. In Figure 6.2 reciprocal spaces maps of various samples containing a carbamazepine/iminostilbene ratio of 1:1.5 are depicted. The samples differ in their processing parameters, i.e. some are spin coated while some are drop casted or the processing temperature is changed. The sample spin coated at room temperature from 4.9 wt% solution reveals Bragg-spots within the entire space map. The smearing along rings is the result of the mosaicity being slightly higher compared to a pure iminostilbene film. Anyway, all spots within the pattern correspond to either the trigonal carbamazepine in a 110 orientation or the iminostilbene in a 010 orientation (see indexation within Figure 6.2a). This confirms the mono-axial alignment of carbamazepine with respect to the substrate surface and or the iminostilbene (010) plane. The situation drastically changes if the same solution (4.9 wt%) is deposited via drop casting at an elevated temperature of 60 °C. The previously spot-like space map shows now a ring-like pattern, the typical Deybe-Scherrer rings obtained for a powder (see Figure 6.2b). Anyway, some more intense regions along the rings are denoted which similarly to the first sample can be indexed by carbamazepine in a 110 and iminostilbene in a 010 orientation. This shows that the degree of order is strongly reduced but a slight texture is still present.

Drop casting a sample from 0.61 wt% solution at room temperature shows a mixture of the first two cases (see Figure 6.2c). Spots corresponding to the iminostilbene are overlayed by weak rings of carbamazepine. Small spots along the rings show that some carbamazepine crystallites are able to cause a sufficiently strong diffraction signal, i.e. they have an adequate size for this process.

The last sample was prepared via drop casting 0.61 wt% at elevated temperatures. Similar to the spin coated sample of Figure 6.2a, a preferred orientation is present (even though a slightly higher mosaic spread exists). This means that preparation induces again a texture of carbamazepine. Increasing the solvent evaporation rate either by changing the preparation method (e.g. to spin coating) or by preparation at

an elevated process temperature both seem a feasible way to enhance the formation of mono-axially aligned carbamazepine, given that the initial concentration is not too close to supersaturation.
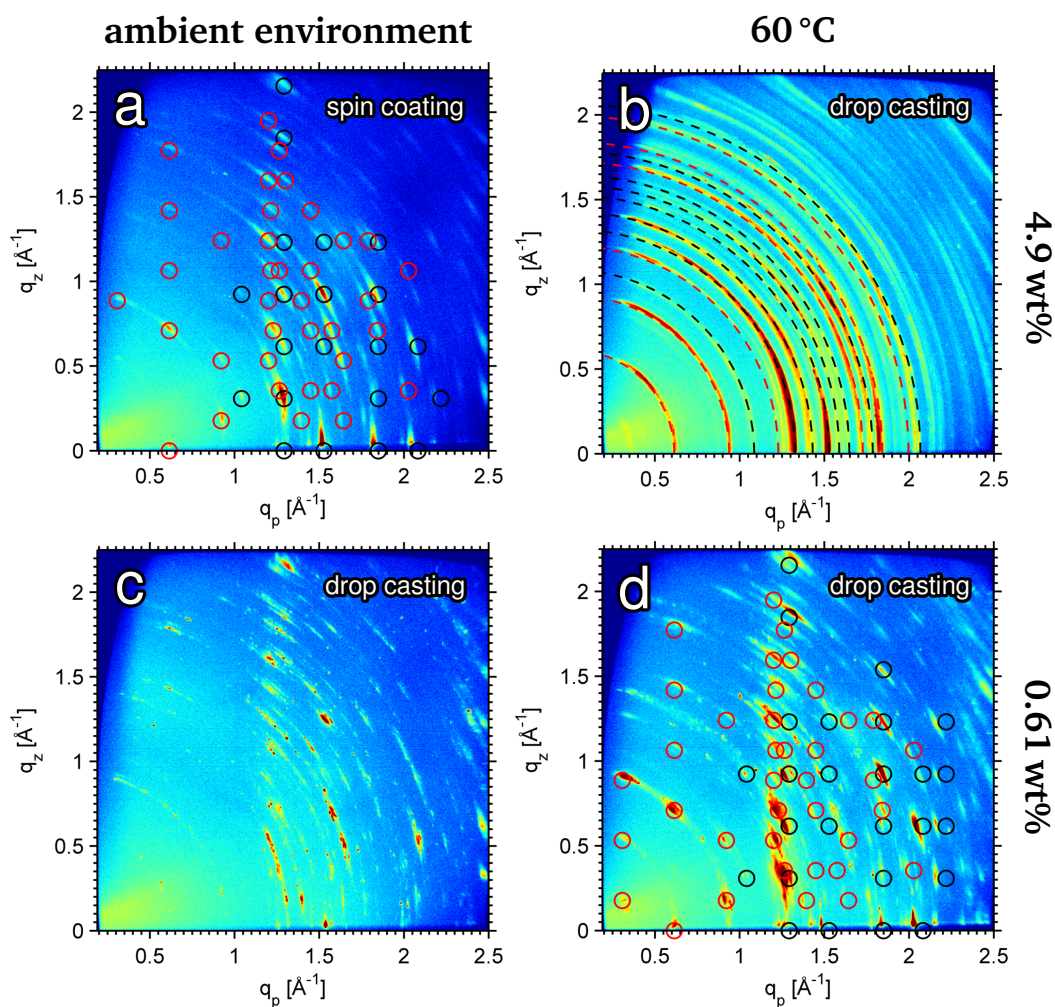
Figure 6.2.: Gracing incidence reciprocal space maps of carbamazepine/iminostilbene in $\sim 1:1.5$ mixing ratio prepared under different conditions from THF. ○ iminostilbene in 010 texture, ○ trigonal carbamazepine in 110 texture. Debye-Scherrer rings are indicated by dashed lines.

6.1.2. Morphology investigation by atomic force microscopy

The morphology of uniaxially aligned carbamazepine in the vicinity of iminostilbene at SiO_x is investigated by atomic force microscopy, with selected images being depicted in Figure 6.3. Drop casting shows the presence of two distinct morphologies: long ranged lines with dendritic side branches grow on the substrate surface whereas smaller needles are found on top or in the space between the former structure (Figure 6.3a,b). Both morphologies show a clear similarity to the structures obtained from the single compounds (compare Figures 5.7a,b and 4.2a,b), hence the former is most likely iminostilbene and the latter carbamazepine. This also means that imi-
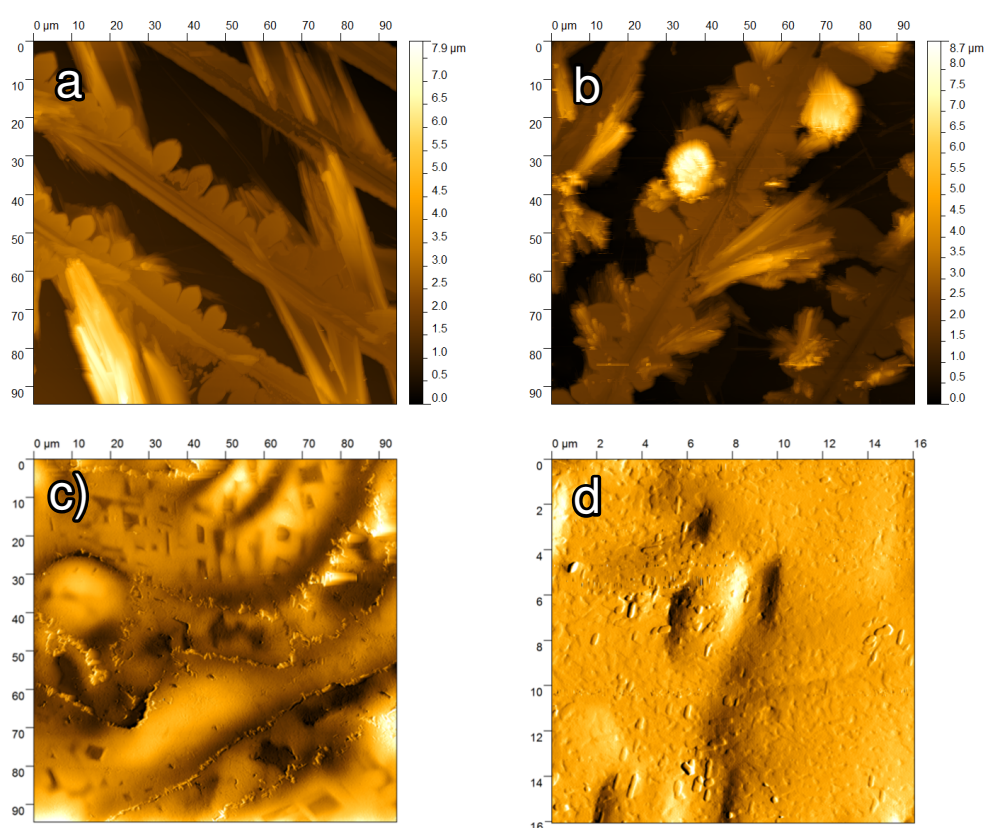
Figure 6.3.: AFM images of carbamazepine/iminostilbene mixtures prepared in 1:1 ratio by drop casting at 60 °C (a,b) and in 1:1.5 ratio by spin coating (c,d) from 0.68 wt% and 4.9 wt% tetrahydrofuran solution, respectively. For better visibility shading is used on images (c,d).

nostilbene is crystallizing prior to carbamazepine as it is growing unimpeded on the substrate surface. This will also decrease the solution concentration thus delaying carbamazepine crystallization.

Compared to the morphologies obtained from drop casting, a very different behavior is observed for spin coated samples as shown in Figure 6.3c,d. The substrate surface is completely covered with a film, making a distinction between the single components difficult. An underlying network of rectangular structures is observed in the upper part of the image (6.3c) or in the center of Figure 6.3d. This might be attributed to iminostilbene for its similarity in shape to the directed, perpendicular growth of the single component. A more detailed image (Figure 6.3d) reveals the presence of small, rod-like structures with a size of roughly $0.5\,\mu$m embedded into the film surface. As the crystallographic orientation is similar to that of drop casted samples, this could mean in analogy that these structures are subsequently crystallizing carbamazepine, thus being located on top. Without a position sensitive method at hand to identify the single compounds, these assumptions, though plausible, remain unverified.

6.1.3. Influence of the mixing ratio

In the previous sections intermixing with iminostilbene has been demonstrated as a possible way to induce a preferred orientation, with respect to the surface, to the otherwise powder-like crystallizing carbamazepine. The degree to which carbamazepine exhibits mono-axial alignment is mainly influenced by the preparation temperature, solvent evaporation rate and the mixing ratio as tested in various experiments. The latter effect is investigated by preparing different mixing ratios of carbamazepine/iminostilbene from $0.67\,$wt% THF solution onto SiO_x surfaces by drop casting both under ambient conditions and at $60\,°$C. The specular X-ray diffraction patterns of the various samples are depicted in Figure 6.4. Samples prepared at room temperature reveal various peaks over the entire scan range. Surprisingly, while the iminostilbene still reveals the orthorhombic phase, the carbamazepine shows various peaks of the trigonal phase as well as of the dihydrate form. The indexation shows furthermore that these two polymorphs again grow in a preferred

orientation. The trigonal form shows a 110 texture and the dihydrate aligns with the 001 plane parallel to the surface. This behavior is independent of the concentration, i.e. increasing the carbamazepine content has no effect on its alignment at ambient conditions.
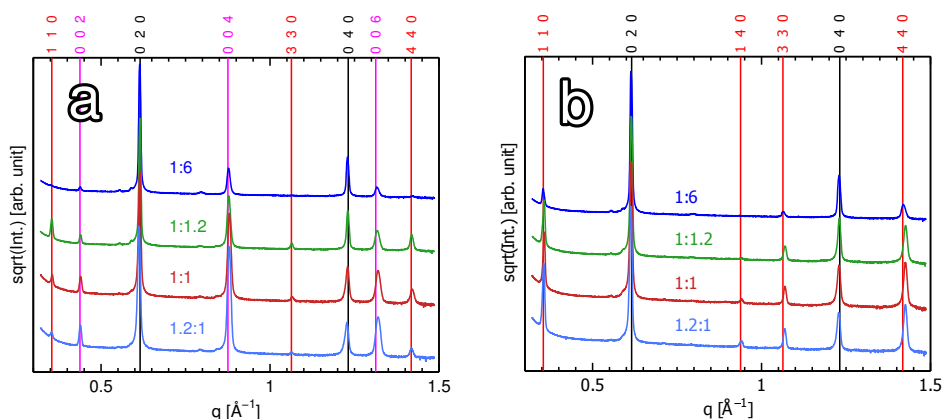
Figure 6.4.: Specular X-ray diffraction pattern for different carbamazepine to iminostilbene ratios. The samples were prepared by drop casting under ambient condition (a) and at 60 °C (b). The vertical lines indicate Bragg reflections for carbamazepine trigonal (red), iminostilbene (black) and carbamazepine dihydrate (magenta), respectively.

For samples prepared at 60 °C the situation changes. Specular X-ray diffraction shows no hydrate formation at all but two higher order peak series corresponding to trigonal carbamazepine in 110 and iminostilbene in 010 orientation, respectively (Figure 6.4b). As the carbamazepine content increases however, a loosening in the alignment is observed by the rise in intensity of the 140 Bragg reflection of carbamazepine, thus indicating the presence of at least another orientation. This peak becomes more dominant as the carbamazepine content surpasses that of iminostilbene. The carbamazepine content in the intermixture should therefore be lower than that of iminostilbene, so that a higher quality of the alignment is achieved.

6.2. Thermal evaporation of carbamazepine onto an iminostilbene template

In the previous section mono-axially aligned carbamazepine has been demonstrated by preparation from an intermixture with iminostilbene, yet the exact mechanism remains elusive. While temperature and solvent evaporation rate dependency suggests an explanation through a change in crystallization kinetics, atomic force microscopy images hint an epitaxial-like growth of carbamazepine on top of the faster crystallizing iminostilbene. Within this section the latter theory is put to test by preparing amorphous carbamazepine on top of an iminostilbene layer, which accordingly is expected to serve as a template in the carbamazepine crystallization process.

Iminostilbene surfaces are prepared by dip coating from 0.51 wt% ethanol solution onto SiO_x and polyimide surfaces at a withdrawal speed of $6\,\mu m\,s^{-1}$ and $3\,\mu m\,s^{-1}$, respectively. The different preparation process will only affect the quality of the iminostilbene in-plane alignment as discussed in 5.2.3 but will not alter the overall morphology in terms of a template. Carbamazepine is then deposited on top by thermal evaporation at a rate of $0.4\,\text{Å}\,s^{-1}$ with a thickness of 50 nm (SiO_x substrate) and 100 nm (polyimide substrate).

The deposited carbamazepine layer is found to be amorphous at first which was tested with optical microscopy and X-ray diffraction (data not shown). This amorphous state is followed by complete crystallization over the course of several days. Optical microscopy (Figure 6.5a,b,c) then reveals morphologies similar to those obtained solely from carbamazepine on SiO_x surfaces. Under ambient conditions the formation of short, randomly oriented needles is observed for one sample (Figure 6.5a), while the other exhibits larger needles with indication of oriented growth (Figure 6.5b). Specular X-ray diffraction (Figure 6.5d) of the former did not show any Bragg reflections corresponding to carbamazepine. The low thickness most likely causes the diffraction signal being below the detection limit of the experiment in use. However, judging from the morphology, it is reasonable to assume that this is the triclinic form. For the other sample crystallized at ambient conditions (Figure 6.5b), the formation of carbamazepine dihydrate is revealed. Furthermore, the
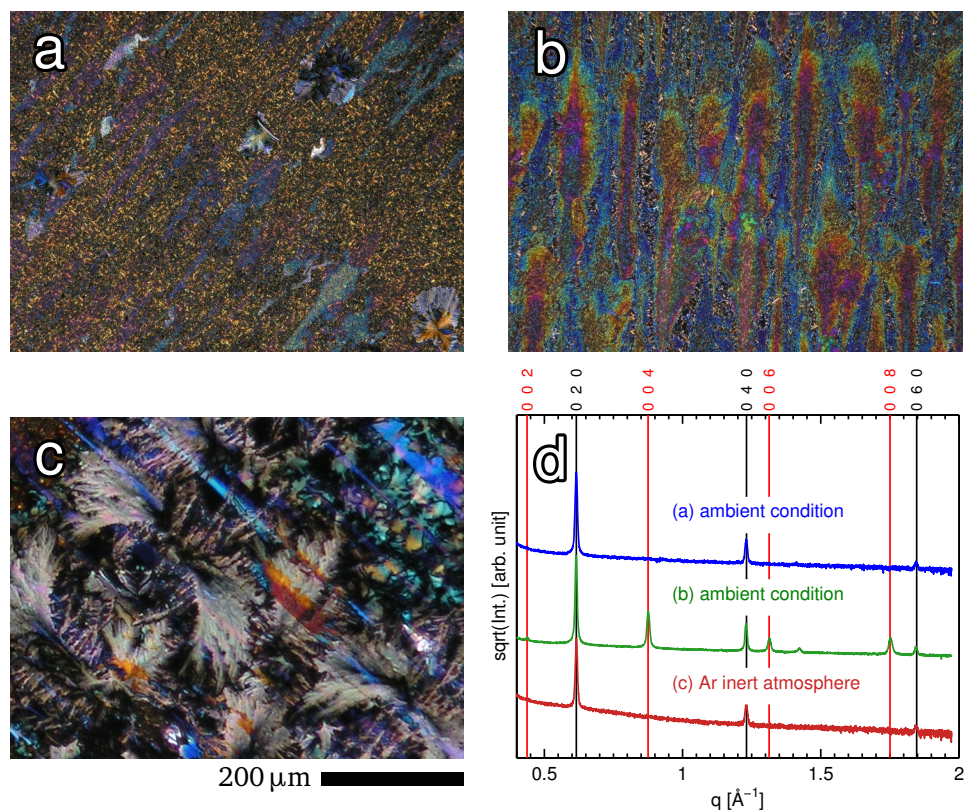
**Figure 6.5.:** Optical microscopy images of carbamazepine on a dip coated iminostilbene template: crystallization under ambient conditions without (a) and with dihydrate formation (b) as well as under argon inert atmosphere (c). In (d) the corresponding specular X-ray diffraction pattern is given with the vertical black/red lines indicating the 010 and 001 peak series of iminostilbene and carbamazepine dihydrate, respectively.

sample exhibits a 001 orientation. The morphology is different to the triclinic form with the structures aligning along the iminostilbene template. This alignment is also proven by pole figure measurements.

Pole figure measurement at $|q| = 1.38\,\text{Å}^{-1}$ (corresponding to the 112 Bragg reflection of the dihydrate) is depicted in Figure 6.6. Poles smeared out along four distinct arcs are found at $\Psi \approx 72°$ corresponding to $\{112\}$ net planes of the carbamazepine dihydrate. This indicates not only the presence of a fiber texture but also of partially bi-axially aligned crystallites inclined approximately 87° in respect to each other. At $\Psi \approx 79°$ distinct spots are distributed along a ring corresponding to $\{111\}$ planes of iminostilbene. This means that the dip coated iminostilbene substrate is not in perfect bi-axial alignment, which might also be the reason for the absence of single, distinct orientations of the on top growing carbamazepine dihydrate.
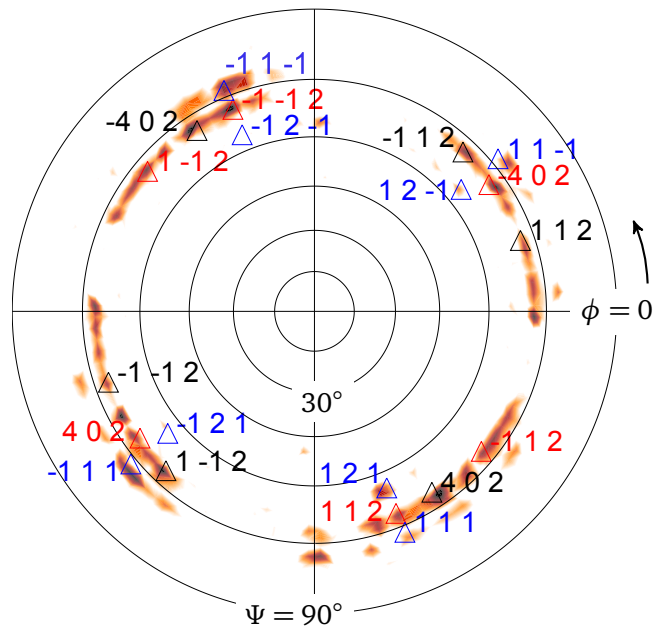
Figure 6.6.: Pole figure taken at $|q| = 1.38\,\text{Å}^{-1}$ of carbamazepine prepared on top of an iminostilbene layer. △, △ Two main orientations of carbamazepine dihyrate with a 001 texture; △ iminostilbene with a 010 texture.

Crystallization under argon inert atmosphere results in the formation of structures (Figure 6.5c) similar to morphologies observed previously under inert gas environment, hence the p-monoclinic form is assumed. The specular X-ray diffraction

pattern (Figure 6.5d) shows only Bragg reflections of the underlying iminostilbene layer.

6.3. The mechanism of carbamazepine alignment

The alignment of carbamazepine on top of a silica surface is achievable by the addition of iminostilbene. Independent of the preparation technique, i.e. spin coating or drop casting, an alignment can be achieved during solution processing. The processing conditions have in addition a great impact on the quality of the alignment. On the on hand, drop casting from high concentrations at elevated temperatures results in poor quality films with the carbamazepine having nearly powder-like properties with only a slight 110 texture. All other processing temperatures and concentration values tested yielded a rather good alignment. Also a variation of the relative amount of both components did not change this behavior, although an additional formation of dihydrate was evident for one set of samples. This may be addressed by the poor environment control which may result in the relative humidity being drastically different during processing, thus dihydrate may have been formed.

The situation for the vacuum deposited samples is different. No clear order of the trigonal form could be found. However, a reasonable alignment was observed for samples which formed the carbamazepine dihydrate. Even a bi-axially alignment is present in such samples, i.e. not only the contact plane is parallel to the surface but also the in-plane alignment with respect to the underlying iminostilbene is noted. Such an alignment may also be present within the solution cast film in Figure 6.3d where most of the crystallites have a very similar inclination.

From these observations two possible molecular arrangements are suggested, depicted in Figure 6.7. Carbamazepine could attach to the iminostilbene ledges and grow from there, possibly even forming some hydrogen bonds (Figure 6.7c). In this context ledge-directed epitaxy (LDE) would be a possible explanation. LDE is a mechanism which describes oriented growth resulting from a lattice matching between the close-packed planes of a substrate ledge site and that of a prenucleation aggregate as reported by Bonafede *et al.* [79]. The geometric lattice modeling rou-
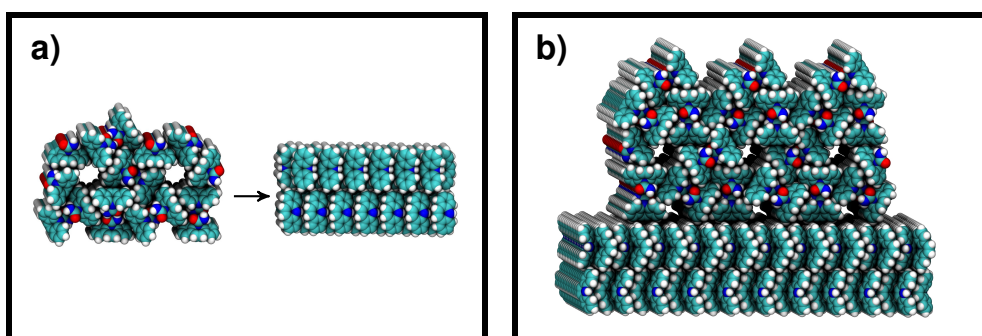
Figure 6.7.: Possible molecular arrangements of carbamazepine: (a) Ledge-directed growth along an iminostilbene edge. (b) Epitaxial growth on top of an iminostilbene layer with a 010 texture. The carbamazepine contact plane is (110).

tine GRACE [80] was used to examine the epitaxial match of carbamzepine and iminostilbene planes in their respective configuration but no conclusive result was obtained. As this routine only investigates a possible lattice match and does not take the change in potential energy for the various configurations into account, further investigation is necessary. Simulations by molecular dynamics (MD) or density functional theory (DFT) could be used to evaluate possible arrangements and may help in understanding the underlying mechanism better.

Lattice matching via GRACE for epitaxial growing carbamazepine is alike inconclusive. Still, manual arrangement shows that the surface morphology of iminostilbene in 010 texture fits to the contact plane of carbamazepine with the configuration depicted in Figure 6.7b. The upright standing iminostilbene molecules lead to a grooved surface into which the tilted carbamazepine molecules of the trigonal structure would perfectly fit. It has to be noted though that the needles observed by AFM, attributed to carbamazepine, are found in more than one orientation on top of the iminostilbene layer, while this explanation would only describe the presence of one distinct direction.

7. Conclusion

Within this work a comprehensive study on the crystallization behavior of carbamazepine and iminostilbene in the vicinity of solid surfaces is presented. The results gained from various preparation techniques and from application of selected surfaces show a significant difference between these two molecules in terms of possible morphology and crystallographic phases, although their chemical structure is very similar. Several routes to control and manipulate these properties are demonstrated so that desirable material properties can be obtained.

Over the course of this work, three of the five known carbamazepine polymorphs were obtained together with the formation of hydrous phases. The active pharmaceutical ingredient usually exhibits powder-like distribution of its crystallites independent of the preparation technique when recrystallized from solution. Also, multiple phases are often observed simultaneously, especially in cases where hydrate formation is encouraged (e.g. by using ethanol as solvent). However, a reliable method to obtain the trigonal and the triclinic polymorph was found as depicted in Figure 7.1.
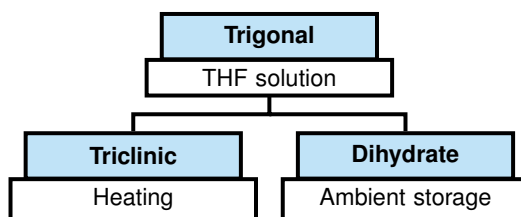

Figure 7.1.: Schematic representation of the carbamazepine polymorphs obtained via drop casting from solution and post deposition treatment.

Drop casting carbamazepine from tetrahydrofuran solution usually results in the formation of the trigonal polymorph. This is in accordance with Ostwald's step rule as

it is also the least stable form. For thin film carbamazepine a thermally induced transition to the triclinic form is observed at approximately 140 °C. This indicates that the substrate is of minor importance as this behavior is similar to the data reported in literature for the bulk material. Likewise, a phase transition to a hydrous form is observed over time upon storage under ambient conditions. Preparation on hydrophilic silicon oxide surfaces further enhances this transition. The same applies for smaller particle sizes, as samples prepared from lower concentration are more likely to exhibit water incorporation. Among the different substrates used (SiO_x, glass, kapton, mylar, mica), only muscovite mica did exhibit an influence on the crystallization process as uniaxial crystal growth was indicated (see Section 4.2.5).

Amorphous carbamazepine was found from films prepared by spin coating as well as thermal evaporation. The latter technique is advantageous as no solvent is needed so solvent effects can be excluded. The amorphous state is not stable, however, and crystallization was observed after a short period of time (see Figure 7.2). This makes the amorphous state impractical within a pharmaceutical application where stable storage over at least 6 months is essential.
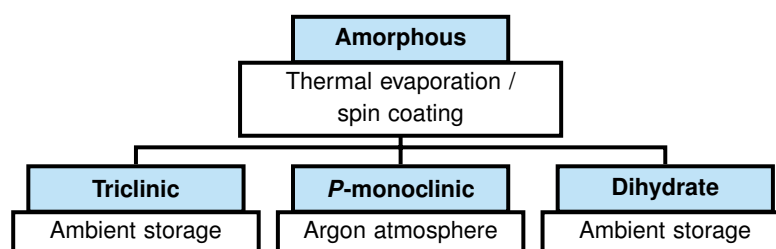

Figure 7.2.: Schematic representation of the carbamazepine polymorphs as obtained via thermal evaporation and spin coating from solution.

Ambient storage usually results in the formation of triclinic carbamazepine, but dihydrate formation is also observed. On the other hand it was indicated that crystallization under argon atmosphere yields the *P*-monoclinic form. As this is the commercial form, this would provide a reliable way to recrystallize carbamazepine in the desired phase independent of the polymorphic composition of the original material. The crystallites are usually randomly oriented with respect to the surface while a slight preferred orientation in 0-11 direction is observed in films prepared by spin coating (Figure 7.3).
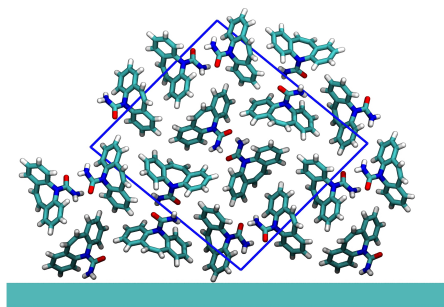
Figure 7.3.: Illustration of the unit cell of the triclinic carbamazepine form with the 0-11 plane contacting the substrate surface.

A different situation is found for iminostilbene which always crystallizes in the single polymorph known in literature, independent of the preparation techniques utilized. Moreover, a 010 texture is present in all the films and dendritic growth is observed along the surface. The iminostilbene molecules *stand* on the substrate surface as depicted in Figure 7.4. The absence of hydrogen bonding and dimer formation (compared to carbamazepine) also promotes faster crystallization, showing that the addition of a small side group has a dramatic effect on the crystallization behavior.
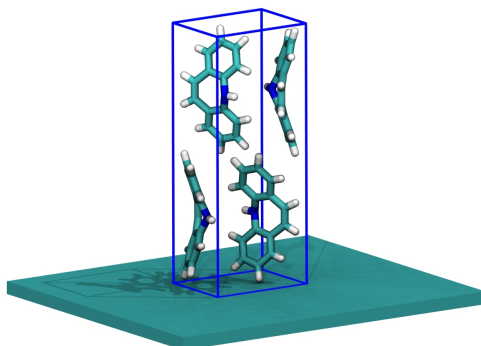

Figure 7.4.: Illustration of the iminostilbene unit cell with the 010 plane oriented parallel to the substrate surface.

Upon intermixing of carbamazepine with iminostilbene a preferred orientation is induced to the former. Iminostilbene is identified as the faster crystallizing component, thus forming undisturbed layers on the substrate surface. The later crys-
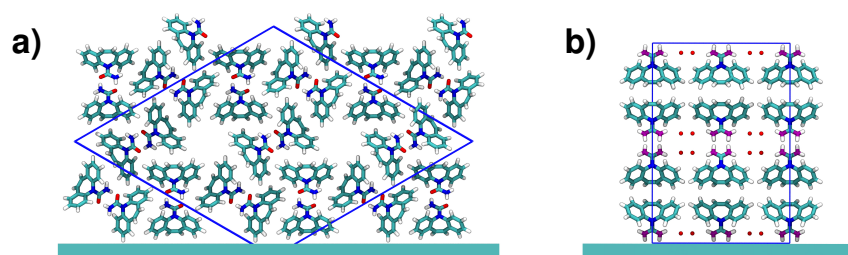
Figure 7.5.: Illustration of the unit cell orientation of the trigonal carbamazepine form (a) and of the orthorhombic dihydrate (b) in respect to the substrate surface. The contact plane is 110 and 001, respectively.

tallizing carbamazepine then orients itself on this template, exhibiting a 110 texture (Figure 7.5a). Both drop casting and spin coating have been demonstrated as a feasible way to achieve this; elevated processing temperatures enhance the oriented carbamazepine growth. As long as the iminostilbene content exceeds that of carbamazepine this effect was observed. Bi-axially aligned iminostilbene was also demonstrated from dip coating onto an aligned polyimide layer which subsequently was used as a template (Section 5.2.3). Directed growth of vacuum deposited carbamazepine could also be shown with the undesired hydrate form exhibiting the highest degree of order (Figure 7.5b). While a final conclusion on the growth mechanism cannot be given within this work, there is some indication that the ledges of the iminostilbene dendrites act as a nucleation/docking site for carbamazepine. Also epitaxial growth seems likewise possible as indicated by atomic force microscopy.

The findings of this work demonstrate how the polymorphic form (and morphology) can be manipulated in the vicinity of a solid surface. This information can directly be applied for various formulations like transdermal patches or nanoparticle coatings. Even though not tested, it can at least be expected that each of the obtained "variations" will directly impact the dissolution and thus the bioavailability. While fast dissolution may be of interest for acute treatment, slow/delayed dissolution allows for long term treatment much more effectively. The sample preparation tested show a practical way to easily manipulate the thin film properties, which might also allow to find new polymorphs/morphologies with advanced properties within other active pharmaceutical ingredients. In the future this may provide new routes to overcome the problem of poor solubility often emerging in therapeutic treatment.

A. Appendix

A.1. GIXD Carbamazepine from tetrahydrofuran

Grazing incidence diffraction was used to investigate the in-plane order of drop casted carbamazepine, prepared from 5 wt% tetrahydrofuran solution. In the reciprocal space map (Figure A.1) high-intensity Bragg reflections are observed. These diffraction spots are located along rings characteristic for a powder. This means that rather large, single crystallites are present in the film, which exhibit a random spatial distribution. From the position of these so-called Deybe-Scherrer rings, the polymorphic phase of carbamazepine is determined to the trigonal form.
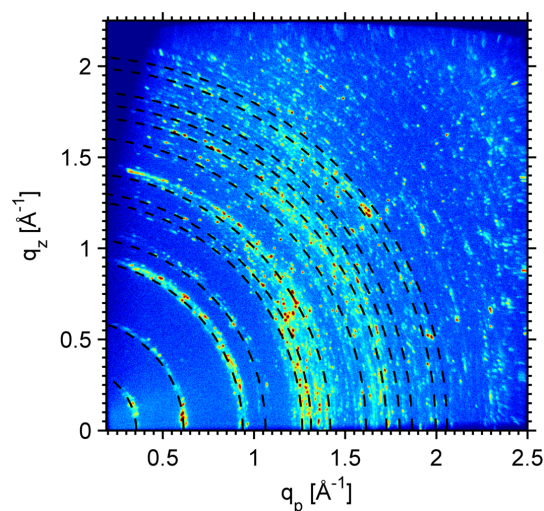

Figure A.1.: Grazing incidence reciprocal space map of carbamazepine drop casted from 5.0 wt % tetrahydrofuran. Deybe-Scherrer rings of high-intensity Bragg reflections of the trigonal carbamazepine form are indicated by dashed lines.

A.2. Carbamazepine on mica

Specular X-ray diffraction of carbamazepine, drop casted from 2.3 wt% ethanol solution on muscovite mica, is inconclusive as both the triclinic and the hydrous phase are possible candidates. In Figure A.2 the experimental diffraction pattern is given with an alternative indexation assuming the hydrate form. In this case the higher-order peak series corresponds to the {001} net planes, indicating a slight preferred texture. However, a shoulder located next to a mica Bragg reflection at $q = 2.51\,\text{Å}^{-1}$, cannot be matched by this form.
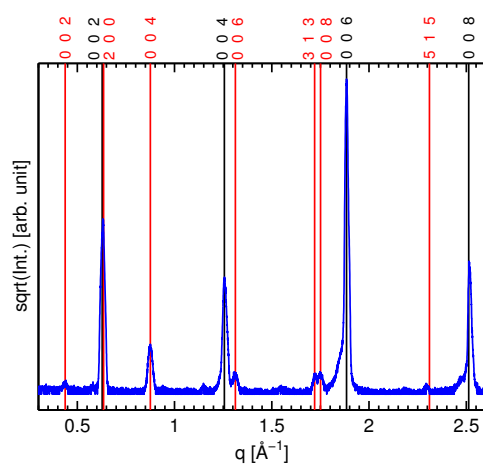
Figure A.2.: Specular X-ray diffraction pattern of carbamazepine drop casted from a 2.3 wt % ethanol solution onto a mica surface. Bragg reflections of the orthorhombic carbamazepine dihydrate (red) and mica (black) are indicated as vertical lines.

A.3. Carbamazepine and iminostilbene mixture from ethanol

Carbamazepine mixed with iminostilbene in 1:1 ratio was prepared in 0.83 wt% ethanol solution. Thin film preparation was then carried out at 60 °C by drop casting onto silicon oxide substrates. Optical polarization microscopy (Figure A.3a) shows a phase separation where a dendritic layer grows on the substrate (long, white nee-

dles), while on top bulky needles are arranged. This is likewise observed in atomic force microscopy (Figure A.3b), which depicts the two distinct morphologies. Specular X-ray diffraction (Figure A.3c) shows two higher-order peak series, corresponding to carbamazepine and iminostilbene in 110 and 010 orientation, respectively. As low-intensity Bragg reflections are also observed at $q = 0.8$ and $0.94\,\text{Å}^{-1}$, this means that also some other orientations are present. The in-plane order is further investigated by grazing incidence diffraction as depicted in Figure A.3d. While the intensity is mostly smeared out along rings, spots of higher intensity are also observed. They
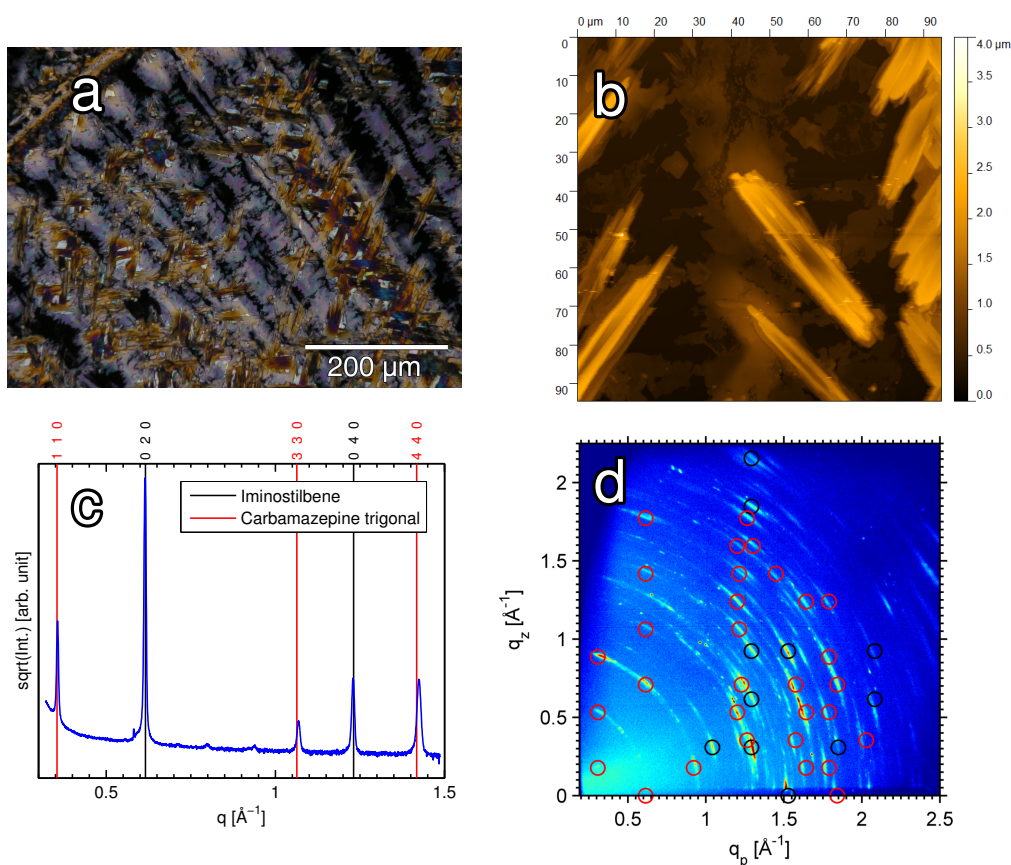
Figure A.3.: Carbamazepine/iminostilbene 1:1 mixture drop casted from 0.83 wt % ethanol solution at 60 °C: Optical microscopy (a), atomic force microscopy image (b), specular X-ray diffraction pattern (c) and gracing incidence reciprocal space map (d). ○ iminostilbene in 010 texture, ○ trigonal carbamazepine in 110 texture.

match carbamazepine and iminostilbene in the orientation already assumed from specular X-ray diffraction. This means that even though the alignment is still more powder-like, a texture has been induced to carbamazepine.

Bibliography

[1] C. Leuner and J. Dressman. "Improving drug solubility for oral delivery using solid dispersions." In: *European Journal of Pharmaceutics and Biopharmaceutics* 50.1 (July 3, 2000), pp. 47–60. DOI: 10.1016/S0939-6411(00)00076-X.

[2] D. J. Hauss. "Oral lipid-based formulations." In: *Advanced Drug Delivery Reviews*. Drug Solubility: How to Measure it, How to Improve it 59.7 (July 30, 2007), pp. 667–676. DOI: 10.1016/j.addr.2007.05.006.

[3] E. Merisko-Liversidge, G. G. Liversidge, and E. R. Cooper. "Nanosizing: a formulation approach for poorly-water-soluble compounds." In: *European Journal of Pharmaceutical Sciences* 18.2 (Feb. 2003), pp. 113–120. DOI: 10.1016/S0928-0987(02)00251-8.

[4] V. P. Torchilin. "Structure and design of polymeric surfactant-based drug delivery systems." In: *Journal of Controlled Release* 73.2 (June 15, 2001), pp. 137–172. DOI: 10.1016/S0168-3659(01)00299-1.

[5] Y. Kawabata, K. Wada, M. Nakatani, S. Yamada, and S. Onoue. "Formulation design for poorly water-soluble drugs based on biopharmaceutics classification system: Basic approaches and practical applications." In: *International Journal of Pharmaceutics* 420.1 (Nov. 25, 2011), pp. 1–10. DOI: 10.1016/j.ijpharm.2011.08.032.

[6] Y. C. Ng, Z. Yang, W. J. McAuley, and S. Qi. "Stabilisation of amorphous drugs under high humidity using pharmaceutical thin films." In: *European Journal of Pharmaceutics and Biopharmaceutics* 84.3 (Aug. 2013), pp. 555–565. DOI: 10.1016/j.ejpb.2013.01.008.

[7]   A. W. Newman and S. R. Byrn. "Solid-state analysis of the active pharmaceutical ingredient in drug products." In: *Drug Discovery Today* 8.19 (Oct. 1, 2003), pp. 898–905. DOI: 10.1016/S1359-6446(03)02832-0.

[8]   A. Llinàs and J. M. Goodman. "Polymorph control: past, present and future." In: *Drug Discovery Today* 13.5 (Mar. 2008), pp. 198–210. DOI: 10.1016/j.drudis.2007.11.006.

[9]   J. V. Parambil, S. K. Poornachary, R. B. H. Tan, and J. Y. Y. Heng. "Template-induced polymorphic selectivity: the effects of surface chemistry and solute concentration on carbamazepine crystallisation." In: *CrystEngComm* 16.23 (May 19, 2014), pp. 4927–4930. DOI: 10.1039/C3CE42622J.

[10]   R. Ruiz et al. "Structure of pentacene thin films." In: *Applied Physics Letters* 85.21 (Nov. 22, 2004), pp. 4926–4928. DOI: 10.1063/1.1826229.

[11]   C. C. Mattheus et al. "Polymorphism in pentacene." In: *Acta Crystallographica Section C* 57.8 (Aug. 1, 2001), pp. 939–941. DOI: 10.1107/S010827010100703X.

[12]   D. J. Gundlach, T. N. Jackson, D. G. Schlom, and S. F. Nelson. "Solvent-induced phase transition in thermally evaporated pentacene films." In: *Applied Physics Letters* 74.22 (May 31, 1999), pp. 3302–3304. DOI: 10.1063/1.123325.

[13]   S. Schiefer, M. Huth, A. Dobrinevski, and B. Nickel. "Determination of the Crystal Structure of Substrate-Induced Pentacene Polymorphs in Fiber Structured Thin Films." In: *Journal of the American Chemical Society* 129.34 (Aug. 1, 2007), pp. 10316–10317. DOI: 10.1021/ja0730516.

[14]   K. S. Paudel et al. "Challenges and opportunities in dermal/transdermal delivery." In: *Therapeutic Delivery* 1.1 (June 25, 2010), pp. 109–131. DOI: 10.4155/tde.10.16.

[15]   O. Werzer, R. Baumgartner, M. Zawodzki, and E. Roblegg. "Particular Film Formation of Phenytoin at Silica Surfaces." In: *Molecular Pharmaceutics* 11.2 (Feb. 3, 2014), pp. 610–616. DOI: 10.1021/mp4006479.

[16]   R. Hilfiker. *Polymorphism: In the Pharmaceutical Industry*. John Wiley & Sons, Aug. 21, 2006. 436 pp.

[17] D. Singhal and W. Curatolo. "Drug polymorphism and dosage form design: a practical perspective." In: *Advanced Drug Delivery Reviews*. Pharmaceutical solid polymorphism in drug development and regulation 56.3 (Feb. 23, 2004), pp. 335–347. DOI: 10.1016/j.addr.2003.10.008.

[18] R. J. Davey, S. L. M. Schroeder, and J. H. ter Horst. "Nucleation of Organic Crystals - A Molecular Perspective." In: *Angewandte Chemie International Edition* 52.8 (Feb. 18, 2013), pp. 2166–2179. DOI: 10.1002/anie.201204824.

[19] M. Volmer and 1885-1965. "Kinetik der phasenbildung." In: (1939).

[20] R. Boistelle and J. P. Astier. "Crystallization mechanisms in solution." In: *Journal of Crystal Growth* 90.1 (July 2, 1988), pp. 14–30. DOI: 10.1016/0022-0248(88)90294-1.

[21] A. C. Zettlemoyer. *Nucleation*. New York: Dekker, 1969. 606 pp.

[22] E. Clouet. "Modeling of Nucleation Processes." In: *arXiv:1001.4131 [cond-mat]* (Jan. 23, 2010).

[23] L. Gránásy. "Comparison of modern theories of vapor condensation." In: *AIP Conference Proceedings*. NUCLEATION AND ATMOSPHERIC AEROSOLS 2000: 15th International Conference. Vol. 534. AIP Publishing, Aug. 2, 2000, pp. 209–212. DOI: 10.1063/1.1361848.

[24] P. G. Vekilov. "Nucleation." In: *Crystal Growth & Design* 10.12 (Dec. 1, 2010), pp. 5007–5019. DOI: 10.1021/cg1011633.

[25] D. Erdemir, A. Y. Lee, and A. S. Myerson. "Nucleation of Crystals from Solution: Classical and Two-Step Models." In: *Accounts of Chemical Research* 42.5 (May 19, 2009), pp. 621–629. DOI: 10.1021/ar800217x.

[26] O. Galkin et al. "Two-Step Mechanism of Homogeneous Nucleation of Sickle Cell Hemoglobin Polymers." In: *Biophysical Journal* 93.3 (Aug. 1, 2007), pp. 902–913. DOI: 10.1529/biophysj.106.103705.

[27] P. Hartman and W. G. Perdok. "On the relations between structure and morphology of crystals. III." In: *Acta Crystallographica* 8.9 (Sept. 1, 1955), pp. 525–529. DOI: 10.1107/S0365110X55001680.

[28] J. J. D. Yoreo and P. G. Vekilov. "Principles of Crystal Nucleation and Growth." In: *Reviews in Mineralogy and Geochemistry* 54.1 (Mar. 1, 2003), pp. 57–93. DOI: 10.2113/0540057.

[29] W. C. McCrone. "Physics and chemistry of the organic solid state." In: *Interscience, New York* (1965).

[30] G. P. Stahly. "Diversity in Single- and Multiple-Component Crystals. The Search for and Prevalence of Polymorphs and Cocrystals." In: *Crystal Growth & Design* 7.6 (June 1, 2007), pp. 1007–1026. DOI: 10.1021/cg060838j.

[31] R. K. Khankari and D. J. Grant. "Pharmaceutical hydrates." In: *Pharmaceuticals and Thermal Analysis* 248 (Jan. 2, 1995), pp. 61–79. DOI: 10.1016/0040-6031(94)01952-D.

[32] N. J. Babu and A. Nangia. "Solubility Advantage of Amorphous Drugs and Pharmaceutical Cocrystals." In: *Crystal Growth & Design* 11.7 (July 6, 2011), pp. 2662–2679. DOI: 10.1021/cg200492w.

[33] R. B. Hammond, K. Pencheva, and K. J. Roberts. "Simulation of Energetic Stability of Facetted l-Glutamic Acid Nanocrystalline Clusters in Relation to Their Polymorphic Phase Stability as a Function of Crystal Size." In: *The Journal of Physical Chemistry B* 109.42 (Oct. 1, 2005), pp. 19550–19552. DOI: 10.1021/jp053546m.

[34] W. Ostwald. "Studien über die Bildung und Umwandlung fester Körper." In: *Zeitschrift für Physikalische Chemie* 22 (1897), pp. 289–330.

[35] T. Aree, N. Chaichit, and C. Engkakul. "Polymorphism in beta-cyclodextrin–benzoic acid inclusion complex: a kinetically controlled crystal growth according to the Ostwald's rule." In: *Carbohydrate Research* 343.14 (Sept. 22, 2008), pp. 2451–2458. DOI: 10.1016/j.carres.2008.06.032.

[36] R. J. Davey, N. Blagden, S. Righini, H. Alison, and E. S. Ferrari. "Nucleation Control in Solution Mediated Polymorphic Phase Transformations: The Case of 2,6-Dihydroxybenzoic Acid." In: *The Journal of Physical Chemistry B* 106.8 (Feb. 1, 2002), pp. 1954–1959. DOI: 10.1021/jp013044i.

[37] C. Stoica et al. "Understanding the Effect of a Solvent on the Crystal Habit." In: *Crystal Growth & Design* 4.4 (July 1, 2004), pp. 765–768. DOI: 10.1021/cg0342314.

[38] W. H. Organization, ed. *WHO Model Lists of Essential Medicines*. Apr. 2013.

[39]   M. Lindenberg, S. Kopp, and J. B. Dressman. "Classification of orally administered drugs on the World Health Organization Model list of Essential Medicines according to the biopharmaceutics classification system." In: *European Journal of Pharmaceutics and Biopharmaceutics*. The International Association of Pharmaceutical Technology (APV) 58.2 (Sept. 2004), pp. 265–278. DOI: 10.1016/j.ejpb.2004.03.001.

[40]   K. Tsinman, A. Avdeef, O. Tsinman, and D. Voloboy. "Powder Dissolution Method for Estimating Rotating Disk Intrinsic Dissolution Rates of Low Solubility Drugs." In: *Pharmaceutical Research* 26.9 (Sept. 1, 2009), pp. 2093–2100. DOI: 10.1007/s11095-009-9921-3.

[41]   J.-B. Arlin, L. S. Price, S. L. Price, and A. J. Florence. "A strategy for producing predicted polymorphs: catemeric carbamazepine form V." In: *Chemical Communications* 47.25 (June 14, 2011), pp. 7074–7076. DOI: 10.1039/C1CC11634G.

[42]   S. L. Childs, P. A. Wood, N. Rodríguez-Hornedo, L. S. Reddy, and K. I. Hardcastle. "Analysis of 50 Crystal Structures Containing Carbamazepine Using the Materials Module of Mercury CSD." In: *Crystal Growth & Design* 9.4 (Apr. 1, 2009), pp. 1869–1888. DOI: 10.1021/cg801056c.

[43]   A. Kogan et al. "Crystallization of Carbamazepine Pseudopolymorphs from Nonionic Microemulsions." In: *Langmuir* 24.3 (Feb. 1, 2008), pp. 722–733. DOI: 10.1021/la702763e.

[44]   W. Humphrey, A. Dalke, and K. Schulten. "VMD: Visual molecular dynamics." In: *Journal of Molecular Graphics* 14.1 (Feb. 1996), pp. 33–38. DOI: 10.1016/0263-7855(96)00018-5.

[45]   A. L. Grzesiak, M. Lang, K. Kim, and A. J. Matzger. "Comparison of the four anhydrous polymorphs of carbamazepine and the crystal structure of form I." In: *Journal of Pharmaceutical Sciences* 92.11 (Nov. 1, 2003), pp. 2260–2271. DOI: 10.1002/jps.10455.

[46]   M. M. Lowes, M. R. Caira, A. P. Lötter, and J. G. Van der Watt. "Physicochemical properties and X-ray structural studies of the trigonal polymorph of carbamazepine." In: *Journal of Pharmaceutical Sciences* 76.9 (Sept. 1987), pp. 744–752.

Bibliography

[47] K. S. Eccles et al. "Evaluation of the Bruker SMART X2S: crystallography for the nonspecialist?" In: *Journal of Applied Crystallography* 44.1 (Feb. 1, 2011), pp. 213–215. DOI: 10.1107/S0021889810042561.

[48] M. Lang, J. W. Kampf, and A. J. Matzger. "Form IV of carbamazepine." In: *Journal of Pharmaceutical Sciences* 91.4 (Apr. 1, 2002), pp. 1186–1190. DOI: 10.1002/jps.10093.

[49] S. G. Fleischman et al. "Crystal Engineering of the Composition of Pharmaceutical Phases: Multiple-Component Crystalline Solids Involving Carbamazepine." In: *Crystal Growth & Design* 3.6 (Nov. 1, 2003), pp. 909–919. DOI: 10.1021/cg034035x.

[50] A. J. C. Cabeza, G. M. Day, W. D. S. Motherwell, and W. Jones. "Solvent inclusion in form II carbamazepine." In: *Chemical Communications* 16 (Apr. 11, 2007), pp. 1600–1602. DOI: 10.1039/B701299C.

[51] R. K. Harris et al. "Structural Studies of the Polymorphs of Carbamazepine, Its Dihydrate, and Two Solvates." In: *Organic Process Research & Development* 9.6 (Nov. 1, 2005), pp. 902–910. DOI: 10.1021/op0500990.

[52] R. Vardanyan and V. Hruby. *Synthesis of Essential Drugs*. Elsevier, Mar. 10, 2006. 636 pp.

[53] J. P. Reboul, B. Cristau, J. C. Soyfer, and J. P. Astier. "5H-Dibenz[b,f]azépinecarboxamide-5 (carbamazépine)." In: *Acta Crystallographica Section B* 37.10 (Oct. 15, 1981), pp. 1844–1848. DOI: 10.1107/S0567740881007383.

[54] B. Wedl. *Structure and morphology of dihexyl-terthiophene thin films*. 2010.

[55] L. E. Scriven. "Physics and Applications of DIP Coating and Spin Coating." In: *Symposium H – Better Ceramics Through Chemistry III*. Vol. 121. MRS Online Proceedings Library. Jan. 1988. DOI: 10.1557/PROC-121-717.

[56] D. W. Schubert and T. Dunkel. "Spin coating from a molecular point of view: its concentration regimes, influence of molar mass and distribution." In: *Materials Research Innovations* 7.5 (Oct. 1, 2003), pp. 314–321. DOI: 10.1007/s10019-003-0270-2.

[57] G. Sauerbrey. "Verwendung von Schwingquarzen zur Wägung dünner Schichten und zur Mikrowägung." In: *Zeitschrift für Physik* 155.2 (Apr. 1, 1959), pp. 206–222. DOI: 10.1007/BF01337937.

[58]   F. J. Giessibl. "Advances in atomic force microscopy." In: *Reviews of Modern Physics* 75.3 (July 29, 2003), pp. 949–983. DOI: `10.1103/RevModPhys.75.949`.

[59]   M. Birkholz. *Thin Film Analysis by X-Ray Scattering*. Wiley-VCH Verlag GmbH & Co. KGaA, 2005.

[60]   A. Moser. *Crystal structure solution based on grazing incidence x-ray diffraction: software development and application to organic films*. 2012.

[61]   O. Werzer. *Structure and Morphology of Thiophene based Polymers and Pentacene for organic electronics: an X-ray based study*. 2007.

[62]   U. Pietsch, V. Holy, and T. Baumbach. *High-Resolution X-Ray Scattering - From Thin Films to Lateral Nanostructures*. 2004. 408 pp.

[63]   A. Brandt, T. Gutberlet, N. Leidel, F. Staier, and A. Vollmer, eds. *Experimental Facilities at BESSY II and BER II*. 14109 Berlin, Germany: Helmholtz-Zentrum Berlin für Materialien und Energie GmbH, Sept. 2014. 256 pp.

[64]   D. Kriegner, E. Wintersberger, and J. Stangl. "xrayutilities: a versatile tool for reciprocal space conversion of scattering data recorded with linear and area detectors." In: *Journal of Applied Crystallography* 46 (Pt 4 Aug. 1, 2013), pp. 1162–1170. DOI: `10.1107/S0021889813017214`.

[65]   I. Salzmann and R. Resel. "*STEREOPOLE* : software for the analysis of X-ray diffraction pole figures with IDL." In: *Journal of Applied Crystallography* 37.6 (Dec. 1, 2004), pp. 1029–1033. DOI: `10.1107/S002188980402165X`.

[66]   C. Rustichelli et al. "Solid-state study of polymorphic drugs: carbamazepine." In: *Journal of Pharmaceutical and Biomedical Analysis* 23.1 (Aug. 1, 2000), pp. 41–54. DOI: `10.1016/S0731-7085(00)00262-4`.

[67]   Y. Kobayashi, S. Ito, S. Itai, and K. Yamamoto. "Physicochemical properties and bioavailability of carbamazepine polymorphs and dihydrate." In: *International Journal of Pharmaceutics* 193.2 (Jan. 5, 2000), pp. 137–146. DOI: `10.1016/S0378-5173(99)00315-4`.

[68]   W. Liu, L. Dang, S. Black, and H. Wei. "Solubility of Carbamazepine (Form III) in Different Solvents from (275 to 343) K." In: *Journal of Chemical & Engineering Data* 53.9 (Sept. 1, 2008), pp. 2204–2206. DOI: `10.1021/je8002157`.

[69]   J. L. Hutter and J. Bechhoefer. "Banded spherulitic growth in a liquid crystal." In: *Journal of Crystal Growth* 217.3 (Aug. 1, 2000), pp. 332–343. DOI: 10. 1016/S0022-0248(00)00479-6.

[70]   L. E. Mcmahon, P. Timmins, A. C. Williams, and P. York. "Characterization of dihydrates prepared from carbamazepine polymorphs." In: *Journal of Pharmaceutical Sciences* 85.10 (Oct. 1, 1996), pp. 1064–1069. DOI: 10.1021/ js960117e.

[71]   O. Werzer et al. "Surface Induced Order of Solution Processed Caffeine Needles on Silica and Muscovite Mica." In: *Crystal Growth & Design* 13.3 (Mar. 6, 2013), pp. 1322–1328. DOI: 10.1021/cg301812m.

[72]   B. C. Hancock and G. Zografi. "Characteristics and significance of the amorphous state in pharmaceutical systems." In: *Journal of Pharmaceutical Sciences* 86.1 (Jan. 1, 1997), pp. 1–12. DOI: 10.1021/js9601896.

[73]   H. Kiessig. "Interferenz von Röntgenstrahlen an dünnen Schichten." In: *Annalen der Physik* 402.7 (Jan. 1, 1931), pp. 769–788. DOI: 10.1002/andp. 19314020702.

[74]   R. D. Deegan et al. "Capillary flow as the cause of ring stains from dried liquid drops." In: *Nature* 389.6653 (Oct. 23, 1997), pp. 827–829. DOI: 10.1038/ 39827.

[75]   H. M. A. Ehmann, A. Zimmer, E. Roblegg, and O. Werzer. "Morphologies in Solvent-Annealed Clotrimazole Thin Films Explained by Hansen-Solubility Parameters." In: *Crystal Growth & Design* 14.3 (Mar. 5, 2014), pp. 1386–1391. DOI: 10.1021/cg401859p.

[76]   S. Kumar, J.-H. Kim, and Y. Shi. "What Aligns Liquid Crystals on Solid Substrates? The Role of Surface Roughness Anisotropy." In: *Physical Review Letters* 94.7 (Feb. 23, 2005), p. 077803. DOI: 10.1103/PhysRevLett.94. 077803.

[77]   P. Vishweshwar, J. A. McMahon, M. Oliveira, M. L. Peterson, and M. J. Zaworotko. "The Predictably Elusive Form II of Aspirin." In: *Journal of the American Chemical Society* 127.48 (Dec. 1, 2005), pp. 16802–16803. DOI: 10. 1021/ja056455b.

[78] S. L. Childs et al. "Screening strategies based on solubility and solution com-position generate pharmaceutically acceptable cocrystals of carbamazepine." In: *CrystEngComm* 10.7 (June 24, 2008), pp. 856–864. DOI: 10.1039/B715396A.

[79] S. J. Bonafede and M. D. Ward. "Selective Nucleation and Growth of an Organic Polymorph by Ledge-Directed Epitaxy on a Molecular Crystal Sub-strate." In: *Journal of the American Chemical Society* 117.30 (Aug. 1, 1995), pp. 7853–7861. DOI: 10.1021/ja00135a001.

[80] C. A. Mitchell, L. Yu, and M. D. Ward. "Selective Nucleation and Discovery of Organic Polymorphs through Epitaxy with Single Crystal Substrates." In: *Journal of the American Chemical Society* 123.44 (Oct. 12, 2001), pp. 10830–10839. DOI: 10.1021/ja004085f.